

Non-Equilibrium Dynamics of Discrete Time Boltzmann  
Systems

by

David Packwood

A thesis submitted to The University of Leicester  
for the degree of Doctor of Philosophy

March 2012

## Abstract

Lattice Boltzmann methods are a fully discrete model and numerical method for simulating fluid dynamics, historically they have been developed as a continuation of lattice gas systems. Another route to a lattice Boltzmann system is a discrete approximation to the Boltzmann equation. An analysis of lattice Boltzmann systems is usually performed from one of these directions.

In this thesis the lattice Boltzmann method is presented ab initio as a fully discrete system in its own right. Using the Invariant Manifold hypothesis the microscopic and macroscopic fluid dynamics arising from such a model are found. In particular this analysis represents a validation for lattice Boltzmann methods far from equilibrium.

Far from equilibrium, at high Reynolds or Mach numbers, lattice Boltzmann methods can exhibit stability problems. In this work a conditional stability theorem for lattice Boltzmann methods is established. Furthermore several practical numerical techniques for stabilizing lattice Boltzmann schemes are tested.

# Acknowledgements

I would like to acknowledge firstly my scientific advisors throughout my education. Until my undergraduate tutor Manolis Georgoulis taught me functional analysis I can say, in hindsight, that I knew almost nothing about mathematics. Following that I have gone on to postgraduate study. For my PhD I have been lucky to have a very good supervisor in Alexander Gorban, not only a good scientist but somebody who has managed me well and put me on the right tracks. If in the fullness of time I can be as good an academic as him I will have done pretty well. Also thanks to all the other staff and students of the Department of Mathematics at the University of Leicester who have been good teachers, colleagues and friends.

Personally I should thank my parents and grandparents without whom, of course, I wouldn't be here. Whether by nature or nurture, any modest talent I have comes from them. Finally and most importantly thanks to my wife Aimee, my best friend and the person who kept me smiling when nothing was working.

# Contents

<b>1</b>	<b>Introduction</b>	<b>1</b>
<b>2</b>	<b>Microscopic Equations for Discrete Time Boltzmann Systems</b>	<b>8</b>
2.1	Continuous and Discrete Time Systems . . . . .	8
2.2	Discrete Space and the Lattice Boltzmann Algorithm . . . . .	10
2.3	The Invariance Equation . . . . .	14
2.4	The expansion of the distribution function following a step in the LBM chain . . . . .	15
2.5	The expansion of the invariance equation following a time step . . . . .	17
2.6	Example First Order Invariant Manifolds . . . . .	18
2.7	Second Order Manifolds and an Example . . . . .	19
2.8	Conditional Stability of Lattice Boltzmann Methods . . . . .	23
<b>3</b>	<b>Macroscopic Equations</b>	<b>31</b>
3.1	Discrete Velocity Examples . . . . .	33
3.1.1	An athermal three velocity lattice (D1Q3) . . . . .	33
3.1.2	An athermal five velocity lattice (D1Q5) . . . . .	36
3.1.3	An athermal nine velocity model (D2Q9) . . . . .	38
3.2	Continuous Velocity Examples . . . . .	42
3.2.1	The athermal 1-D model . . . . .	43

3.2.2	The athermal 2D model . . . . .	46
3.3	Macroscopic Stability . . . . .	50
3.3.1	The D1Q3 model . . . . .	50
3.3.2	The D1Q5 model . . . . .	52
3.3.3	The D2Q9 model . . . . .	53
3.4	Constructed Examples . . . . .	58
3.4.1	A constructed thermal example with 8 velocities . . . . .	62
3.5	Macroscopic Stability of Constructed Examples . . . . .	75
3.5.1	The Thermal 1D System . . . . .	75
3.6	The Thermal 2D system . . . . .	78
<b>4</b>	<b>Generalizations of BGK</b>	<b>82</b>
4.1	ELBM . . . . .	82
4.2	Entropic Limiting . . . . .	89
4.3	MRT . . . . .	91
4.3.1	Lallemand and Luo's MRT . . . . .	93
4.3.2	Dellar's MRT . . . . .	97
<b>5</b>	<b>Numerical Experiments</b>	<b>101</b>
5.1	1D Shock Tube . . . . .	101
5.2	2D Lid Driven Cavity . . . . .	105
5.2.1	First Hopf Bifurcation . . . . .	110
<b>6</b>	<b>Conclusions</b>	<b>118</b>
<b>A</b>	<b>First order populations for the D2Q9 lattice with standard polynomial quasi-equilibria</b>	<b>125</b>
<b>B</b>	<b>Populations for the constructed 2D thermal example</b>	<b>128</b>

B.1	Zero order populations for the 8 velocity lattice with a thermal moment	128
B.2	Example first order populations for the 8 velocity lattice with a thermal moment	129

# Chapter 1

## Introduction

The most common approach to solving a fluid dynamics problem is to attempt a direct numerical simulation of a discrete approximation to the Navier-Stokes equations [4]. The Navier-Stokes equations are simply given by conservation laws applied to a continuum. Such a description of a fluid may, although being a convenient model, be considered somehow non-physical. A model more related to reality is to specifically recognise that a fluid is composed of a large number of individual particles moving and interacting with each other through a potential energy. Such an intuitive and physical model is unfortunately far too expensive to implement for almost all fluid dynamics problems.

Lattice Boltzmann algorithms have been developed as a discrete algorithm used to approximate fluid dynamics. In such algorithms the dynamics of a statistical distribution of particles is simulated, rather than either the direct solution of macroscopic equations or a microscopic molecular dynamics type simulation of individual particles. The usual model hierarchy with respect to macro vs microscopic dynamics is Navier-Stokes, Boltzmann Equation, Molecular Dynamics. The lattice Boltzmann method takes the place of the Boltzmann equation for a A lattice Boltzmann system is computationally practical to use while retaining some of the physical intuitive-

ness of the molecular dynamics type simulations. A more straight forward handling of inter-species reactions and boundary conditions can be a boon in certain fluid dynamics problems, for example in complex fluids. [66]

A lattice Boltzmann algorithm can be arrived at from a number of directions. Historically one motivation is as a development of a lattice gas automata system [14, 23, 35], for a review see [51]. Such a system could operate on the same discrete velocity principle as a lattice Boltzmann system. On each edge of the lattice there is a binary option of whether a particle exists or does not. These particles advect along these edges to nodes where the edges intersect. At that point a probabilistic collision operation is applied and the particles leave the node along newly selected edges. It can be shown that the emergent macroscopic dynamics of such a system are the Navier-Stokes equations (with some appropriate assumptions).

Such a system can be viewed as a rather coarse approximation to a molecular dynamics simulation. A great advantage is that the number of degrees in the freedom is dramatically reduced. For a direct molecular dynamicis simulation of a fluid then the number of degrees of freedom would be of the order of Avagadro's constant, which is impractically high for todays computers. Another benefit of such an algorithm is that it is extremely local, during each time step each node is only concerned with the usually small number of edges connecting it to its neighbours. This makes such an algorithm rather easy to parallelize, simply be assigning a subdomain of the system to each processor. However such an approach also has its negatives. In particular, although the desired macroscopic dynamics may be achieved theoretically, due to the binary nature of the ‘fluid’ the results may be noisy. One way to arrive at lattice Boltzmann type system then, is to remove the condition that the particle populations moving along each edge must be binary. Allowing a floating point value for particles along these edges implies a *density* of particles. With an appropriate modification of the collision operation one arrives at a lattice Boltzmann system.

Another, perhaps more modern, derivation of a lattice Boltzmann system is as a direct discretization of Boltzmann's kinetic transport equation (Eq 2.1) See e.g. [34, 60, 62]. The transport equation, along with some inseparable attendant concepts (entropy and the Maxwellian distribution) represents the foundation of non-equilibrium statistical mechanics. It gives the time evolution for a one particle statistical distribution function of particles. Most importantly pairwise interactions between particles are not considered. Rather, through the assumption of ‘molecular chaos’, collisions between particles are modelled as a local increase in entropy towards the equilibrium distribution.

Although any discrete time approximation qualitatively changes the nature of the system in comparison with the fully continuous Boltzmann transport equation, one idea remains key. The notion of the local equilibrium (the Maxwell distribution in a continuous space system) defines the system. Supposed collisions between particles introduce entropy, or dissipation, which drives the system towards the equilibrium locally and the equilibrium can be defined as the fixed point of the collisions, the position of maximum entropy.

In a continuous time system the equilibrium can be considered as a particular branch of the dynamics, which represents the limit where local production of entropy is maximized. Analogously in the discrete time system, a chain of states, each element of which is locally at equilibrium, represents a branch of the discrete time dynamics.

An analysis of the continuous time system is usually based on a separation of the dynamics into fast/slow components. In particular the collision time scale  $\tau$  is assumed to be small and may then be used in a Chapman-Enskog [13] expansion. The rate of attraction towards the local equilibrium is inversely proportional to the amount of dissipation produced in the system. Therefore this rate is usually selected to model a fluid at a particular viscosity and therefore Reynolds num-

ber. An alternative method for closing the microscopic system is given by Grad's approximation[1, 31, 60]. Here an approximation to the Boltzmann equation is made by expanding the distribution function in terms of Hermite polynomials in velocity space. The coefficients of these polynomials are directly related to observable macroscopic fluid variables.

In the discrete time system collisions occur instantaneously every  $\epsilon$  units of time. On this basis the collision parameter  $\tau$  is not a time scale, it still however controls the amount of dissipation produced in the system and thereby the local contraction to equilibrium. Altogether then the amount of dissipation in a discrete time system depends on both parameters  $\epsilon$  and  $\tau$ , which respectively control the frequency and magnitude of the injections of dissipation into the system.

The introduction of a second parameter into the system may complicate a complete asymptotic analysis of the dynamics, as different cases based on the *relative* sizes of these parameters should be compared.

Lattice Boltzmann methods are often applied for fluids where the real physical time scale  $\tau$  is indeed small, but with relatively large time steps. In such systems the meaning of the parameter  $\tau$  must be lost and the Chapman-Enskog analysis of the continuous system cannot be called on. This suggests that a proper analysis of the discrete time system is best performed using asymptotics in the small difference parameter  $\epsilon$  only.

An analysis of the microscopic dynamics of a single relaxation time lattice Boltzmann system represents the first chapter of this work. This analysis is based on asymptotic expansions of the small parameter  $\epsilon$ , combined with an application of the *invariance equation*. The invariance equation is the key tool used in this work to calculate the microscopic lattice Boltzmann dynamics.

The state of any lattice Boltzmann system cannot be completely described by the state of its corresponding macroscopic variables. There is at least one (and

frequently more than one) degree of freedom in the system which controls dissipation. An equivalent statement is that the dimension of the space which the statistical distribution functions operate in as at least one more than the dimension of the space of the macroscopic variables.

The invariance manifold hypothesis tells us that using the change of macroscopics due to free flight of particles between collision operations gives a unique chain of states in this higher dimensional space. This chain of states belong to the *invariant manifold* which can in principle be calculated up to an arbitrary finite order.

The zero order approximation to the dynamics is given by a chain of local equilibrium states. The form of the higher order corrections are presented. These are necessary to calculate the macroscopic dynamics up to the same order. They depend on the space derivatives of the distribution function and the derivatives of the local equilibrium along the macroscopic moments, as well as the parameter  $\tau$ . In this work the microscopic dynamics of the single relaxation time system are calculated up to the second order.

Under some hypotheses about the magnitude of these derivatives then the size of these corrections are bounded. In that case we can make some statements regarding the proximity of the dynamics to equilibrium chain.

The macroscopic dynamics of a lattice Boltzmann system are also given by an infinite order expansion in the small parameter  $\epsilon$ . A usual selection of the equilibrium gives the Euler equations at the zero order. At the first order a Navier-Stokes type correction appears. Here there may arise some additional error terms due to the necessary finite velocity approximation used to produce a discrete algorithm. In particular this occurs if the velocity set is not sufficiently large to accurately match the third order moments of the Maxwellian. If the velocity set is large enough to calculate these moments accurately the Navier-Stokes viscous stress is produced exactly [65]. Higher order macroscopic dynamics which are not calculated in this

work are dependent on the higher order moments of the equilibrium.

In the microscopic dynamics a stable branch of the dynamics is given by a chain of states all at local equilibrium. When a lattice Boltzmann system becomes unstable we can consider that the problem is that we are too far from this stable branch and that we should return nearer to it. An obvious problem is that the rate of progress toward the equilibrium is used to control the production of dissipation and therefore Reynolds number and viscosity. This means that any modification of the dissipation made to improve stability should be carefully made so as not to affect the hydrodynamic dissipation, at least on average.

In variance with the continuous Boltzmann transport equation, the usual equilibrium of a fully discrete lattice Boltzmann method does not respect a H-theorem [67, 68]. It has been suggested that a discrete H-theorem and corresponding equilibrium could be introduced to benefit lattice Boltzmann systems [7, 41, 38, 42]. In a stability context a discrete H-theorem provides a Lyapunov function for the collision operation. The usual relaxation type collision operations can easily shown to be linearly stable, however in some circumstances H-stability may be a stronger requirement.

Another idea on how to stabilize a lattice Boltzmann system is simply to manufacture additional dissipation in the parts of the domain furthest from equilibrium, this has been termed ‘entropic limiting’ [8, 9, 10]. Other more general types of filtering, including directly filtering the macroscopic moments have also been proposed [57]. Such methods may be considered as a particular example of general flux limiter schemes for fluid dynamics [44].

In fact in a lattice Boltzmann system many instabilities arise from extremely localized singularities and shockwaves, a feature of linear second-order difference schemes [32]. These produce non-physical dispersive oscillations which then propagate and threaten the stability of the system. To prevent nonphysical oscillations,

most upwind schemes employ limiters that reduce the spatial accuracy to first order through shock waves. A mixed-order scheme may be defined as a numerical method where the formal order of the truncation error varies either spatially, for example, at a shock wave, or for different terms in the governing equations, for example, third-order convection with second-order diffusion [58].

It may be sufficient to target the source of any oscillations and suppress them before they pollute the system. Such a suppression would be achieved by implementing a lower order scheme locally. In an implementation of entropic filtering the size of the non-equilibrium component of the dynamics is measured in some way. Should it exceed some pre-defined threshold then additional entropy is injected in order to return nearer to equilibrium. Due to this threshold the percentage of the domain where extra entropy may be injected is rather small and should not affect low viscosity hydrodynamics on average.

One more technique used to stabilize lattice Boltzmann methods is termed Multiple Relaxation Time (MRT) lattice Boltzmann [18, 16, 20, 21, 46, 47]. In many velocity systems used in lattice Boltzmann systems symmetry requires a higher number of velocities than strictly required to recover the Navier-Stokes equations. This leads to a number of ‘spare’ degrees of freedom in the system, in the standard single relaxation time lattice Boltzmann systems these are not exploited. MRT lattice Boltzmann uses these degrees of freedom to modify dissipation at different orders of the dynamics. Hence the higher order components of the dynamics can be smoothed without compromising the Navier-Stokes component of the macroscopics.

In the last part of this work some more details about these enhancements are made and finally they are put to some numerical tests.

# Chapter 2

## Microscopic Equations for Discrete Time Boltzmann Systems

### 2.1 Continuous and Discrete Time Systems

Lattice Boltzmann Systems are discrete systems used to solve fluid dynamics and more [62]. For fluids, such systems can be derived as a discretization of the Boltzmann Equation

$$\partial_t f + \mathbf{v} \cdot \partial_{\mathbf{x}} f = Q(f) \quad (2.1)$$

where  $f \equiv f(\mathbf{x}, \mathbf{v}, t)$  is a one particle distribution function over space and velocity space at time  $t$ , The operator  $Q(f)$  represents the interaction between particles, sometimes called a collision operation. A particular example of the interaction  $Q(f)$  is the Bhatnagar-Gross-Krook[6, 15] operator

$$Q(f) = -\frac{1}{\tau}(f - f^{\text{eq}}). \quad (2.2)$$

The BGK operation represents a relaxation towards the local equilibrium  $f^{\text{eq}}$  with rate  $1/\tau$ . The distribution  $f^{\text{eq}}$  is given by the Maxwell Boltzmann distribution,

$$f^{\text{eq}} = \frac{\rho}{(2\pi T)^{D/2}} \exp\left(\frac{-(\mathbf{v} - \mathbf{u})^2}{2T}\right). \quad (2.3)$$

The macroscopic quantities are available as integrals over velocity space of the distribution function,

$$\begin{aligned} \rho &= \int f \, d\mathbf{v}, \\ \rho \mathbf{u} &= \int f \mathbf{v} \, d\mathbf{v}, \\ \rho \mathbf{u}^2 + \rho T &= \int f \mathbf{v}^2 \, d\mathbf{v}. \end{aligned} \quad (2.4)$$

In the standard presentation[34, 62] a quadrature approximation to these integrals is the first ingredient to discretize this system. The second is a time integration along the discrete velocities given by the quadrature. The scalar field of the population function (over space, vector space and time) becomes a sequence of vector fields (over space) in time  $f_i(\mathbf{x}, n_t \epsilon), n_t \in \mathbb{Z}$ , where the elements of the vector each correspond with an element of the quadrature. Explicitly the macroscopic moments are given by,

$$\begin{aligned} \rho &= \sum_{i=1}^n f_i, \\ \rho \mathbf{u} &= \sum_{i=1}^n f_i \mathbf{v}_i, \\ \rho \mathbf{u}^2 + T &= \sum_{i=1}^n f_i \mathbf{v}_i^2. \end{aligned} \quad (2.5)$$

The complete discrete scheme is given by

$$f_i(\mathbf{x} + \epsilon \mathbf{v}_i, t + \epsilon) = f_i + \omega(f_i - f_i^{\text{eq}}) \quad (2.6)$$

where  $\epsilon$  is the time step. For this system a discrete equilibrium must be used, one way to find a discrete equilibrium is simply to evaluate a second order Mach number expansion of the Maxwellian distribution at each quadrature node. The second order expansion is taken in order to guarantee the exact zero order hydrodynamics (the Euler equations). In the collision operation there is a new notation  $\omega$  for the relaxation rate. This indicates that this parameter has a qualitatively different effect in the discrete system from the continuous one.

In the continuous time system the parameter  $1/\tau$  is a true rate, in the discrete time system the relaxations occur every  $\epsilon$  units of time, the parameter  $\omega$  rather controls the magnitude of the relaxation. The introduction of a second parameter, the time step, complicates the analysis of discrete time systems. In the continuous time system the parameter  $\tau$  can be assumed small and an asymptotic expansion of the dynamics around the equilibrium can be made. In the discrete time system the introduction of a second small parameter (the time step) complicates this and the relative size of these two parameters is important. If the time step  $\epsilon$  is significantly larger than the physical time scale  $\tau$  those microscopic dynamics cannot hope to be captured. Because of this the Chapman-Enskog procedure using  $\tau$  cannot be called on. An asymptotic analysis of the microscopic and macroscopic dynamics with respect to the parameter  $\epsilon$  only represents the first part of this thesis.

## 2.2 Discrete Space and the Lattice Boltzmann Algorithm

The path to a fully discrete system is completed by an appropriate choice of quadrature. The set of all quadrature nodes is denoted  $\mathcal{V} = \{\mathbf{v}_1, \dots, \mathbf{v}_n\}$ . This set can be chosen such that it defines a discrete subgroup of space  $\mathcal{L}$  called the lattice. This

definition if given by the automorphism

$$\mathcal{L} + \epsilon\mathcal{V} = \mathcal{L}. \quad (2.7)$$

If the quadrature is chosen such that Eq. 2.7 holds, then the space discretization is exact. Of course for some domain geometries this exact discretization is not possible, in that case it becomes necessary to perform an interpolation onto the lattice. This introduces an additional error. Normally an interpolation of at least second order is chosen, in order to match the order of the error in the hydrodynamic part of the system.

Although Eq. 2.6 represents the most computationally efficient implementation of the algorithm, a different implementation is possibly more instructive. This involves separating the algorithm into two superposed components, advection and relaxation. In this work the  $\mapsto$  notation is used in the sense of computer memory, that is during a step in the algorithm the information in the memory on the left side of the  $\mapsto$  is mapped onto the information on the right side. Advection is the linear and non-local component of the algorithm,

$$f_i(\mathbf{x}) \mapsto f_i(\mathbf{x} + \epsilon\mathbf{v}_i). \quad (2.8)$$

Relaxation is the non-linear and local component of the algorithm,

$$f_i \mapsto f_i + \omega(f_i^{\text{eq}} - f_i). \quad (2.9)$$

The non-linearity of relaxation may not be obvious, it is contained within the non-linear dependence of the local equilibrium on the macroscopic moments. Later in this work more general forms of the relaxation operation will be considered. To allow for this generality the collision operation can just be denoted  $F$ , using this the

complete lattice Boltzmann algorithm can be written as the superposition,

$$f_i(\mathbf{x}) \mapsto f_i(\mathbf{x} - \epsilon \mathbf{v}_i) \mapsto F(f_i(\mathbf{x} - \epsilon \mathbf{v}_i)). \quad (2.10)$$

This separation of the lattice Boltzmann algorithm into two superposed operations will be used in the analysis of the dynamics of the system.

As mentioned previously the analysis in this work is based on the discrete time algorithm, the time step is denoted  $\epsilon$  hence our sequence of LBM states exists at the time points given by the discrete subgroup  $\epsilon\mathbb{Z} \subset \mathbb{R}$ . All of our asymptotic expansions will be taken in  $\epsilon$  which is assumed small.

We require that the domain for our algorithm is a smooth finite dimensional manifold which we call  $X$ , usually this will be Euclidean space. The eponymous lattice  $\mathcal{L} \subset X$  is a subset of discrete points.

In this section the general form for the microscopic dynamics of a discrete time Boltzmann system are given. In this analysis we use gothic notation for fields and bold for vectors. The discrete velocity system is given by the vector field of distribution functions  $\mathbf{f}$ , the  $i$ th component of this, a scalar field corresponding to a single element of the discrete velocity set would be  $f_i$  or the complete vector at a particular point in space is  $\mathbf{f}(\mathbf{x})$ . In the case where it is useful to use a generic vector of values of the distribution function the notation  $\mathbf{f}$  is used. There is also a corresponding vector field of macroscopic moments  $\mathfrak{M}$  and based on these macroscopic moments a vector field of local equilibrium values  $\mathbf{f}_{\mathfrak{M}}^{\text{eq}}$  also exists which is defined pointwise through the moments from  $\mathbf{f}$  using the operator  $m$ ,  $\mathfrak{M} = m(\mathbf{f})$ . The local equilibrium may also be called the quasi-equilibrium. In order to make this analysis some assumptions about the relaxation operation and the smoothness of these vector fields needs to be made.

We assume that collisions are stable, and for any admissible initial state  $\mathbf{f}$  it-

erations  $F^p(\mathbf{f})$  converge to a unique equilibrium point  $\mathbf{f}^{\text{eq}}$  exponentially fast and uniformly:

$$\|F^p(\mathbf{f}) - \mathbf{f}_{m(\mathbf{f})}^{\text{eq}}\| < C \exp(-\lambda p) \|\mathbf{f} - \mathbf{f}_{m(\mathbf{f})}^{\text{eq}}\|, \quad (2.11)$$

where the Lyapunov exponent  $\lambda > 0$  and pre-factor  $C > 0$  are the same for all admissible  $\mathbf{f}$ . In the limit  $\epsilon = 0$  there is no free flight, the field of macroscopic variables  $\mathfrak{M}$  does not change, and the field of distributions  $\mathbf{f}$  converges to the local equilibrium field  $\mathbf{f}_{\mathfrak{M}}^{\text{eq}}$  by repeated application of the collision operation independently at every point in space. Since each collision occurs instantaneously, the superposed collisions become a projection onto the local equilibrium in zero time.

In order to discuss small  $\epsilon > 0$  it is necessary to evaluate the change of macroscopic variables in free flight during time step  $\epsilon$ . To find the  $q$ th order in  $\epsilon$  term of the non-equilibrium density function of a discrete velocity system, there are two assumptions:

- The derivatives of order  $q$  or less of  $\mathbf{f}$  along the vectors  $\mathbf{v}_i$  exist and are uniformly bounded.
- The derivatives of order  $q$  or less of  $\mathbf{f}_{\mathfrak{M}}^{\text{eq}}$  with respect to the field of macroscopic moments  $\mathfrak{M}$  exist and are uniformly bounded.

Our expression for the manifold will be of the form of an asymptotic expansion in the small parameter  $\epsilon$ ,

$$\mathbf{f} = \mathbf{f}_{\mathfrak{M}}^{(0)} + \epsilon \mathbf{f}_{\mathfrak{M}}^{(1)} + \epsilon^2 \mathbf{f}_{\mathfrak{M}}^{(2)} + o(\epsilon^2). \quad (2.12)$$

Our first goal is to find a prescription for this  $\mathbf{f}_{\mathfrak{M}}^{(1)}$  term. The zero order term of this is simply given by the quasi-equilibrium distributions, that is  $\mathbf{f}_{\mathfrak{M}}^{(0)} \equiv \mathbf{f}_{\mathfrak{M}}^{\text{eq}}$ . For the first order term we will take expansions of the distribution functions in terms of time and of macroscopic moments and equate them. That is for each order in  $\epsilon$  we

can take the effect of a complete LBM step (advection and collision) and match the effect on the distribution function to that of taking the Taylor approximation of the distribution functions through the macroscopic moments up to the same order. In other words we match the dynamics of the microscopic and macroscopic scales on an order by order basis.

## 2.3 The Invariance Equation

The procedure we use is due to the invariant manifold hypothesis. Coupled steps of advection and collision form a chain of states of the population function belonging to a manifold. Since the number of discrete velocities used is normally larger than the number of macroscopic moments, there are an infinite number of possible population distributions which can give rise to the same configuration of macroscopic moments, however only one of these distributions exists on the manifold. We use a Taylor approximation to the manifold and match it with a single coupled step to find the components, at different orders of the time step, of the distribution function.

If we consider  $\mathbf{f}$  to be the field of population distributions on the manifold with corresponding field of macroscopic moments  $\mathbf{M}$  then in a continuous time system this invariance property can be defined as

$$\partial_t \mathbf{f} = \partial_{\mathbf{M}} \mathbf{f} \cdot \partial_t \mathbf{M}. \quad (2.13)$$

Here the derivative  $\partial_{\mathbf{M}}$  indicates the derivative through the field of macroscopic moments  $\mathbf{M}$ , which the field of distributions on the manifold  $\mathbf{f}$  is parameterized by. Altogether the rate of change of the population function is equal to the rate of change of the macroscopic moments multiplied by the change of the populations with respect to the macroscopic moments. The discrete time analogy of this is given

by,

$$\mathbf{f}'_{\mathfrak{M}} = \mathbf{f}_{\mathfrak{M}'} . \quad (2.14)$$

where the prime notates the next time step, therefore the left hand side of this equation can be given by Eq. 2.10.

## 2.4 The expansion of the distribution function following a step in the LBM chain

The first ingredient for the time step expansion is the Taylor series of the advection operation up to the required order in  $\epsilon$ . For the first order we have

$$\mathbf{f}(\mathbf{x} - \epsilon \mathbf{v}) = \mathbf{f}(\mathbf{x}) - \epsilon \mathbf{v} \cdot \partial_{\mathbf{x}} \mathbf{f}(\mathbf{x}) + o(\epsilon) . \quad (2.15)$$

Combining this with (2.12) we have to the first order,

$$\mathbf{f}(\mathbf{x} - \epsilon \mathbf{v}) = \mathbf{f}_{\mathfrak{M}}^{(0)}(\mathbf{x}) - \epsilon \mathbf{v} \cdot \partial_{\mathbf{x}} \mathbf{f}_{\mathfrak{M}}^{(0)}(\mathbf{x}) + \epsilon \mathbf{f}_{\mathfrak{M}}^{(1)}(\mathbf{x}) + o(\epsilon) . \quad (2.16)$$

Applying a collision operation gives the complete, composite discrete time step,

$$\mathbf{f}' = F \left( \mathbf{f}_{\mathfrak{M}}^{(0)} - \epsilon \mathbf{v} \cdot \partial_{\mathbf{x}} \mathbf{f}_{\mathfrak{M}}^{(0)} + \epsilon \mathbf{f}_{\mathfrak{M}}^{(1)} + o(\epsilon) \right) . \quad (2.17)$$

The second ingredient is to use a linearised version of the collision operation, this is sufficient to get the first order populations correctly. To understand these derivatives we recall that any admissible  $F$  is completely local in  $X$ . We can therefore think of  $F$  as a vector of  $n$  functionals (1 per distribution function), each mapping from the vector of  $n$  local values of the distribution functions to a single component of a new vector of values. Since the scalar field underlying the distribution functions is

usually  $\mathbb{R}$  or  $\mathbb{R}^+$  these functionals are usually quite simple. For a lattice Boltzmann method the collision operation takes place instantaneously in time and the field of macroscopic moments is fixed. For the purposes of this linearization then we consider the macroscopic moments to be constants rather than functions of the distribution functions. For a diagonal relaxation type collision then the only non-zero derivative is the first derivative with the index matching the functional itself and this derivative is a scalar.

Here the linearisation is made about the equilibrium corresponding to the populations to be collided,

$$\mathbf{f} \mapsto \mathbf{f}_{m(\mathbf{f})}^{\text{eq}} + (D_f F)_{\mathbf{f}_{m(\mathbf{f})}^{\text{eq}}} \left( \mathbf{f} - \mathbf{f}_{m(\mathbf{f})}^{\text{eq}} \right). \quad (2.18)$$

Due to the linearity we can move the error term in Eq 2.17 outside the collision altogether. The linearisation is then made about the equilibrium defined by the macroscopic moments of the first order advected populations

$$\mathfrak{M}'_1 = m \left( \mathfrak{f}_{\mathfrak{M}}^{(0)} - \epsilon \mathbf{v} \cdot \partial_{\mathbf{x}} \mathfrak{f}_{\mathfrak{M}}^{(0)} \right) = \mathfrak{f} + m \left( -\epsilon \mathbf{v} \cdot \partial_{\mathbf{x}} \mathfrak{f}_{\mathfrak{M}}^{(0)} \right), \quad (2.19)$$

Finally then for the first order approximation to the next step through the time step expansion we have,

$$\mathfrak{f}'_{\mathfrak{M}} = \mathfrak{f}_{\mathfrak{M}'_1}^{\text{eq}} + (D_f F)_{\mathfrak{f}_{\mathfrak{M}'_1}^{\text{eq}}} \left( \mathfrak{f}_{\mathfrak{M}}^{(0)} + \epsilon \mathfrak{f}_{\mathfrak{M}}^{(1)} - \epsilon \mathbf{v} \cdot \partial_{\mathbf{x}} \mathfrak{f}_{\mathfrak{M}}^{(0)} - \mathfrak{f}_{\mathfrak{M}'_1}^{\text{eq}} \right) + o(\epsilon). \quad (2.20)$$

## 2.5 The expansion of the invariance equation following a time step

With the expansion of the left hand of (2.14) complete we consider the right hand side. Here we find the Taylor expansion of the invariant manifold up to the linear term so,

$$\mathbf{f}_{\mathfrak{M}'} = \mathbf{f} + (\partial_{\mathfrak{M}} \mathbf{f}) \cdot m (-\epsilon \mathbf{v} \cdot \partial_{\mathbf{x}} \mathbf{f}) + o(\epsilon). \quad (2.21)$$

Substituting (2.12) into (2.21) we have

$$\mathbf{f}_{\mathfrak{M}'} = \mathbf{f}_{\mathfrak{M}}^{(0)} + \epsilon \mathbf{f}_{\mathfrak{M}}^{(1)} + (\partial_{\mathfrak{M}} \mathbf{f}^{(0)})_{\mathfrak{M}} \cdot m \left( -\epsilon \mathbf{v} \cdot \partial_{\mathbf{x}} \mathbf{f}_{\mathfrak{M}}^{(0)} \right) + o(\epsilon). \quad (2.22)$$

We can now equate (2.20) and (2.22) for a first order approximation to (2.14),

$$\begin{aligned} \mathbf{f}_{\mathfrak{M}'_1}^{\text{eq}} + (D_f F)_{\mathbf{f}_{\mathfrak{M}'_1}^{\text{eq}}} \left( \mathbf{f}_{\mathfrak{M}}^{(0)} + \epsilon \mathbf{f}_{\mathfrak{M}}^{(1)} - \epsilon \mathbf{v} \cdot \partial_{\mathbf{x}} \mathbf{f}_{\mathfrak{M}}^{(0)} - \mathbf{f}_{\mathfrak{M}'_1}^{\text{eq}} \right) \\ = \mathbf{f}_{\mathfrak{M}}^{(0)} + \epsilon \mathbf{f}_{\mathfrak{M}}^{(1)} + (\partial_{\mathfrak{M}} \mathbf{f}_{\mathfrak{M}}^{(0)}) \cdot m \left( -\epsilon \mathbf{v} \cdot \partial_{\mathbf{x}} \mathbf{f}_{\mathfrak{M}}^{(0)} \right). \end{aligned} \quad (2.23)$$

Of course in a similar style to (2.21),

$$\mathbf{f}_{\mathfrak{M}'_1}^{\text{eq}} = \mathbf{f}_{\mathfrak{M}}^{(0)} + (\partial_{\mathfrak{M}} \mathbf{f}^{(0)})_{\mathfrak{M}} \cdot m \left( -\epsilon \mathbf{v} \cdot \partial_{\mathbf{x}} \mathbf{f}_{\mathfrak{M}}^{(0)} \right). \quad (2.24)$$

Substituting back into (2.23) we have

$$(D_f F)_{\mathbf{f}_{\mathfrak{M}'_1}^{\text{eq}}} \left( \epsilon \mathbf{f}_{\mathfrak{M}}^{(1)} - \epsilon \mathbf{v} \cdot \partial_{\mathbf{x}} \mathbf{f}_{\mathfrak{M}}^{(0)} - (\partial_{\mathfrak{M}} \mathbf{f}_{\mathfrak{M}}^{(0)}) \cdot m \left( -\epsilon \mathbf{v} \cdot \partial_{\mathbf{x}} \mathbf{f}_{\mathfrak{M}}^{(0)} \right) \right) = \epsilon \mathbf{f}_{\mathfrak{M}}^{(1)} \quad (2.25)$$

This equation forms the prototype to find  $\mathbf{f}_{\mathfrak{M}}^{(1)}$  for different possible collision operations. It implicitly gives the first order approximation to the invariance equation (2.14). It depends on the choice of the velocity set, the quasiequilibrium and the

collision integral.

## 2.6 Example First Order Invariant Manifolds

We consider two possible examples of collisions. The first example is the simple Ehrenfest step [22, 27],

$$F(\mathbf{f}) = \mathbf{f}_{m(\mathbf{f})}^{\text{eq}} \quad (2.26)$$

we immediately have,

$$(D_f F)_{\mathbf{f}^{\text{eq}}}(\mathbf{f}) = 0. \quad (2.27)$$

Substituting back into (2.25),

$$\mathfrak{f}_{\mathfrak{M}}^{(1)} = 0. \quad (2.28)$$

This of course expected since using Ehrenfests steps for the collisions we should expect to return at every time step to the quasi-equilibrium manifold.

The second example of a collision operator is the BGK collision [6],

$$F(\mathbf{f}) = \mathbf{f} + \omega \left( \mathbf{f}_{m(\mathbf{f})}^{\text{eq}} - \mathbf{f} \right). \quad (2.29)$$

Differentiating we have

$$(D_f F)_{\mathbf{f}_{m(\mathbf{f})}^{\text{eq}}}(\mathbf{f}) = (1 - \omega) \mathbf{f} \quad (2.30)$$

Substituting this into (2.25),

$$(1 - \omega) \cdot \left( \epsilon \mathfrak{f}_{\mathfrak{M}}^{(1)} - \epsilon \mathbf{v} \cdot \partial_{\mathbf{x}} \mathfrak{f}_{\mathfrak{M}}^{(0)} - (\partial_{\mathfrak{M}} \mathfrak{f}_{\mathfrak{M}}^{(0)}) \cdot m \left( -\epsilon \mathbf{v} \cdot \partial_{\mathbf{x}} \mathfrak{f}_{\mathfrak{M}}^{(0)} \right) \right) = \epsilon \mathfrak{f}_{\mathfrak{M}}^{(1)}. \quad (2.31)$$

We can multiply out (2.31) and solve for,  $f_M^{(1)}$ .

$$\frac{\omega}{1 - \omega} \mathfrak{f}_{\mathfrak{M}}^{(1)} = \left( -\mathbf{v} \cdot \partial_{\mathbf{x}} \mathfrak{f}_{\mathfrak{M}}^{(0)} \right) - (\partial_{\mathfrak{M}} \mathfrak{f}_{\mathfrak{M}}^{(0)}) \cdot m \left( -\mathbf{v} \cdot \partial_{\mathbf{x}} \mathfrak{f}_{\mathfrak{M}}^{(0)} \right) \quad (2.32)$$

Figure 2.1 graphically demonstrates the  $\mathbf{f}_M^{(1)}$  for the BGK collision type. In particular for this example there is a critical parameter value at  $\omega = 1$ . For  $\omega = 1$  we recover the Ehrenfest step, for  $\omega > 1$  we have the normal BGK over-relaxation where both of the coupled steps of advection and collision cross the quasiequilibrium manifold, one in each direction.

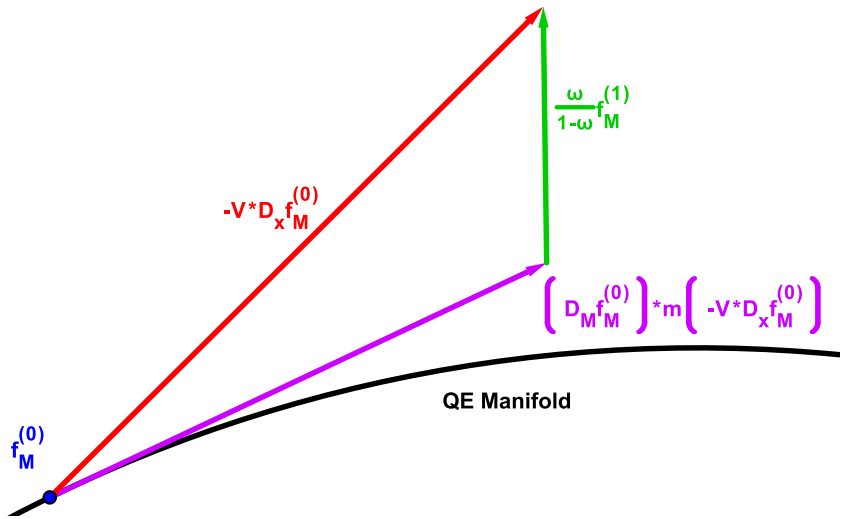


Figure 2.1: Graphical representation of the  $\mathbf{f}_M^{(1)}$  for the BGK collision. Adding the  $\mathbf{f}_M^{(1)}$  term to the quasiequilibrium manifold gives the invariant manifold to first order in  $\epsilon$ . In particular the collision parameter  $\omega$  is critical, for  $\omega > 1$  the direction of the  $\mathbf{f}_M^{(1)}$  term is inverted and consequently the invariant manifold is below (in the sense of this illustration) the quasiequilibrium. Therefore at each step the advection operation crosses the quasiequilibrium and the collision returns below it.

## 2.7 Second Order Manifolds and an Example

The next goal is to find an equation analogous to (2.25) for the second order term of the invariant manifold. During the next section we use a linear collision operation, in this case the linearised collision we use produces the exact same result as the original collision. We restart the procedure using second order expansions where

appropriate, the first of these is the Taylor expansion of the advected populations,

$$\mathbf{f}(\mathbf{x} - \epsilon \mathbf{v}) = \mathbf{f}(\mathbf{x}) - \epsilon \mathbf{v} \cdot \partial_{\mathbf{x}} \mathbf{f}(\mathbf{x}) + \frac{\epsilon^2}{2} \mathbf{v} \cdot \partial_{\mathbf{x}} (\mathbf{v} \cdot \partial_{\mathbf{x}} \mathbf{f}(\mathbf{x})) + o(\epsilon^2). \quad (2.33)$$

The second order population expansion is also used,

$$\mathbf{f} = \mathbf{f}_{\mathfrak{M}}^{(0)} + \epsilon \mathbf{f}_{\mathfrak{M}}^{(1)} + \epsilon^2 \mathbf{f}_{\mathfrak{M}}^{(2)} + o(\epsilon^2). \quad (2.34)$$

Altogether the second order expansion of the advected populations is,

$$\begin{aligned} \mathbf{f}(\mathbf{x} - \epsilon \mathbf{v}) &= \mathbf{f}_{\mathfrak{M}}^{(0)}(\mathbf{x}) - \epsilon \mathbf{v} \cdot \partial_{\mathbf{x}} \mathbf{f}_{\mathfrak{M}}^{(0)}(\mathbf{x}) + \frac{\epsilon^2}{2} \mathbf{v} \cdot \partial_{\mathbf{x}} \left( \mathbf{v} \cdot \partial_{\mathbf{x}} \mathbf{f}_{\mathfrak{M}}^{(0)}(\mathbf{x}) \right) \\ &\quad + \epsilon \mathbf{f}_{\mathfrak{M}}^{(1)}(\mathbf{x}) - \epsilon^2 \mathbf{v} \cdot \partial_{\mathbf{x}} \mathbf{f}_{\mathfrak{M}}^{(1)}(\mathbf{x}) + \epsilon^2 \mathbf{f}_{\mathfrak{M}}^{(2)}(\mathbf{x}) + o(\epsilon^2). \end{aligned} \quad (2.35)$$

We define  $\mathfrak{M}'_2$  as the macroscopic moments of the post advection populations to *second* order,

$$\mathfrak{M}'_2 = m \left( \mathbf{f}_{\mathfrak{M}}^{(0)} - \epsilon \mathbf{v} \cdot \partial_{\mathbf{x}} \mathbf{f}_{\mathfrak{M}}^{(0)} + \frac{\epsilon^2}{2} \mathbf{v} \cdot \partial_{\mathbf{x}} \left( \mathbf{v} \cdot \partial_{\mathbf{x}} \mathbf{f}_{\mathfrak{M}}^{(0)} \right) - \epsilon^2 \mathbf{v} \cdot \partial_{\mathbf{x}} \mathbf{f}_{\mathfrak{M}}^{(1)} \right), \quad (2.36)$$

It will be convenient to introduce notation for the change in macroscopic moments following the advection operation, we denote this quantity  $\Delta M$ ,

$$\Delta \mathfrak{M} = m (\mathbf{f}(\mathbf{x} - \epsilon \mathbf{v}) - \mathbf{f}(\mathbf{x})). \quad (2.37)$$

The second order approximation to this  $\Delta \mathfrak{M}_2$  is the difference between the macroscopic moments of the post and pre advection populations to second order,

$$\Delta \mathfrak{M}_2 = m \left( -\epsilon \mathbf{v} \cdot \partial_{\mathbf{x}} \mathbf{f}_{\mathfrak{M}}^{(0)} + \frac{\epsilon^2}{2} \mathbf{v} \cdot \partial_{\mathbf{x}} \left( \mathbf{v} \cdot \partial_{\mathbf{x}} \mathbf{f}_{\mathfrak{M}}^{(0)} \right) - \epsilon^2 \mathbf{v} \cdot \partial_{\mathbf{x}} \mathbf{f}_{\mathfrak{M}}^{(1)} \right) = \mathfrak{M}'_2 - \mathfrak{M}. \quad (2.38)$$

We use the linearized collision integral in replacement of the original collision operation,

$$\begin{aligned} \mathbf{f}'_{\mathfrak{M}} &= \mathbf{f}_{\mathfrak{M}_2}^{\text{eq}} + (D_f F)_{\mathbf{f}_{\mathfrak{M}_2}^{\text{eq}}} \left( \mathbf{f}_{\mathfrak{M}}^{(0)} - \epsilon \mathbf{v} \cdot \partial_{\mathbf{x}} \mathbf{f}_{\mathfrak{M}}^{(0)} + \frac{\epsilon^2}{2} \mathbf{v} \cdot \partial_{\mathbf{x}} \left( \mathbf{v} \cdot \partial_{\mathbf{x}} \mathbf{f}_{\mathfrak{M}}^{(0)} \right) \right. \\ &\quad \left. + \epsilon \mathbf{f}_{\mathfrak{M}}^{(1)} - \epsilon^2 \mathbf{v} \cdot \partial_{\mathbf{x}} \mathbf{f}_{\mathfrak{M}}^{(1)} + \epsilon^2 \mathbf{f}_{\mathfrak{M}}^{(2)} - \mathbf{f}_{\mathfrak{M}_2}^{\text{eq}} \right) + o(\epsilon^2). \end{aligned} \quad (2.39)$$

For the right hand side of (2.14) we use a second order approximation to the invariant manifold,

$$\mathbf{f}_{\mathfrak{M}'} = \mathbf{f} + \Delta \mathfrak{M}_2 \cdot \partial_{\mathfrak{M}} \mathbf{f} + \frac{1}{2} \Delta \mathfrak{M}_2 \cdot \partial_{\mathfrak{M}} (\Delta \mathfrak{M}_2 \cdot \partial_{\mathfrak{M}} \mathbf{f}) + o((\Delta \mathfrak{M}_2)^2). \quad (2.40)$$

Substituting (2.34) and (2.38) into (2.40) we have

$$\begin{aligned} \mathbf{f}_{\mathfrak{M}'} &= \mathbf{f}_{\mathfrak{M}}^{(0)} + \epsilon \mathbf{f}_{\mathfrak{M}}^{(1)} + \epsilon^2 \mathbf{f}_{\mathfrak{M}}^{(2)} + m \left( -\epsilon \mathbf{v} \cdot \partial_{\mathbf{x}} \mathbf{f}_{\mathfrak{M}}^{(0)} + \frac{\epsilon^2}{2} \mathbf{v} \cdot \partial_{\mathbf{x}} \left( \mathbf{v} \cdot \partial_{\mathbf{x}} \mathbf{f}_{\mathfrak{M}}^{(0)} \right) \right. \\ &\quad \left. - \epsilon^2 \mathbf{v} \cdot \partial_{\mathbf{x}} \mathbf{f}_{\mathfrak{M}}^{(1)} \right) \cdot \partial_{\mathfrak{M}} \mathbf{f}_{\mathfrak{M}}^{(0)} \\ &\quad + \frac{1}{2} m \left( -\epsilon \mathbf{v} \cdot \partial_{\mathbf{x}} \mathbf{f}_{\mathfrak{M}}^{(0)} \right) \cdot \partial_{\mathfrak{M}} \left( m \left( -\epsilon \mathbf{v} \cdot \partial_{\mathbf{x}} \mathbf{f}_{\mathfrak{M}}^{(0)} \right) \cdot \partial_{\mathfrak{M}} \mathbf{f}_{\mathfrak{M}}^{(0)} \right) \\ &\quad + \epsilon m \left( -\epsilon \mathbf{v} \cdot \partial_{\mathbf{x}} \mathbf{f}_{\mathfrak{M}}^{(0)} \right) \cdot \partial_{\mathfrak{M}} \mathbf{f}_{\mathfrak{M}}^{(1)} + o(\epsilon^2). \end{aligned} \quad (2.41)$$

With the expansions of both sides complete we can equate (2.39) and (2.41),

$$\begin{aligned} &\mathbf{f}_{\mathfrak{M}_2}^{\text{eq}} + (D_f F)_{\mathbf{f}_{\mathfrak{M}_2}^{\text{eq}}} \left( \mathbf{f}_{\mathfrak{M}}^{(0)} - \epsilon \mathbf{v} \cdot \partial_{\mathbf{x}} \mathbf{f}_{\mathfrak{M}}^{(0)} + \frac{\epsilon^2}{2} \mathbf{v} \cdot \partial_{\mathbf{x}} \left( \mathbf{v} \cdot \partial_{\mathbf{x}} \mathbf{f}_{\mathfrak{M}}^{(0)} \right) + \epsilon \mathbf{f}_{\mathfrak{M}}^{(1)} \right. \\ &\quad \left. - \epsilon^2 \mathbf{v} \cdot \partial_{\mathbf{x}} \mathbf{f}_{\mathfrak{M}}^{(1)} + \epsilon^2 \mathbf{f}_{\mathfrak{M}}^{(2)} - \mathbf{f}_{\mathfrak{M}_2}^{\text{eq}} \right) \\ &= \mathbf{f}_{\mathfrak{M}}^{(0)} + \epsilon \mathbf{f}_{\mathfrak{M}}^{(1)} + \epsilon^2 \mathbf{f}_{\mathfrak{M}}^{(2)} \\ &\quad + m \left( -\epsilon \mathbf{v} \cdot \partial_{\mathbf{x}} \mathbf{f}_{\mathfrak{M}}^{(0)} + \frac{\epsilon^2}{2} \mathbf{v} \cdot \partial_{\mathbf{x}} \left( \mathbf{v} \cdot \partial_{\mathbf{x}} \mathbf{f}_{\mathfrak{M}}^{(0)} \right) - \epsilon^2 \mathbf{v} \cdot \partial_{\mathbf{x}} \mathbf{f}_{\mathfrak{M}}^{(1)} \right) \cdot \partial_{\mathfrak{M}} \mathbf{f}_{\mathfrak{M}}^{(0)} \\ &\quad + \frac{1}{2} m \left( -\epsilon \mathbf{v} \cdot \partial_{\mathbf{x}} \mathbf{f}_{\mathfrak{M}}^{(0)} \right) \cdot \partial_{\mathfrak{M}} \left( m \left( -\epsilon \mathbf{v} \cdot \partial_{\mathbf{x}} \mathbf{f}_{\mathfrak{M}}^{(0)} \right) \cdot \partial_{\mathfrak{M}} \mathbf{f}_{\mathfrak{M}}^{(0)} \right) \\ &\quad + \epsilon m \left( -\epsilon \mathbf{v} \cdot \partial_{\mathbf{x}} \mathbf{f}_{\mathfrak{M}}^{(0)} \right) \cdot \partial_{\mathfrak{M}} \mathbf{f}_{\mathfrak{M}}^{(1)} \end{aligned} \quad (2.42)$$

Analogously to the first order case we note that,

$$\begin{aligned} \mathbf{f}_{\mathfrak{M}_2}^{\text{eq}} = & \mathbf{f}_{\mathfrak{M}}^{(0)} + m \left( -\epsilon \mathbf{v} \cdot \partial_{\mathbf{x}} \mathbf{f}_{\mathfrak{M}}^{(0)} + \frac{\epsilon^2}{2} \mathbf{v} \cdot \partial_{\mathbf{x}} \left( \mathbf{v} \cdot \partial_{\mathbf{x}} \mathbf{f}_{\mathfrak{M}}^{(0)} \right) - \right. \\ & \left. \epsilon^2 \mathbf{v} \cdot \partial_{\mathbf{x}} \mathbf{f}_{\mathfrak{M}}^{(1)} \right) \cdot \partial_{\mathfrak{M}} \mathbf{f}_{\mathfrak{M}}^{(0)} \\ & + m \left( -\epsilon \mathbf{v} \cdot \partial_{\mathbf{x}} \mathbf{f}_{\mathfrak{M}}^{(0)} \right) \cdot \partial_{\mathfrak{M}} \left( m \left( -\epsilon \mathbf{v} \cdot \partial_{\mathbf{x}} \mathbf{f}_{\mathfrak{M}}^{(0)} \right) \cdot \partial_{\mathfrak{M}} \mathbf{f}_{\mathfrak{M}}^{(0)} \right). \end{aligned} \quad (2.43)$$

Substituting this back into (2.42) we have the final prototype for  $\mathbf{f}^{(2)}$  which this time is given implicitly,

$$\begin{aligned} (D_f F)_{\mathbf{f}_{\mathfrak{M}_2}^{\text{eq}}} = & \left( -\epsilon \mathbf{v} \cdot \partial_{\mathbf{x}} \mathbf{f}_{\mathfrak{M}}^{(0)} + \frac{\epsilon^2}{2} \mathbf{v} \cdot \partial_{\mathbf{x}} \left( \mathbf{v} \cdot \partial_{\mathbf{x}} \mathbf{f}_{\mathfrak{M}}^{(0)} \right) + \epsilon \mathbf{f}_{\mathfrak{M}}^{(1)} - \epsilon^2 \mathbf{v} \cdot \partial_{\mathbf{x}} \mathbf{f}_{\mathfrak{M}}^{(1)} + \epsilon^2 \mathbf{f}_{\mathfrak{M}}^{(2)} \right. \\ & - m \left( -\epsilon \mathbf{v} \cdot \partial_{\mathbf{x}} \mathbf{f}_{\mathfrak{M}}^{(0)} + \frac{\epsilon^2}{2} \mathbf{v} \cdot \partial_{\mathbf{x}} \left( \mathbf{v} \cdot \partial_{\mathbf{x}} \mathbf{f}_{\mathfrak{M}}^{(0)} \right) - \epsilon^2 \mathbf{v} \cdot \partial_{\mathbf{x}} \mathbf{f}_{\mathfrak{M}}^{(1)} \right) \cdot \partial_{\mathfrak{M}} \mathbf{f}_{\mathfrak{M}}^{(0)} \\ & \left. - \frac{1}{2} m \left( -\epsilon \mathbf{v} \cdot \partial_{\mathbf{x}} \mathbf{f}_{\mathfrak{M}}^{(0)} \right) \cdot \partial_{\mathfrak{M}} \left( m \left( -\epsilon \mathbf{v} \cdot \partial_{\mathbf{x}} \mathbf{f}_{\mathfrak{M}}^{(0)} \right) \cdot \partial_{\mathfrak{M}} \mathbf{f}_{\mathfrak{M}}^{(0)} \right) \right) \\ = & \epsilon \mathbf{f}_{\mathfrak{M}}^{(1)} + \epsilon^2 \mathbf{f}_{\mathfrak{M}}^{(2)} + \epsilon m \left( -\epsilon \mathbf{v} \cdot \partial_{\mathbf{x}} \mathbf{f}_{\mathfrak{M}}^{(0)} \right) \cdot \partial_{\mathfrak{M}} \mathbf{f}_{\mathfrak{M}}^{(1)}. \end{aligned} \quad (2.44)$$

We return to the BGK collision for a specific example of an  $\mathbf{f}_{\mathfrak{M}}^{(2)}$  term. (2.44) becomes,

$$\begin{aligned} (1 - \omega) \left( & -\epsilon \mathbf{v} \cdot \partial_{\mathbf{x}} \mathbf{f}_{\mathfrak{M}}^{(0)} + \frac{\epsilon^2}{2} \mathbf{v} \cdot \partial_{\mathbf{x}} \left( \mathbf{v} \cdot \partial_{\mathbf{x}} \mathbf{f}_{\mathfrak{M}}^{(0)} \right) + \epsilon \mathbf{f}_{\mathfrak{M}}^{(1)} - \epsilon^2 \mathbf{v} \cdot \partial_{\mathbf{x}} \mathbf{f}_{\mathfrak{M}}^{(1)} + \epsilon^2 \mathbf{f}_{\mathfrak{M}}^{(2)} \right. \\ & - m \left( -\epsilon \mathbf{v} \cdot \partial_{\mathbf{x}} \mathbf{f}_{\mathfrak{M}}^{(0)} + \frac{\epsilon^2}{2} \mathbf{v} \cdot \partial_{\mathbf{x}} \left( \mathbf{v} \cdot \partial_{\mathbf{x}} \mathbf{f}_{\mathfrak{M}}^{(0)} \right) - \epsilon^2 \mathbf{v} \cdot \partial_{\mathbf{x}} \mathbf{f}_{\mathfrak{M}}^{(1)} \right) \cdot \partial_{\mathfrak{M}} \mathbf{f}_{\mathfrak{M}}^{(0)} \\ & \left. - \frac{1}{2} m \left( -\epsilon \mathbf{v} \cdot \partial_{\mathbf{x}} \mathbf{f}_{\mathfrak{M}}^{(0)} \right) \cdot \partial_{\mathfrak{M}} \left( m \left( -\epsilon \mathbf{v} \cdot \partial_{\mathbf{x}} \mathbf{f}_{\mathfrak{M}}^{(0)} \right) \cdot \partial_{\mathfrak{M}} \mathbf{f}_{\mathfrak{M}}^{(0)} \right) \right) \\ = & \epsilon \mathbf{f}_{\mathfrak{M}}^{(1)} + \epsilon^2 \mathbf{f}_{\mathfrak{M}}^{(2)} + \epsilon m \left( -\epsilon \mathbf{v} \cdot \partial_{\mathbf{x}} \mathbf{f}_{\mathfrak{M}}^{(0)} \right) \cdot \partial_{\mathfrak{M}} \mathbf{f}_{\mathfrak{M}}^{(1)} \end{aligned} \quad (2.45)$$

. Rearranging and equating terms with  $\epsilon$  order 2 gives us,

$$\begin{aligned} \frac{\omega}{1-\omega} \mathbf{f}_{\mathfrak{M}}^{(2)} = & \frac{1}{2} \mathbf{v} \cdot \partial_{\mathbf{x}} \left( \mathbf{v} \cdot \partial_{\mathbf{x}} \mathbf{f}_{\mathfrak{M}}^{(0)} \right) - \mathbf{v} \cdot \partial_{\mathbf{x}} \mathbf{f}_{\mathfrak{M}}^{(1)} \\ & - m \left( \frac{1}{2} \mathbf{v} \cdot \partial_{\mathbf{x}} \left( \mathbf{v} \cdot \partial_{\mathbf{x}} \mathbf{f}_{\mathfrak{M}}^{(0)} \right) - \mathbf{v} \cdot \partial_{\mathbf{x}} \mathbf{f}_{\mathfrak{M}}^{(1)} \right) \cdot \partial_{\mathbf{x}} \mathbf{f}_{\mathfrak{M}}^{(0)} \\ & - \frac{1}{2} m \left( -\mathbf{v} \cdot \partial_{\mathbf{x}} \mathbf{f}_{\mathfrak{M}}^{(0)} \right) \cdot \partial_{\mathbf{m}} \left( m \left( -\mathbf{v} \cdot \partial_{\mathbf{x}} \mathbf{f}_{\mathfrak{M}}^{(0)} \right) \cdot \partial_{\mathbf{m}} \mathbf{f}_{\mathfrak{M}}^{(0)} \right) \\ & - \frac{1}{1-\omega} m \left( -\mathbf{v} \cdot \partial_{\mathbf{x}} \mathbf{f}_{\mathfrak{M}}^{(0)} \right) \cdot \partial_{\mathbf{m}} \mathbf{f}_{\mathfrak{M}}^{(1)}. \end{aligned} \quad (2.46)$$

We will not use these populations in the examples of macroscopic dynamics which we calculate in the next chapter. For the Navier-Stokes dynamics the first order populations are sufficient. We expect that this second order part should give rise to macroscopic dynamics equating to the Burnett equations in a continuous velocity system, with some additional error terms due to the quadrature approximation to the Maxwellian distribution.

## 2.8 Conditional Stability of Lattice Boltzmann Methods

Usually when a finite difference scheme is used to solve a differential equation the solution is not exact. The error term generally includes an infinite number of higher order derivatives multiplied with increasing powers of the finite difference parameter (or stepsize) often denoted  $h$ . If these higher order derivatives become unbounded then the convergence of the finite difference scheme under decreasing  $h$  may be compromised. We can illustrate this with the example of the commonly used forward Euler scheme for a time dependent variable  $u$ ,

$$\frac{d}{dt} u(t) \approx \frac{u(t+h) - u(t)}{h}. \quad (2.47)$$

In fact the exact difference scheme calculates,

$$\frac{u(t+h) - u(t)}{h} = \frac{d}{dt}u(t) + \sum_{i=2}^n \frac{h^{i-1}}{i!} \frac{d^i}{dt^i}u(t) + \frac{h^n}{(n+1)!} \frac{d^{n+1}}{dt^{n+1}}u(t+ah), \quad a \in (0, 1). \quad (2.48)$$

If the derivatives in the spurious terms on the right hand side are unbounded then no matter how small  $h$  is chosen, the solution calculated by this difference scheme will ‘blow up’. If, however, the first  $n+1$  derivatives are bounded, then we can always make the  $n$ th order in  $h$  component of the error arbitrarily small by decreasing  $h$ , we can then say that the difference scheme is *conditionally stable* up to the  $n$ th order in  $h$ .

We are interested in order by order conditional stability theorems for lattice Boltzmann methods, which we prove inductively. For a first order theorem corresponding to the base case we have the following requirements.

Before we state our theorem we create some extra notation. We define an operator to perform advection

$$\text{adv}(\mathbf{f}(\mathbf{x})) = \mathbf{f}(\mathbf{x} - \epsilon \mathbf{v}), \quad (2.49)$$

and another operator giving us the 1st order Taylor approximation to advection,

$$\text{adv}_1(\mathbf{f}) = \mathbf{f} - \epsilon \mathbf{v} \cdot \partial_{\mathbf{x}} \mathbf{f} \quad (2.50)$$

For a distribution function  $\mathbf{f}$  with corresponding field of macroscopic moments  $\mathfrak{M} = m(\mathbf{f})$  we can call  $\mathbf{g}_{\mathfrak{M}}^{(n)}$  the  $n$ th order ‘jet’ of the invariant manifold. If it exists it satisfies the invariance equation up to the  $n$ th order. That is the difference between an LBM time step of a distribution on the jet parameterized by macroscopic moments  $\mathfrak{M}$ , and the distribution on the jet parameterized by the change in

macroscopic moments in that time step is  $o(\epsilon^n)$ ,

$$\left( \mathbf{g}_{\mathfrak{M}}^{(n)} \right)' - \mathbf{g}_{m(\text{adv}(\mathbf{g}_{\mathfrak{M}}^{(n)}))}^{(n)} = o(\epsilon^n). \quad (2.51)$$

The necessary derivatives required for the existence of the jet will be written as an asymptotic expansion,

$$\mathbf{g}_{\mathfrak{M}}^{(n)} = \sum_{i=0}^n \epsilon^i \mathbf{f}_{\mathfrak{M}}^{(i)}, \quad (2.52)$$

where  $\mathbf{f}_{\mathfrak{M}}^{(0)} = \mathbf{f}_{\mathfrak{M}}^{\text{eq}}$ .

We would also like to project a distribution function onto its  $n$ th order jet given in Eq 2.52. By definition for the starting distribution we know that this is,

$$\text{proj}_n(\mathbf{f}) = \mathbf{g}_{\mathfrak{M}}^{(n)}. \quad (2.53)$$

The projection onto the equilibrium is given by  $\text{proj}_0$ .

**Assumption (1).** *We have a linear operator  $A$  used in a relaxation type collision,*

$$F(\mathbf{f}) = \mathbf{f}^{\text{eq}} + A(\mathbf{f} - \mathbf{f}^{\text{eq}}) \quad (2.54)$$

*Applications of this operator decrease the norm of a population function,*

$$\|A\mathbf{f}\| < r\|\mathbf{f}\| \quad 0 \leq r < 1. \quad (2.55)$$

*This assumption is just linear stability of the collision operation.*

**Assumption (2<sub>1</sub>).** *If the local equilibrium  $\mathbf{f}_{\mathfrak{M}}^{\text{eq}}$  exists and is uniformly bounded then so are the derivatives  $\partial_{\mathfrak{M}} \mathbf{f}_{\mathfrak{M}}^{\text{eq}}$ . If the macroscopic moments exist and are bounded then this assumption is guaranteed by a sensible choice of equilibrium.*

**Hypothesis (1).** For a time interval  $t \in [0, T]$ , the distribution  $\mathbf{f}$  and its first space derivatives  $\partial_{\mathbf{x}} \mathbf{f}$  exist and are uniformly bounded. This hypothesis guarantees the macroscopic moments also exist and are bounded hence Assumption 2.8 holds.

**Theorem (Base Case).** For a distribution function  $\mathbf{f}$  with corresponding field of macroscopic moments  $\mathfrak{M} = m(\mathbf{f})$  under Assumptions 1, 2<sub>1</sub> then for the time interval where Hypothesis 1 holds there exists a ball of radius  $\epsilon B^{(1)}$ , where  $B^{(1)}$  is a constant, around the equilibrium. The interior of this ball forms an absorbing set, that is if the norm of the nonequilibrium populations is bigger than this radius, that is  $\|\mathbf{f} - \mathbf{f}_{\mathfrak{M}}^{\text{eq}}\| > \epsilon B^{(1)}$ , then in a time step this norm decreases by a coefficient  $\alpha$  which satisfies the inequality  $r < \alpha < 1$ , where  $\alpha$  does not depend on  $\epsilon$ .

We can say that the condition for first order stability of a lattice Boltzmann method satisfying Assumptions 1, 2 is that Hypothesis 1 holds.

*Proof.* We begin with a distribution function  $\mathbf{f}$  with field of macroscopic moments  $\mathfrak{M} = m(\mathbf{f})$ , which has a non-equilibrium part  $\mathbf{d}^{(1)} = \mathbf{f} - \mathbf{f}_{\mathfrak{M}}^{\text{eq}}$ . We are interested in the size of this deviation following a time step  $\|\mathbf{d}^{(1)'}\| = \|\mathbf{f}' - \text{proj}_0(\mathbf{f}')\|$ .

We take an LBM step of  $\mathbf{f}$ ,

$$\mathbf{f}' = \text{proj}_0(\text{adv}(\mathbf{f})) + A(\text{adv}(\mathbf{f}) - \text{proj}_0(\text{adv}(\mathbf{f}))), \quad (2.56)$$

we would like to calculate the distance from this distribution to its equilibrium projection,

$$\mathbf{d}^{(1)'} = \mathbf{f}' - \text{proj}_0(\text{adv}(\mathbf{f})). \quad (2.57)$$

To bound the norm of this we begin by comparing an LBM step of both  $\mathbf{f}$  and  $\mathbf{f}_{\mathfrak{M}}^{\text{eq}}$ , the step from the equilibrium is given,

$$\mathbf{f}_{\mathfrak{M}}^{\text{eq}'} = \text{proj}_0(\text{adv}(\mathbf{f}_{\mathfrak{M}}^{\text{eq}})) + A(\text{adv}(\mathbf{f}_{\mathfrak{M}}^{\text{eq}}) - \text{proj}_0(\text{adv}(\mathbf{f}_{\mathfrak{M}}^{\text{eq}}))) \quad (2.58)$$

If Hypothesis 1 holds then the difference of these is bounded, ,

$$\begin{aligned}
\|\mathbf{f}' - \mathbf{f}_M^{\text{eq}'}\| &\leq (1+r) \|\text{proj}_0(\text{adv}(\mathbf{f})) - \text{proj}_0(\text{adv}(\mathbf{f}_M^{\text{eq}}))\| \\
&\quad + r \|\text{adv}_1(\mathbf{f}) - \text{adv}_1(\mathbf{f}_M^{\text{eq}})\| + o(\epsilon) \\
&\leq (1+r)\epsilon C_1^{(1)} + r \left( \|\mathbf{d}^{(1)}\| + \epsilon C_2^{(1)} \right)
\end{aligned} \tag{2.59}$$

where  $C_1^{(1)}, C_2^{(1)}$  are some constants based on the magnitude of the derivatives.

We next take the difference between the LBM step of the equilibrium and its projection back onto the equilibrium manifold, by Equation 2.51,

$$\|\mathbf{f}_M^{\text{eq}'} - \text{proj}_0(\text{adv}(\mathbf{f}_M^{\text{eq}}))\| \leq \epsilon C_3^{(1)} \tag{2.60}$$

Finally we re-use the difference between the projections onto the equilibrium manifold of both  $\text{adv}(\mathbf{f})$  and  $\text{adv}(\mathbf{f}_M^{\text{eq}})$ , again under Hypothesis 1 and the Invariance equation this difference is bounded

$$\|\text{proj}_0(\text{adv}(\mathbf{f}_M^{\text{eq}})) - \text{proj}_0(\text{adv}(\mathbf{f}))\| \leq \epsilon C_1^{(1)}. \tag{2.61}$$

Following some rearrangement, using Equations 2.59, 2.60, 2.61 we arrive at,

$$\|\mathbf{d}^{(1)'}\| \leq \left( r \|\mathbf{d}^{(1)}\| + \epsilon(2+r)C_1^{(1)} \right) + r\epsilon C_2^{(1)} + \epsilon C_3^{(1)}. \tag{2.62}$$

We are now interested in the circumstances under which this distance is less than  $\mathbf{d}^{(1)}$ , that is we look for a value  $\alpha < 1$  such that,

$$\left( r \|\mathbf{d}^{(1)}\| + \epsilon(2+r)C_1^{(1)} \right) + r\epsilon C_2^{(1)} + \epsilon C_3^{(1)} < \alpha \|\mathbf{d}^{(1)}\|. \tag{2.63}$$

After some trivial rearrangement,

$$||\mathbf{d}^{(1)}|| > \frac{\epsilon}{\alpha - r} \left( (2 + r)C_1^{(1)} + rC_2^{(1)} + C_3^{(1)} \right). \quad (2.64)$$

Therefore  $\epsilon B^{(1)}$  is given by the right side of Equation 2.64 and we can choose any  $\alpha$  satisfying  $r < \alpha < 1$ .  $\square$

This theorem may be generalized to a statement about conditional stability up to an arbitrary order in  $\epsilon$ , a proof can be built inductively. Some more general assumptions and hypotheses are required.

**Assumption (2<sub>n+1</sub>).** *If the local equilibrium  $\mathbf{f}_{\mathfrak{M}}^{\text{eq}}$  exists and is uniformly bounded then so are the derivatives derivatives  $\partial_{\mathbf{M}_\psi} \mathbf{f}_{\mathfrak{M}}^{\text{eq}}$  where  $|\psi| \leq n + 1$ . If the macroscopic moments exist and are bounded then this assumption is guaranteed by a sensible choice of equilibrium.*

**Hypothesis (1<sub>n+1</sub>).** *For a time interval  $t \in [0, T]$ , the distribution  $\mathbf{f}$  and its space derivatives  $\partial_{\mathbf{x}_\beta} \mathbf{f}$  where  $|\beta| \leq n + 1$  exist and are uniformly bounded. This hypothesis guarantees the macroscopic moments also exist and are bounded hence Assumption 2.8 holds.*

**Theorem (Induction Step).** *If for a distribution function  $\mathbf{f}$  with corresponding field of macroscopic moments  $\mathfrak{M} = m(\mathbf{f})$  there exists a constant  $B^{(n)}$  such that  $||\mathbf{f} - \mathbf{g}_{\mathfrak{M}}^{(n-1)}|| < \epsilon^n B^{(n)}$ , then under Assumption 2<sub>n+1</sub> and where Hypothesis 1<sub>n+1</sub> holds there exists a ball of radius  $\epsilon^{n+1} B^{(n+1)}$  around the jet  $\mathbf{g}_{\mathfrak{M}}^{(n)}$ . The interior of this ball forms an absorbing set, that is if the norm of the nonequilibrium populations is bigger than this radius, that is  $||\mathbf{f} - \mathbf{g}_{\mathfrak{M}}^{(n)}|| > \epsilon^{n+1} B^{(n+1)}$ , then in a time step this norm decreases by a coefficient  $\alpha$  which satisfies the inequality  $r < \alpha < 1$ , where  $\alpha$  does not depend on  $\epsilon$ .*

We can say that the condition for  $n + 1$ th order stability of a lattice Boltzmann method satisfying Assumptions 1,  $2_{n+1}$  is that Hypothesis  $1_{n+1}$  holds.

*Proof.* We begin with a distribution function  $\mathbf{f}$  with corresponding field of macroscopic moments  $\mathfrak{M} = m(\mathbf{f})$ , the distribution function is within a ball of radius  $\epsilon^n B^{(n)}$  around the  $n - 1$  order jet ( $\|\mathbf{f} - \mathbf{g}_{\mathfrak{M}}^{(n-1)}\| < \epsilon^n B^{(n)}$ ).

The distribution function has an error term from the  $n$ th order jet  $\mathbf{d}^{(n+1)} = \mathbf{f} - \mathbf{g}_{\mathfrak{M}}^{(n)}$ . We are interested in the size of this deviation following a time step  $\|\mathbf{d}^{(n+1)'}\| = \|\mathbf{f}' - \text{proj}_n(\mathbf{f}')\|$ .

We again use LBM step of  $\mathbf{f}$  from Equation 2.56, we would like to calculate the distance from this distribution to its projection onto the  $n$ th order jet

$$\mathbf{d}^{(n+1)'} = \mathbf{f}' - \text{proj}_n(\text{adv}(\mathbf{f})). \quad (2.65)$$

To bound the norm of this we compare  $\mathbf{f}'$  with an LBM step of  $\mathbf{g}_{\mathfrak{M}}^{(n)}$ ,

$$\mathbf{g}_{\mathfrak{M}}^{(n)'} = \text{proj}_0 \left( \text{adv} \left( \mathbf{g}_{\mathfrak{M}}^{(n)} \right) \right) + A \left( \text{adv} \left( \mathbf{g}_{\mathfrak{M}}^{(n)} \right) - \text{proj}_0 \left( \text{adv} \left( \mathbf{g}_{\mathfrak{M}}^{(n)} \right) \right) \right) \quad (2.66)$$

If Hypothesis 1 holds then the difference of these is bounded at the  $n + 1$ th order,

$$\begin{aligned} \|\mathbf{f}' - \mathbf{g}_{\mathfrak{M}}^{(n)'}\| &\leq (1 + r) \left\| \text{proj}_0(\text{adv}(\mathbf{f})) - \text{proj}_0 \left( \text{adv} \left( \mathbf{g}_{\mathfrak{M}}^{(n)} \right) \right) \right\| \\ &\quad + r \left\| \text{adv}_1(\mathbf{f}) - \text{adv}_1 \left( \mathbf{g}_{\mathfrak{M}}^{(n)} \right) \right\| + o(\epsilon^{n+1}) \\ &\leq (1 + r) \epsilon^{n+1} C_1^{(n+1)} + r \left( \|\mathbf{d}^{(n+1)}\| + \epsilon^{n+1} C_2^{(n+1)} \right) \end{aligned} \quad (2.67)$$

where  $C_1^{(n+1)}, C_2^{(n+1)}$  are some constants based on the magnitude of the derivatives.

We next take the difference between the LBM step of the equilibrium and its projection back onto the  $n$ th order jet of the manifold, by Equation 2.51 this projection represents the  $n$ th order component of the post LBM step dynamics, so the

remainder is order  $n + 1$ ,

$$\left\| \mathbf{g}_{\mathfrak{M}}^{(n)'} - \text{proj}_n \left( \text{adv} \left( \mathbf{g}_{\mathfrak{M}}^{(n)} \right) \right) \right\| \leq \epsilon^{n+1} C_3^{(n+1)} \quad (2.68)$$

Finally we use the difference between the projections onto the  $n$ th order jet of both  $\text{adv}(\mathbf{f})$  and  $\text{adv}(\mathbf{g}_{\mathfrak{M}}^{(n)})$ , again under Hypothesis 1<sub>1</sub> and the Invariance equation this difference is bounded at the  $n + 1$ th order

$$\left\| \text{proj}_n \left( \text{adv} \left( \mathbf{g}_{\mathfrak{M}}^{(n)} \right) \right) - \text{proj}_n (\text{adv}(\mathbf{f})) \right\| \leq \epsilon C_4^{(n+1)}. \quad (2.69)$$

In the arbitrary order system this is a new constant  $C_4^{(n+1)}$ , in the base case where  $n = 0$  this was not necessary.

Following some rearrangement, using Equations 2.67, 2.68, 2.69 we arrive at,

$$\left\| \mathbf{d}^{(n+1)'} \right\| \leq (1+r)\epsilon^{n+1}C_1^{(n+1)} + r \left( \left\| \mathbf{d}^{(n+1)} \right\| + \epsilon^{n+1}C_2^{(n+1)} \right) + r\epsilon^{n+1}C_3^{(n+1)} + \epsilon^{n+1}C_4^{(n+1)}. \quad (2.70)$$

We are now interested in the circumstances under which this distance is less than  $\mathbf{d}^{(n+1)}$ , that is we look for a value  $\alpha < 1$  such that,

$$(1+r)\epsilon^{n+1}C_1^{(n+1)} + r \left( \left\| \mathbf{d}^{(n+1)} \right\| + \epsilon^{n+1}C_2^{(n+1)} \right) + r\epsilon^{n+1}C_3^{(n+1)} + \epsilon^{n+1}C_4^{(n+1)} < \alpha \left\| \mathbf{d}^{(n+1)} \right\|. \quad (2.71)$$

After some trivial rearrangement,

$$\left\| \mathbf{d}^{(n+1)} \right\| > \frac{\epsilon^{n+1}}{\alpha - r} \left( (1+r)C_1^{(n+1)} + rC_2^{(n+1)} + C_3^{(n+1)} + C_4^{(n+1)} \right). \quad (2.72)$$

Therefore  $\epsilon^{n+1}B^{(n+1)}$  is given by the right side of Equation 2.72. We can choose  $\alpha$  subject to the inequality  $r < \alpha < 1$ .  $\square$

# Chapter 3

## Macroscopic Equations

In this section we are concerned with deriving equations for the macroscopic dynamics arising from several different example lattices. We expect that the lattice parameter  $\epsilon$  should partly govern these dynamics and that the 1st order macroscopic dynamics should be governed by the 1st order population functions.

In order to find these dynamics we project the microscopic flow (advection) up to the required order, following one time step, onto the invariant manifold up to the same order [28, 30].

We can immediately perform a Taylor expansion in time on the macroscopic dynamics,

$$\mathfrak{M}' = \mathfrak{M} + \epsilon \partial_t \mathfrak{M} + o(\epsilon) \quad (3.1)$$

We expect that the final model should be given in terms of a time derivative of the macroscopic moments, we write this in a power series in terms of  $\epsilon$ ,

$$\partial_t \mathfrak{M} = \Psi^{(0)} + \epsilon \Psi^{(1)} + o(\epsilon) \quad (3.2)$$

Combining these two we have

$$\mathfrak{M}' = \mathfrak{M} + \epsilon \Psi^{(0)} + o(\epsilon) \quad (3.3)$$

Equating (2.19) and (3.3) we have

$$\Psi^{(0)} = m \left( -\mathbf{v} \cdot \partial_{\mathbf{x}} \mathfrak{f}_{\mathfrak{M}}^{(0)} \right) \quad (3.4)$$

The corresponding second order approximation of the macroscopic moments in time is

$$\mathfrak{M}' = \mathfrak{M} + \epsilon (\Psi^{(0)} + \epsilon \Psi^{(1)}) + \frac{\epsilon^2}{2} \partial_t \Psi^{(0)} + o(\epsilon^2) \quad (3.5)$$

Equating terms on the second order of  $\epsilon$  we have,

$$m \left( \frac{1}{2} \mathbf{v} \cdot \partial_{\mathbf{x}} \left( \mathbf{v} \cdot \partial_{\mathbf{x}} \mathfrak{f}_{\mathfrak{M}}^{(0)} \right) \right) + m \left( -\mathbf{v} \cdot \partial_{\mathbf{x}} \mathfrak{f}_{\mathfrak{M}}^{(1)} \right) = \Psi^{(1)} + \frac{1}{2} \partial_t \Psi^{(0)} \quad (3.6)$$

or

$$\Psi^{(1)} = m \left( \frac{1}{2} \mathbf{v} \cdot \partial_{\mathbf{x}} \left( \mathbf{v} \cdot \partial_{\mathbf{x}} \mathfrak{f}_{\mathfrak{M}}^{(0)} \right) \right) + m \left( -\mathbf{v} \cdot \partial_{\mathbf{x}} \mathfrak{f}_{\mathfrak{M}}^{(1)} \right) - \frac{1}{2} \partial_t \Psi^{(0)} \quad (3.7)$$

Later we will calculate the final term of this equation by the chain rule, for a system with only one conserved moment this would be written,

$$\partial_t \Psi^{(0)} = (\partial_{\rho} \Psi^{(0)}) (\partial_t \rho). \quad (3.8)$$

To get the dynamics at the proper order we would use the zero order component of the time derivative of  $\rho$ . In the usual Chapman-Enskog analysis of Boltzmann equation this might be signified by explicitly introducing time derivative operators at different orders of  $\epsilon$ . In this work we don't introduce any extra notation and just say that where these time derivatives are given they should be taken to the correct

order of  $\epsilon$ .

The macroscopic dynamics of the continuous velocity, discrete time system could be written in nearly the same format. The vector field  $\mathbf{f}$  would be replaced by a scalar field  $f$  which would also be over the continuous velocity space, the moment operator  $m$  would take a continuous form (integrals rather than the quadrature). In the next two sections we calculate some example, equivalent, discrete and continuous systems, in order to compare them.

### 3.1 Discrete Velocity Examples

We will now demonstrate the exact first order dynamics of a popular choice of lattice scheme in one and two dimensions. The athermal schemes we consider are typically described in shorthand by the dimension within which they operate and the number of velocities used to form the lattice in the form DmQn, where  $m$  and  $n$  are integers representing the number of dimensions and velocities respectively. The general quasi-equilibrium for these systems, including the two examples we use can be written in a general form,

$$f_i^{\text{eq}} = W_i \rho \left( 1 + \frac{\mathbf{v}_i \cdot \mathbf{u}}{c_s^2} + \frac{(\mathbf{v}_i \cdot \mathbf{u})^2}{2c_s^4} - \frac{\mathbf{u}^2}{2c_s^2} \right). \quad (3.9)$$

This equilibrium defines an athermal system where the temperature is fixed. To complete the definition of the discrete system requires only the selection of a velocity set and some accompanying weights  $W_\alpha$ .

#### 3.1.1 An athermal three velocity lattice (D1Q3)

Our 1-D example lattice is one of the most common, the athermal 1-D lattice with 3 velocities. In this example the velocity vectors are  $\{-1, 0, 1\}$  and the speed of sound

$c_s = 1/\sqrt{3}$ . The equilibrium populations are derived from the general formula for athermal quasi-equilibria in any dimension where the additional parameters the weights  $W_i$  are  $\{\frac{1}{6}, \frac{2}{3}, \frac{1}{6}\}$ .

For this case the populations are,

$$\frac{1}{6} \left\{ \rho(1 - 3u + 3u^2), 4\rho \left(1 - \frac{3u^2}{2}\right), \rho(1 + 3u + 3u^2) \right\}. \quad (3.10)$$

For this lattice with unit distances we note that  $v^4 = v^2$ ,  $v^1 = v^3$  etc. We calculate the two components of  $\Psi^{(0)}$  using the formulas for the macroscopic moments. We have for the density derivative,

$$\Psi_1^{(0)} = - \sum_i v_i \partial_x f_i^{(0)} = -\partial_x \sum_i v_i f_i^{(0)} = -\partial_x \rho u, \quad (3.11)$$

and for the momentum derivative

$$\Psi_2^{(0)} = - \sum_i v_i^2 \partial_x f_i^{(0)} = -\partial_x \sum_i v_i^2 f_i^{(0)} = -\partial_x \left( \frac{\rho}{3} + \rho u^2 \right), \quad (3.12)$$

Now we examine the individual macroscopic moments of the first order part in the case of the one dimensional lattice, as before we begin with the density,

$$\Psi_1^{(1)} = \frac{1}{2} \sum_i v_i^2 \partial_{x^2} f_i^{(0)} - \sum_i v_i \partial_x f_i^{(1)} - \frac{1}{2} \partial_t \Psi_1^{(0)}. \quad (3.13)$$

The second term here is the space derivative of the momentum of the  $f_M^{(1)}$  which equals zero due to all macroscopic moments of non equilibrium components being zero and the first term can be calculated immediately from the quasi-equilibrium. Therefore,

$$\Psi_1^{(1)} = \frac{1}{2} \partial_{x^2} \left( \frac{\rho}{3} + \rho u^2 \right) - \frac{1}{2} \partial_t \Psi_1^{(0)}. \quad (3.14)$$

The time derivative of  $\Psi_1^{(0)}$  can be calculated by the chain rule,

$$\partial_t \Psi_1^{(0)} = \left( \partial_\rho \Psi_1^{(0)} \right) (\partial_t \rho) + \left( \partial_{\rho u} \Psi_1^{(0)} \right) (\partial_t \rho u) - \partial_x \Psi_2^{(0)} = \partial_{x^2} \left( \frac{\rho}{3} + \rho u^2 \right) \quad (3.15)$$

Substituting this back in we have,

$$\Psi_1^{(1)} = \frac{1}{2} \partial_{x^2} \left( \frac{\rho}{3} + \frac{(\rho u)^2}{\rho} \right) - \frac{1}{2} \partial_{x^2} \left( \frac{\rho}{3} + \rho u^2 \right) = 0. \quad (3.16)$$

For the momentum moment we have

$$\Psi_2^{(1)} = \frac{1}{2} \sum_i v_i^3 \partial_{x^2} f_i^{(0)} - \sum_i v_i^2 \partial_x f_i^{(1)} - \frac{1}{2} \partial_t \Psi_2^{(0)}. \quad (3.17)$$

Recalling that that  $v^3 = v^1$  we can simplify the first term so,

$$\frac{1}{2} \sum_i v_i^3 \partial_{x^2} f_i^{(0)} = \frac{1}{2} \sum_i v_i \partial_{x^2} f_i^{(0)} = \frac{1}{2} \partial_{x^2} \rho u. \quad (3.18)$$

For the second term we need to calculate the  $f_i^{(1)}$  terms. To do this we need to specify a collision type, we use the BGK collision described above (2.32).

$$\begin{aligned} \frac{\omega}{1-\omega} f_i^{(1)} &= \partial_x \left( 2u \partial_x \rho + (-2 - 3u^2) \partial_x \rho u + 6u \partial_x \rho u^2 \right), \\ &\quad - u \frac{\partial_x}{\rho} + \left( 1 + \frac{3}{2}u^2 \right) \partial_x \rho u - 3u \partial_x \rho u^2, \\ &\quad 2u \partial_x \rho + (-2 - 3u^2) \partial_x \rho u + 6u \partial_x \rho u^2. \end{aligned} \quad (3.19)$$

This gives then

$$\sum_i v_i^2 \partial_x f_i^{(1)} = \frac{1-\omega}{\omega} \partial_x \left( \frac{2}{3}u \partial_x \rho + \left( -\frac{2}{3} - u^2 \right) \partial_x \rho u + 2u \partial_x \rho u^2 \right). \quad (3.20)$$

Again using the chain rule,

$$\begin{aligned}\partial_t \Psi_2^{(0)} &= \left(\partial_\rho \Psi_2^{(0)}\right) (\partial_t \rho) + \left(\partial_{\rho u} \Psi_2^{(0)}\right) (\partial_t \rho u) = -\partial_x \left(\frac{1}{3} - u^2\right) \Psi_1^{(0)} - \partial_x 2u \Psi_2^{(0)} \\ &= \partial_x \left(\frac{2}{3}u \partial_x \rho + \left(\frac{1}{3} - u^2\right) \partial_x \rho u + 2u \partial_x \rho u^2\right).\end{aligned}\quad (3.21)$$

Substituting this all back in we have,

$$\begin{aligned}\Psi_2^{(1)} &= \left(\frac{\omega-1}{\omega} - \frac{1}{2}\right) \partial_x \left(\frac{2}{3}u \partial_x \rho + \left(-\frac{2}{3} - u^2\right) \partial_x \rho u + 2u \partial_x \rho u^2\right) \\ &= \frac{\omega-2}{2\omega} \partial_x \left(\frac{2}{3}u \partial_x \rho + \left(-\frac{2}{3} - u^2\right) \partial_x \rho u + 2u \partial_x \rho u^2\right) \\ &= \frac{\omega-2}{2\omega} \partial_x \left(u^3 \partial_x \rho + \rho \left(3u^2 - \frac{2}{3}\right) \partial_x u\right).\end{aligned}\quad (3.22)$$

The moment gradients are then to first order in  $\epsilon$ ,

$$\begin{aligned}\partial_t \rho &= -\partial_x \rho u \\ \partial_t \rho u &= -\partial_x \left(\frac{1}{3}\rho + \rho u^2\right) - \epsilon \frac{2-\omega}{2\omega} \partial_x \left(u^3 \partial_x \rho + \rho \left(3u^2 - \frac{2}{3}\right) \partial_x u\right)\end{aligned}\quad (3.23)$$

### 3.1.2 An athermal five velocity lattice (D1Q5)

To increase the speed of sound more velocities can be added, we consider using the velocity set  $(-2, -1, 0, 1, 2)$  and corresponding weights  $(\frac{1}{12}, \frac{2}{12}, \frac{6}{12}, \frac{2}{12}, \frac{1}{12})$  giving equilibrium populations

$$\frac{1}{12} \left\{ \rho \left(1 - 2u + \frac{3u^2}{2}\right), 2\rho(1-u), 6\rho \left(1 - \frac{u^2}{2}\right), 2\rho(1+u), \rho \left(1 + 2u + \frac{3u^2}{2}\right) \right\}\quad (3.24)$$

On this lattice the speed of sound is  $c_s = 1$ . The first order density moment remain the same as the three velocity 1-D lattice, the momentum density term is very

similar,

$$\Psi_2^{(0)} = - \sum_i v_i^2 \partial_{\mathbf{x}} \mathfrak{f}_i^{(0)} = -\partial_{\mathbf{x}} \sum_i v_i^2 \mathfrak{f}_i^{(0)} = -\partial_{\mathbf{x}} (\rho + \rho u^2), \quad (3.25)$$

In the case of the second order macroscopic moments the density moment is again 0 by exactly the same argument, for the momentum density we have

$$\Psi_2^{(1)} = \frac{1}{2} \sum_i v_i^3 \partial_{x^2} \mathfrak{f}_i^{(0)} - \sum_i v_i \partial_x \mathfrak{f}_i^{(1)} - \frac{1}{2} \partial_t \Psi_2^{(0)} \quad (3.26)$$

For the first term we have

$$\sum_i v_i^3 \partial_{x^2} \mathfrak{f}_i^{(0)} = 3\partial_{x^2} \rho u \quad (3.27)$$

For the second term we calculate the first order populations

$$\begin{aligned} \frac{\omega}{1-\omega} \mathfrak{f}_i^{(1)} &= \partial_x \left( 3u\partial_x \rho + \left( -3 - \frac{3}{2}u^2 \right) \partial_x \rho u + (1+3u)\partial_x \rho u^2, -2\partial_x \rho u^2 \right. \\ &\quad \left. - u\partial_x \rho + \left( 1 + \frac{1}{2}u^2 \right) \partial_x \rho u - u\partial_x \rho u^2, 2\partial_x \rho u^2, \right. \\ &\quad \left. 3u\partial_x \rho + \left( -3 - \frac{3}{2}u^2 \right) \partial_x \rho u + (-1+3u)\partial_x \rho u^2 \right) \end{aligned} \quad (3.28)$$

and thereby the term

$$\sum_i v_i^2 \partial_x \mathfrak{f}_i^{(1)} = \frac{1-\omega}{\omega} \partial_x (2u\partial_x \rho + (-2-u^2)\partial_x \rho u + 2u\partial_x \rho u^2) \quad (3.29)$$

Again using the chain rule,

$$\begin{aligned} \partial_t \Psi_2^{(0)} &= \left( \partial_\rho \Psi_2^{(0)} \right) (\partial_t \rho) + \left( \partial_{\rho u} \Psi_2^{(0)} \right) (\partial_t \rho u) = -\partial_x (1-u^2) \Psi_1^{(0)} - \partial_x 2u \Psi_2^{(0)} \\ &= \partial_x (2u\partial_x \rho + (1-u^2)\partial_x \rho u + 2u\partial_x \rho u^2) \end{aligned} \quad (3.30)$$

Substituting this back in we have,

$$\begin{aligned}
\Psi_2^{(1)} &= \left( \frac{\omega - 1}{\omega} - \frac{1}{2} \right) \partial_x (2u\partial_x\rho + (1 - u^2)\partial_x\rho u + 2u\partial_x\rho u^2) \\
&= \frac{\omega - 2}{2\omega} \partial_x (2u\partial_x\rho + (-2 - u^2)\partial_x\rho u + 2u\partial_x\rho u^2) \\
&= \frac{\omega - 2}{2\omega} \partial_x (u^3\partial_x\rho + \rho(3u^2 - 2)\partial_x u). \quad (3.31)
\end{aligned}$$

For the 5 velocity lattice we have then the moment gradients

$$\begin{aligned}
\partial_t\rho &= -\partial_x\rho u + o(\epsilon) \\
\partial_t\rho u &= -\partial_x(\rho + \rho u^2) - \epsilon \frac{2 - \omega}{2\omega} \partial_x(u^3\partial_x\rho + \rho(3u^2 - 2)\partial_x u) + o(\epsilon) \quad (3.32)
\end{aligned}$$

### 3.1.3 An athermal nine velocity model (D2Q9)

The 2-D example we consider is a popular 2d lattice consisting of 9 different velocities. If we identify  $v_1$  as the horizontal component of a vector and  $v_2$  the vertical component then the set of velocities is

$$\begin{aligned}
v_1 &= (0, 1, 0, -1, 0, 1, -1, -1, 1) \\
v_2 &= (0, 0, 1, 0, -1, 1, 1, -1, -1). \quad (3.33)
\end{aligned}$$

The equilibrium is then given by the polynomial formula (3.9) with corresponding weights

$$w_i = \left\{ \frac{4}{9}, \frac{1}{9}, \frac{1}{9}, \frac{1}{9}, \frac{1}{9}, \frac{1}{36}, \frac{1}{36}, \frac{1}{36}, \frac{1}{36} \right\} \quad (3.34)$$

As before we calculate the components of  $\Psi^{(0)}$  using the formulas for the macroscopic moments although this time we have two momentum density momentums for

the two dimensions. We have for the density derivative,

$$\begin{aligned}
\Psi_1^{(0)} &= \sum_i \left( -\mathbf{v}_i \cdot \partial_{\mathbf{x}} \mathbf{f}_i^{(0)} \right) \\
&= -\partial_{x_1} \sum_i v_{i,1} \mathbf{f}_i^{(0)} - \partial_{x_2} \sum_i v_{i,2} \mathbf{f}_i^{(0)} \\
&= -\partial_{x_1} \rho u_1 - \partial_{x_2} \rho u_2,
\end{aligned} \tag{3.35}$$

for the first momentum derivative

$$\begin{aligned}
\Psi_2^{(0)} &= \sum_i v_{i,1} \left( -\mathbf{v}_i \cdot \partial_{\mathbf{x}} \mathbf{f}_i^{(0)} \right) \\
&= -\partial_{x_1} \sum_i v_{i,1}^2 \mathbf{f}_i^{(0)} - \partial_{x_2} \sum_i v_{i,1} v_{i,2} \mathbf{f}_i^{(0)} \\
&= -\partial_{x_1} \left( \frac{1}{3} \rho + \rho u_1^2 \right) - \partial_{x_2} \rho u_1 u_2,
\end{aligned} \tag{3.36}$$

and for the second momentum derivative

$$\begin{aligned}
\Psi_3^{(0)} &= \sum_i v_{i,2} \left( -\mathbf{v}_i \cdot \partial_{\mathbf{x}} \mathbf{f}_i^{(0)} \right) \\
&= -\partial_{x_1} \sum_i v_{i,1} v_{i,2} \mathbf{f}_i^{(0)} - \partial_{x_2} \sum_i v_{i,2}^2 \mathbf{f}_i^{(0)} \\
&= -\partial_{x_1} \rho u_1 u_2 - \partial_{x_2} \left( \frac{1}{3} \rho + \rho u_2^2 \right).
\end{aligned} \tag{3.37}$$

The first order density moment is given by,

$$\Psi_1^{(1)} = \frac{1}{2} \sum_i \left( \mathbf{v}_i \cdot \partial_{\mathbf{x}} \left( \mathbf{v}_i \cdot \partial_{\mathbf{x}} \mathbf{f}_i^{(0)} \right) \right) + \sum_i \left( -\mathbf{v}_i \cdot \partial_{\mathbf{x}} \mathbf{f}_i^{(1)} \right) - \frac{1}{2} \partial_t \Psi_1^{(0)}. \tag{3.38}$$

Again we observe that the second term is the space gradient multiplied with the momentum densities of the first order populations and hence is zero, for the first

term we have

$$\begin{aligned}
& \sum_i \left( \mathbf{v}_i \cdot \partial_{\mathbf{x}} \left( \mathbf{v}_i \cdot \partial_{\mathbf{x}} \mathfrak{f}_i^{(0)} \right) \right) \\
&= \sum_i \left( \partial_{x_1^2} v_{i,1}^2 \mathfrak{f}_i^{(0)} + 2\partial_{x_1 x_2} v_{i,1} v_{i,2} \mathfrak{f}_i^{(0)} + \partial_{x_2^2} v_{i,2}^2 \mathfrak{f}_i^{(0)} \right) \\
&= \partial_{x_1^2} \left( \frac{1}{3} \rho + \rho u_1^2 \right) + 2\partial_{x_1 x_2} \rho u_1 u_2 + \partial_{x_2^2} \left( \frac{1}{3} \rho + \rho u_2^2 \right), \quad (3.39)
\end{aligned}$$

and for the third term

$$\begin{aligned}
\partial_t \Psi_1^{(0)} &= \left( \partial_\rho \Psi_1^{(0)} \right) (\partial_t \rho) + \left( \partial_{\rho u_1} \Psi_1^{(0)} \right) (\partial_t \rho u_1) + \left( \partial_{\rho u_2} \Psi_1^{(0)} \right) (\partial_t \rho u_2) = -\partial_{x_1} \Psi_2^{(0)} - \partial_{x_2} \Psi_3^{(0)} \\
&= -\partial_{x_1} \left( -\partial_{x_1} \left( \frac{1}{3} \rho + \rho u_1^2 \right) - \partial_{x_2} \rho u_1 u_2 \right) \\
&\quad - \partial_{x_2} \left( -\partial_{x_1} \rho u_1 u_2 - \partial_{x_2} \left( \frac{1}{3} \rho + \rho u_2^2 \right) \right). \quad (3.40)
\end{aligned}$$

hence subtracting these we have  $\Psi_1^{(1)} = 0$ .

For the first second order momentum density we have

$$\Psi_2^{(1)} = \frac{1}{2} \sum_i v_{i,1} \left( \mathbf{v}_i \cdot \partial_{\mathbf{x}} \left( \mathbf{v}_i \cdot \partial_{\mathbf{x}} \mathfrak{f}_i^{(0)} \right) \right) + \sum_i v_{i,1} \left( -\mathbf{v}_i \cdot \partial_{\mathbf{x}} \mathfrak{f}_i^{(1)} \right) - \frac{1}{2} \partial_t \Psi_2^{(0)}. \quad (3.41)$$

Examining each term in turn more closely we have for the first term

$$\begin{aligned}
& \sum_i v_{i,1} \left( \mathbf{v}_i \cdot \partial_{\mathbf{x}} \left( \mathbf{v}_i \cdot \partial_{\mathbf{x}} \mathfrak{f}_i^{(0)} \right) \right) \\
&= \sum_i v_{i,1} \left( \partial_{x_1^2} v_{i,1}^2 \mathfrak{f}_i^{(0)} + 2\partial_{x_1 x_2} v_{i,1} v_{i,2} \mathfrak{f}_i^{(0)} + \partial_{x_2^2} (v_{i,2})^2 \mathfrak{f}_i^{(0)} \right) \\
&= \partial_{x_1} \left( \rho \partial_{x_1} u_1 + u_1 \partial_{x_1} \rho + \frac{1}{3} \rho \partial_{x_2} u_2 + \frac{1}{3} u_2 \partial_{x_2} \rho \right) \\
&\quad + \partial_{x_2} \left( \frac{1}{3} \rho \partial_{x_1} u_2 + \frac{1}{3} u_2 \partial_{x_1} \rho + \frac{1}{3} \rho \partial_{x_2} u_1 + \frac{1}{3} u_1 \partial_{x_2} \rho \right). \quad (3.42)
\end{aligned}$$

The first order populations are given in Appendix A, these give us for the second

term

$$\begin{aligned}
& \sum_i v_{i,1} \left( -\mathbf{v}_i \cdot \partial_{\mathbf{x}} \mathfrak{f}_i^{(1)} \right) = - \sum_i v_{i,1} \left( \partial_{x_1} v_{i,1} \mathfrak{f}_i^{(1)} + \partial_{x_2} v_{i,2} \mathfrak{f}_i^{(1)} \right) \\
&= \frac{\omega - 1}{\omega} \left( \partial_{x_1} \left( u_1^3 \partial_{x_1} \rho + u_1^2 u_2 \partial_{x_2} \rho + \left( 3\rho u_1^2 - \frac{2}{3}\rho \right) \partial_{x_1} u_1 \right. \right. \\
&\quad \left. \left. + 2\rho u_1 u_2 \partial_{x_2} u_1 + \rho u_1^2 \partial_{x_2} u_2 \right) \right. \\
&\quad \left. + \partial_{x_2} \left( u_1^2 u_2 \partial_{x_1} \rho + u_1 u_2^2 \partial_{x_2} \rho + 2\rho u_1 u_2 \partial_{x_1} u_1 + 2\rho u_1 u_2 \partial_{x_2} u_2 \right. \right. \\
&\quad \left. \left. + \left( \rho u_2^2 - \frac{1}{3}\rho \right) \partial_{x_2} u_1 + \left( \rho u_1^2 - \frac{1}{3}\rho \right) \partial_{x_1} u_2 \right) \right). \tag{3.43}
\end{aligned}$$

and for the third term

$$\begin{aligned}
\partial_t \Psi_2^{(0)} &= \left( \partial_\rho \Psi_2^{(0)} \right) (\partial_t \rho) + \left( \partial_{\rho u_1} \Psi_2^{(0)} \right) (\partial_t \rho u_1) + \left( \partial_{\rho u_2} \Psi_2^{(0)} \right) (\partial_t \rho u_2) \\
&= \left( \frac{\partial}{\partial x_1} \left( -\frac{1}{3}u^2 + u_1^2 \right) + \partial_{x_2} u_1 u_2 \right) \Psi_1^{(0)} \\
&\quad + (-2\partial_{x_1} u_1 - \partial_{x_2} u_2) \Psi_2^{(0)} - \partial_{x_2} u_1 \Psi_3^{(0)} \\
&= \partial_{x_1} \left( (u_1 + u_1^3) \partial_{x_1} \rho + \left( \frac{1}{3}u_2 + u_1^2 u_2 \right) \partial_{x_2} \rho \right. \tag{3.44} \\
&\quad \left. + \left( \frac{1}{3}\rho + 3\rho u_1^2 \right) \partial_{x_1} u_1 + \left( \frac{1}{3}\rho + \rho u_1^2 \right) \partial_{x_2} u_2 + 2\rho u_1 u_2 \partial_{x_2} u_1 \right) \\
&\quad + \partial_{x_2} \left( \left( \frac{1}{3}u_2 + u_1^2 u_2 \right) \partial_{x_1} \rho + \left( \frac{1}{3}u_1 + u_1 u_2^2 \right) \partial_{x_2} \rho \right. \\
&\quad \left. + 2\rho u_1 u_2 \partial_{x_1} u_1 + \rho u_2^2 \partial_{x_2} u_1 + \rho u_1^2 \partial_{x_1} u_2 + 2\rho u_1 u_2 \partial_{x_2} u_2 \right).
\end{aligned}$$

Combining all three terms we have,

$$\begin{aligned}
\Psi_2^{(1)} &= \left( \frac{\omega - 1}{\omega} - \frac{1}{2} \right) \left( \partial_{x_1} \left( u_1^3 \partial_{x_1} \rho + u_1^2 u_2 \partial_{x_2} \rho + \left( 3\rho u_1^2 - \frac{2}{3}\rho \right) \partial_{x_1} u_1 \right. \right. \\
&\quad \left. \left. + 2\rho u_1 u_2 \partial_{x_2} u_1 + \rho u_1^2 \partial_{x_2} u_2 \right) \right. \\
&\quad \left. + \partial_{x_2} \left( u_1^2 u_2 \partial_{x_1} \rho + u_1 u_2^2 \partial_{x_2} \rho + 2\rho u_1 u_2 \partial_{x_1} u_1 + 2\rho u_1 u_2 \partial_{x_2} u_2 \right. \right. \\
&\quad \left. \left. + \left( \rho u_2^2 - \frac{1}{3}\rho \right) \partial_{x_2} u_1 + \left( \rho u_1^2 - \frac{1}{3}\rho \right) \partial_{x_1} u_2 \right) \right). \tag{3.45}
\end{aligned}$$

The final macroscopic equations for this particular lattice and quasiequilibrium then

are to first order

$$\begin{aligned}
\partial_t \rho &= -\partial_{\mathbf{x}} \rho \mathbf{u} \\
\partial_t \rho u_1 &= -\partial_{x_1} \left( \frac{\rho}{3} + \rho u_1^2 \right) - \partial_{x_2} \rho u_1 u_2 \\
&\quad - \epsilon \frac{2-\omega}{2\omega} \left( \partial_{x_1} \left( u_1^3 \partial_{x_1} \rho + u_1^2 u_2 \partial_{x_2} \rho + \left( 3\rho u_1^2 - \frac{2}{3}\rho \right) \partial_{x_1} u_1 \right. \right. \\
&\quad \left. \left. + 2\rho u_1 u_2 \partial_{x_2} u_1 + \rho u_1^2 \partial_{x_2} u_2 \right) \right. \\
&\quad \left. + \partial_{x_2} \left( u_1^2 u_2 \partial_{x_1} \rho + u_1 u_2^2 \partial_{x_2} \rho + 2\rho u_1 u_2 \partial_{x_1} u_1 + 2\rho u_1 u_2 \partial_{x_2} u_2 \right. \right. \\
&\quad \left. \left. + \left( \rho u_2^2 - \frac{1}{3}\rho \right) \partial_{x_2} u_1 + \left( \rho u_1^2 - \frac{1}{3}\rho \right) \partial_{x_1} u_2 \right) \right)
\end{aligned} \tag{3.46}$$

The second momentum density is available easily through symmetry. With some care this can be rearranged to a more readable form

$$\begin{aligned}
\partial_t \rho &= -\partial_{\mathbf{x}} \rho \mathbf{u} \\
\partial_t \rho u_1 &= -\partial_{x_1} \left( \frac{\rho}{3} + \rho u_1^2 \right) - \partial_{x_2} \rho u_1 u_2 \\
&\quad + \epsilon \left( \frac{2-\omega}{2\omega} \right) \left( \partial_{x_1} \left( \frac{2}{3}\rho \partial_{x_1} u_1 - \partial_{\mathbf{x}} \rho u_1^2 \mathbf{u} \right) + \partial_{x_2} \left( \frac{1}{3}\rho (\partial_{x_1} u_2 + \partial_{x_2} u_1) - \partial_{\mathbf{x}} \rho u_1 u_2 \mathbf{u} \right) \right).
\end{aligned} \tag{3.47}$$

Evidently the errors are third order in the Mach number as the expansion of the Maxwellian was taken to second order.

## 3.2 Continuous Velocity Examples

In this section the macroscopic moments approximated by the LBM chain in a continuous velocity system are calculated. We select two examples, chosen to match the previous discrete velocity schemes. The methodology is exactly the same as in the discrete velocity system with the calculation of the macroscopic moments replaced by the integral and the vector field of distributions replaced by a scalar

field over the continuous velocity space.

### 3.2.1 The athermal 1-D model

The first continuous velocity model we will examine is one chosen to match the zero order dynamics of the discrete model studied in section 3.1.1, the one dimensional system with the three discrete velocities  $\{-1, 0, 1\}$ . The continuous population function acting as the quasi-equilibrium is a specific case of the Maxwell distribution where the temperature is fixed, in this case to  $1/3$ .

$$f^{(0)} = \rho \sqrt{\frac{3}{2\pi}} \exp\left(-\frac{3}{2}(v-u)^2\right) \quad (3.48)$$

With such a system the macroscopic variables are calculated as integrals rather than the sums in the discrete case.

$$\begin{aligned} \int_{-\infty}^{\infty} f^{(0)} dv &= \rho \\ \int_{-\infty}^{\infty} v f^{(0)} dv &= \rho u \\ \int_{-\infty}^{\infty} v^2 f^{(0)} dv &= \frac{1}{3}\rho + \rho u^2 \end{aligned} \quad (3.49)$$

Clearly this matches the macroscopic moments retrieved in the discrete velocity case. Due to this we can, analogously to the discrete case, immediately write down the zero order macroscopic dynamics following equation 3.4.

$$\Psi_0^{(1)} = - \int_{-\infty}^{\infty} v (\partial_x f^{(0)}) dv = -\partial_x \int_{-\infty}^{\infty} v f^{(0)} dv = -\partial_x \rho u \quad (3.50)$$

$$\Psi_0^{(2)} = - \int_{-\infty}^{\infty} v^2 (\partial_x f^{(0)}) dv = -\partial_x \int_{-\infty}^{\infty} v^2 f^{(0)} dv = -\partial_x \left(\frac{1}{3}\rho + \rho u^2\right) \quad (3.51)$$

In order to calculate the first order macroscopic moments we expect that we shall require the first order continuous populations. These are also derived exactly as in

the discrete case with the replacement of the sum, by the integral, in the calculation of the macroscopic moments. Since we replicate the discrete case the collision we select is again the BGK collision and we derive the first order populations from equation 2.32.

$$\frac{\omega}{1-\omega} f^{(1)} = \rho \sqrt{\frac{3}{2\pi}} \exp\left(-\frac{3}{2}(v-u)^2\right) \cdot (1 - 3v^2 + 6vu - 3u^2) \cdot (\partial_x u) \quad (3.52)$$

Again we calculate the first order macroscopic moments from the template given by equation 3.7

$$\Psi_1^{(1)} = \frac{1}{2} \int_{\infty}^{\infty} v^2 (\partial_{x^2} f^{(0)}) dv - \int_{\infty}^{\infty} v (\partial_x f^{(1)}) dv - \frac{1}{2} \partial_t \Psi_1^{(0)} \quad (3.53)$$

Exactly as the discrete case the second term here is the space derivative of the momentum of the  $f^{(1)}$  which equals zero due to all macroscopic moments of non equilibrium components being zero and the first term can be calculated immediately from the quasi-equilibrium therefore,

$$\Psi_1^{(1)} = \frac{1}{2} \partial_{x^2} \left( \frac{\rho}{3} + \rho u^2 \right) - \frac{1}{2} \partial_t \Psi_1^{(0)}. \quad (3.54)$$

Again the time derivative of  $\Psi^{(0)}$  can be calculated by the chain rule,

$$\partial_t \Psi_1^{(0)} = \left( \partial_{\rho} \Psi_1^{(0)} \right) (\partial_t \rho) + \left( \partial_{\rho u} \Psi_1^{(0)} \right) (\partial_t \rho u) = -\partial_x \Psi_2^{(0)} = \partial_{x^2} \left( \frac{\rho}{3} + \rho u^2 \right) \quad (3.55)$$

Substituting we have,

$$\Psi_1^{(1)} = \frac{1}{2} \partial_{x^2} \left( \frac{\rho}{3} + \rho u^2 \right) - \frac{1}{2} \partial_{x^2} \left( \frac{\rho}{3} + \rho u^2 \right) = 0. \quad (3.56)$$

For the continuous velocity momentum moment we have

$$\Psi_2^{(1)} = \frac{1}{2} \int_{\infty}^{\infty} v^3 (\partial_{x^2} f^{(0)}) dv - \int_{\infty}^{\infty} v^2 (\partial_x f^{(1)}) dv - \frac{1}{2} \partial_t \Psi_2^{(0)} \quad (3.57)$$

Rearranging and performing the first two integrals gives us

$$\Psi_2^{(1)} = \frac{1}{2} \partial_{x^2} (\rho u + \rho u^3) - \partial_x \left( -\frac{2}{3} \rho (\partial_x u) \right) - \frac{1}{2} \partial_t \Psi_2^{(0)} \quad (3.58)$$

Again using the chain rule, this term is exactly as in the discrete case,

$$\begin{aligned} \partial_t \Psi_2^{(0)} (\partial_{\rho} \partial \Psi_2^{(0)}) (\partial_t \rho) + (\partial_{\rho u} \Psi_2^{(0)}) (\partial_t \rho u) &= -\partial_x \left( \frac{1}{3} - u^2 \right) \Psi_1^{(0)} - \partial_x 2u \Psi_2^{(0)} \\ &= \partial_x \left( \frac{2}{3} u \partial_x \rho + \left( \frac{1}{3} - u^2 \right) \partial_x \rho u + 2u \partial_x \rho u^2 \right) \end{aligned} \quad (3.59)$$

Substituting this all back in we have,

$$\Psi_2^{(1)} = \left( \frac{\omega - 1}{\omega} - \frac{1}{2} \right) \partial_x \left( -\frac{2}{3} \rho \partial_x u \right) = \frac{\omega - 2}{2\omega} \partial_x \left( -\frac{2}{3} \rho \partial_x u \right). \quad (3.60)$$

The moment gradients are then, for the continuous velocity system, to first order in  $\epsilon$ ,

$$\begin{aligned} \partial_t \rho &= -\partial_x \rho u + o(\epsilon) \\ \partial_t \rho u &= -\partial_x \left( \frac{1}{3} \rho + \rho u^2 \right) - \epsilon \frac{2 - \omega}{2\omega} \partial_x \left( -\frac{2}{3} \rho \partial_x u \right) + o(\epsilon) \end{aligned} \quad (3.61)$$

We immediately observe that several of the dissipative terms that appeared in the discrete velocity system do not occur when we use continuous velocities

### 3.2.2 The athermal 2D model

The next continuous velocity model we examine is the widely used athermal 2d model. Again we use a specific choice of the Maxwellian distribution which matches the zero order macroscopic moments given by the discrete velocity set.

$$f^{(0)} = \rho \frac{3}{2\pi} \exp\left(-\frac{3}{2}(\mathbf{v} - \mathbf{u})^2\right) \quad (3.62)$$

Again macroscopic variables are calculated by integrals over velocity space

$$\begin{aligned} \int_{\mathbb{R}^2} f^{(0)} d\mathbf{v} &= \rho \\ \int_{\mathbb{R}^2} v_1 f^{(0)} d\mathbf{v} &= \rho u_1 \\ \int_{\mathbb{R}^2} v_2 f^{(0)} d\mathbf{v} &= \rho u_2 \\ \int_{\mathbb{R}^2} \mathbf{v}^2 f^{(0)} d\mathbf{v} &= \frac{2}{3}\rho + \rho \mathbf{u}^2 \end{aligned} \quad (3.63)$$

Again we calculate the zero order macroscopic moments,

$$\begin{aligned} \Psi_1^{(0)} &= \int_{\mathbb{R}^2} -\mathbf{v} \cdot \partial_{\mathbf{x}} f^{(0)} d\mathbf{v} \\ &= -\partial_{x_1} \int_{\mathbb{R}^2} v_1 f^{(0)} d\mathbf{v} - \partial_{x_2} \int_{\mathbb{R}^2} v_2 f^{(0)} d\mathbf{v} \\ &= -\partial_{x_1} \rho u_1 - \partial_{x_2} \rho u_2 \end{aligned} \quad (3.64)$$

and for the first momentum derivative

$$\begin{aligned} \Psi_2^{(0)} &= \int_{\mathbb{R}^2} v_1 (-\mathbf{v} \cdot \partial_{\mathbf{x}} f^{(0)}) d\mathbf{v} \\ &= -\partial_{x_1} \int_{\mathbb{R}^2} v_1^2 f^{(0)} d\mathbf{v} - \partial_{x_2} \int_{\mathbb{R}^2} v_1 v_2 f^{(0)} d\mathbf{v} \\ &= -\partial_{x_1} \left( \frac{1}{3}\rho + \rho u_1^2 \right) - \partial_{x_2} \rho u_1 u_2 \end{aligned} \quad (3.65)$$

for the second momentum derivative

$$\begin{aligned}
\Psi_3^{(0)} &= \int_{\mathbb{R}^2} v_2 (-\mathbf{v} \cdot \partial_{\mathbf{x}} f^{(0)}) d\mathbf{v} \\
&= -\partial_{x_1} \int_{\mathbb{R}^2} v_1 v_2 f^{(0)} d\mathbf{v} - \partial_{x_2} \int_{\mathbb{R}^2} v_2^2 f^{(0)} d\mathbf{v} \\
&= -\partial_{x_1} \rho u_1 u_2 - \partial_{x_2} \left( \frac{1}{3} \rho + \rho u_2^2 \right)
\end{aligned} \tag{3.66}$$

We again calculate the first order populations following equation 2.32.

$$\begin{aligned}
\frac{\omega}{1-\omega} f^{(1)} &= \\
\rho \frac{3}{2\pi} \exp \left( -\frac{3}{2} ((v_1 - u_1)^2 + (v_2 - u_2)^2) \right) &\cdot ((1 - 3v_1^2 + 6v_1 u_1 - 3u_1^2) \partial_{x_1} u_1 \\
+ (-3v_1 v_2 + 3v_1 u_2 + 3v_2 u_1 - 3u_1 u_2) \partial_{x_2} u_1 \\
+ (-3v_1 v_2 + 3v_1 u_2 + 3v_2 u_1 - 3u_1 u_2) \partial_{x_1} u_2 \\
+ (1 - 3v_2^2 + 6v_2 u_2 - 3u_2^2) \partial_{x_2} u_2)
\end{aligned} \tag{3.67}$$

The first order density moment is given by,

$$\Psi_1^{(1)} = \frac{1}{2} \int_{\mathbb{R}^2} \mathbf{v} \cdot \partial_{\mathbf{x}} (\mathbf{v} \cdot \partial_{\mathbf{x}} f^{(0)}) d\mathbf{v} - \int_{\mathbb{R}^2} \mathbf{v} \cdot \partial_{\mathbf{x}} f^{(1)} d\mathbf{v} - \frac{1}{2} \partial_t \Psi_1^{(0)} \tag{3.68}$$

Performing the integrals of the first two terms we note that the second term is again zero therefore

$$\Psi_1^{(1)} = \frac{1}{2} \partial_{x_1^2} \left( \frac{1}{3} \rho + \rho u_1^2 \right) + \partial_{x_1 x_2} \rho u_1 u_2 + \frac{1}{2} \partial_{x_2^2} \left( \frac{1}{3} \rho + \rho u_2^2 \right) - \frac{1}{2} \partial_t \Psi_1^{(0)} \tag{3.69}$$

and exactly as in the discrete velocity system we have for the third term

$$\begin{aligned}
\partial_t \Psi_1^{(0)} &= \left( \partial_\rho \Psi_1^{(0)} \right) (\partial_t \rho) + \left( \partial_{\rho u_1} \Psi_1^{(0)} \right) (\partial_t \rho u_1) + \left( \partial_{\rho u_2} \Psi_1^{(0)} \right) (\partial_t \rho u_2) \\
&= -\partial_{x_1} \Psi_2^{(0)} - \partial_{x_2} \Psi_3^{(0)} \\
&= -\partial_{x_1} \left( -\partial_{x_1} \left( \frac{1}{3} \rho + \rho u_1^2 \right) - \partial_{x_2} \rho u_1 u_2 \right) \\
&\quad - \partial_{x_2} \left( -\partial_{x_1} \rho u_1 u_2 - \partial_{x_2} \left( \frac{1}{3} \rho + \rho u_2^2 \right) \right)
\end{aligned} \tag{3.70}$$

hence subtracting these we have  $\Psi_1^{(1)} = 0$ .

For the first second order momentum density we have

$$\Psi_2^{(1)} = \frac{1}{2} \int_{\mathbb{R}^2} v_1 \left( \mathbf{v} \cdot \partial_{\mathbf{x}} (\mathbf{v} \cdot \partial_{\mathbf{x}} \mathbf{f}^{(0)}) \right) d\mathbf{v} + \int_{\mathbb{R}^2} v_1 \left( -\mathbf{v} \cdot \partial_{\mathbf{x}} \mathbf{f}^{(1)} \right) d\mathbf{v} - \frac{1}{2} \partial_t \Psi_2^{(0)} \tag{3.71}$$

Again performing the integrations from the first two terms we have

$$\begin{aligned}
\Psi_2^{(1)} &= \frac{1}{2} \left( \partial_{x_1^2} (\rho u_1^3 + \rho u_1) + \partial_{x_1 x_2} \left( \frac{1}{3} \rho u_2 + \rho u_1^2 u_2 \right) \right. \\
&\quad \left. + \frac{\partial^2}{\partial x_2^2} \left( \frac{1}{3} \rho u_1 + \rho u_1 u_2^2 \right) \right) \\
&\quad + \frac{\omega - 1}{2\omega} \left( \partial_{x_1} \left( -\frac{2}{3} \rho \partial_{x_1} u_1 \right) \right. \\
&\quad \left. - \partial_{x_2} \left( -\frac{1}{3} \rho (\partial_{x_1} u_2 + \partial_{x_2} u_1) \right) \right) - \frac{1}{2} \partial_t \Psi_2^{(0)}
\end{aligned} \tag{3.72}$$

and for the third term

$$\begin{aligned}
\partial_t \Psi_2^{(0)} &= \left( \partial_\rho \Psi_2^{(0)} \right) (\partial_t \rho) + \left( \partial_{\rho u_1} \Psi_2^{(0)} \right) (\partial_t \rho u_1) + \left( \partial_{\rho u_2} \Psi_2^{(0)} \right) (\partial_t \rho u_2) \\
&= \left( \frac{\partial}{\partial x_1} \left( -\frac{1}{3} u^2 + u_1^2 \right) + \partial_{x_2} u_1 u_2 \right) \Psi_1^{(0)} \\
&\quad + (-2\partial_{x_1} u_1 - \partial_{x_2} u_2) \Psi_2^{(0)} - \partial_{x_2} u_1 \Psi_3^{(0)} \\
&= \partial_{x_1} \left( (u_1 + u_1^3) \partial_{x_1} \rho + \left( \frac{1}{3} u_2 + u_1^2 u_2 \right) \partial_{x_2} \rho \right. \\
&\quad \left. + \left( \frac{1}{3} \rho + 3\rho u_1^2 \right) \partial_{x_1} u_1 + \left( \frac{1}{3} \rho + \rho u_1^2 \right) \partial_{x_2} u_2 + 2\rho u_1 u_2 \partial_{x_2} u_1 \right) \\
&\quad + \partial_{x_2} \left( \left( \frac{1}{3} u_2 + u_1^2 u_2 \right) \partial_{x_1} \rho + \left( \frac{1}{3} u_1 + u_1 u_2^2 \right) \partial_{x_2} \rho + 2\rho u_1 u_2 \partial_{x_1} u_1 \right. \\
&\quad \left. + \rho u_2^2 \partial_{x_2} u_1 + \rho u_1^2 \partial_{x_1} u_2 + 2\rho u_1 u_2 \partial_{x_2} u_2 \right)
\end{aligned} \tag{3.73}$$

Combining all three terms we have

$$\begin{aligned}
\Psi_2^{(1)} &= \left( \frac{\omega - 1}{\omega} - \frac{1}{2} \right) \left( \partial_{x_1} \left( -\frac{2}{3} \rho \partial_{x_1} u_1 \right) \right. \\
&\quad \left. - \partial_{x_2} \left( -\frac{1}{3} \rho (\partial_{x_1} u_2 + \partial_{x_2} u_1) \right) \right)
\end{aligned} \tag{3.74}$$

The final macroscopic equations for this particular lattice and quasiequilibrium then are

$$\begin{aligned}
\partial_t \rho &= -\partial_x \rho u \\
\partial_t \rho u_1 &= -\partial_{x_1} \left( \frac{\rho}{3} + \rho u_1^2 \right) - \partial_{x_2} \rho u_1 u_2 \\
&\quad - \epsilon \frac{2 - \omega}{2\omega} \left( \partial_{x_1} \left( -\frac{2}{3} \rho \partial_{x_1} u_1 \right) - \partial_{x_2} \left( -\frac{1}{3} \rho (\partial_{x_1} u_2 + \partial_{x_2} u_1) \right) \right)
\end{aligned} \tag{3.75}$$

and again the second momentum density can be found by reflection. Once again many of the dissipative terms vanish in the continuous velocity system.

### 3.3 Macroscopic Stability

In the previous sections we have demonstrated the discrete velocity systems studied do not recover the exact macroscopic dissipative dynamics of the continuous system. We are now concerned with the stability of the discrete dynamics under a short wave perturbation. In each example we are concerned with the stability of the linear part of the dynamics (as calculated above) only. We should reinforce that this linear macroscopic stability is not equivalent to stability of the complete microscopic dynamics.

#### 3.3.1 The D1Q3 model

We consider perturbations by a Fourier mode around a constant flow, that is we write

$$\begin{aligned}\rho &= \rho_0 + Ae^{i(\lambda t + \kappa x)} \\ u &= u_0 + Be^{i(\lambda t + \kappa x)}\end{aligned}\tag{3.76}$$

We combine this with a composite coefficient for the first order part

$$\nu = \epsilon \frac{2 - \omega}{2\omega}\tag{3.77}$$

Substituting these into the macroscopic equations and with some rearrangement for the  $u$  term we have

$$\begin{aligned}A\lambda &= -\rho_0 B\kappa - u_0 A\kappa \\ B\lambda &= -\frac{1}{3\rho_0} A\kappa - u_0 B\kappa - \nu \left( \frac{u_0^3}{\rho_0} A i \kappa^2 + \left( 3u_0^2 - \frac{2}{3} \right) B i \kappa^2 \right)\end{aligned}\tag{3.78}$$

We take eigenvalues of the matrix

$$\begin{pmatrix} -u_0\kappa & -\rho_0\kappa \\ -\frac{1}{3\rho_0}\kappa - \nu\frac{u_0^3}{\rho_0}i\kappa^2 & -u_0\kappa - \nu\left(3u_0^2 - \frac{2}{3}\right)i\kappa^2 \end{pmatrix} \quad (3.79)$$

which give us two values for  $\lambda$

$$\lambda = \kappa \left( -u_0 - \frac{3}{2}\nu u_0^2 i\kappa + \frac{1}{3}\nu i\kappa \pm \sqrt{\nu u_0^3 i\kappa - \frac{9}{4}\nu^2 u_0^4 \kappa^2 + \nu^2 u_0^2 \kappa^2 - \frac{1}{9}\nu^2 \kappa^2 + \frac{1}{3}} \right) \quad (3.80)$$

In order for the manifold to remain bounded in time we investigate parameters which give  $\Im(\lambda) \geq 0$ . We begin by checking asymptotics of two parameters, for large  $\kappa$  we have

$$\begin{aligned} \lambda &= \nu\kappa^2 \left( -\frac{3}{2}u_0^2 i + \frac{1}{3}i \pm \sqrt{-\left(\frac{3}{2}u_0^2 + \frac{1}{3}\right)} \right) \\ &= 0, \nu\kappa^2 \left( -3u_0^2 + \frac{2}{3} \right) i \end{aligned} \quad (3.81)$$

and for large  $u_0$

$$\begin{aligned} \lambda &= \kappa \left( -\frac{3}{2}\nu u_0^2 i\kappa \pm \sqrt{-\frac{9}{4}\nu^2 u_0^4 \kappa^2} \right) \\ &= 0, -3\nu u_0^2 i\kappa^2 \end{aligned} \quad (3.82)$$

We can see from this that for non-zero  $\kappa$  the first condition that should be satisfied for stability is  $u_0^2 < 2/9$ , for large  $u_0$  it is necessary for  $\kappa$  to equal 0. Additionally, stability is absolutely contingent on the composite coefficient  $\nu$  being positive, this is the dual condition that time steps are positive and that relaxation parameter of the collision  $\omega$  is in the interval  $0 \leq \omega \leq 2$  (repeated steps of the collision integral in isolation go towards the quasiequilibrium). In the case that either  $\nu$  is negative or that  $u_0$  is outside the given region, the magnitude of the Fourier perturbation will

grow exponentially causing a rapid divergence from the constant flow.

We can confirm these results numerically by plotting the contours of the two eigenvalues equal to zero. In fact in Figure(3.1) we additionally plot contours below zero to show the decay from stability.

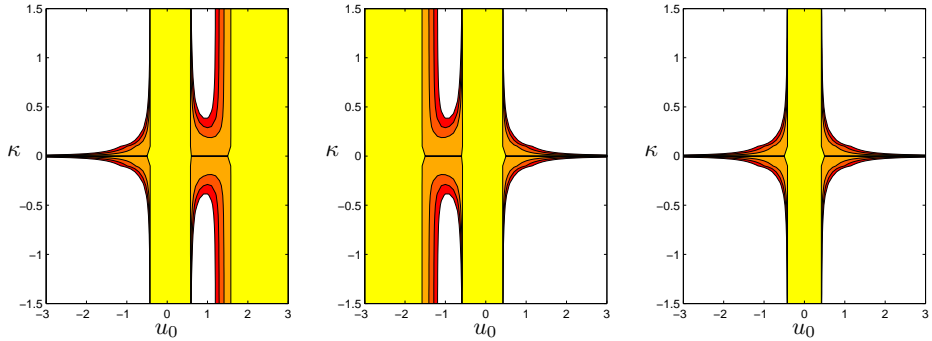


Figure 3.1: The first two figures show stability for each of the two eigenvalues in the D1Q3 system with  $\nu = 1$ , the third figure plots the minimum of the two. Contours are plotted at  $\Im(\lambda) = (-0.3, -0.2, -0.1, 0)$ , the yellow region and its boundary indicate the stable region and, the other colours, the decay from stability.

### 3.3.2 The D1Q5 model

The stability of the D1Q5 system can be calculated in exactly the same way, substituting the same Fourier perturbation into the macroscopic equations we have,

$$\begin{aligned} A\lambda &= -\rho_0 B\kappa - u_0 A\kappa, \\ B\lambda &= -\frac{1}{\rho_0} A\kappa - u_0 B\kappa - \nu \left( \frac{u_0^3}{\rho_0} A i\kappa^2 + (3u_0^2 - 2) B i\kappa^2 \right). \end{aligned} \quad (3.83)$$

We take eigenvalues of the matrix

$$\begin{pmatrix} -u_0\kappa & -\rho_0\kappa \\ -\frac{1}{\rho_0} - \nu \frac{u_0^3}{\rho_0} i\kappa^2 & -u_0\kappa - \nu (3u_0^2 - 2) i\kappa^2 \end{pmatrix} \quad (3.84)$$

in this case the two values for  $\lambda$  are

$$\lambda = \kappa \left( -u_0 - \frac{3}{2}\nu u_0^2 i\kappa + \nu i\kappa \pm \sqrt{\nu u_0^3 i\kappa - \frac{9}{4}\nu^2 u_0^4 \kappa^2 + 3\nu^2 u_0^2 \kappa^2 - \nu^2 \kappa^2 + 1} \right) \quad (3.85)$$

Again we investigate parameters which give  $\Im(\lambda) \geq 0$ . We begin by checking asymptotics of two parameters, for large  $\kappa$  we have

$$\begin{aligned} \lambda &= \nu\kappa^2 \left( -\frac{3}{2}u_0^2 i + i \pm \sqrt{-\left(\frac{3}{2}u_0^2 + 1\right)} \right) \\ &= 0, \nu\kappa^2 (-3u_0^2 + 2) i \end{aligned} \quad (3.86)$$

and for large  $u_0$

$$\begin{aligned} \lambda &= \kappa \left( -\frac{3}{2}\nu u_0^2 i\kappa \pm \sqrt{-\frac{9}{4}\nu^2 u_0^4 \kappa^2} \right) \\ &= 0, -3\nu u_0^2 i\kappa^2 \end{aligned} \quad (3.87)$$

We can see this time that for non-zero  $\kappa$  the condition that should be satisfied for stability is  $u_0^2 < 2/3$ , that is that  $u_0$  can be much larger while retaining stability. Again we can confirm this numerically by plotting the contours of the two eigenvalues equal to zero, in the same format, in Figure(3.2).

### 3.3.3 The D2Q9 model

We extend the stability analysis from the one dimensional case with a perturbation in the additional space direction. The perturbed system is given by,

$$\begin{aligned} \rho &= \rho_0 + A e^{i(\lambda t + \kappa_1 x_1 + \kappa_2 x_2)} \\ u_1 &= u_{10} + B_1 e^{i(\lambda t + \kappa_1 x_1 + \kappa_2 x_2)} \\ u_2 &= u_{20} + B_2 e^{i(\lambda t + \kappa_1 x_1 + \kappa_2 x_2)} \end{aligned} \quad (3.88)$$

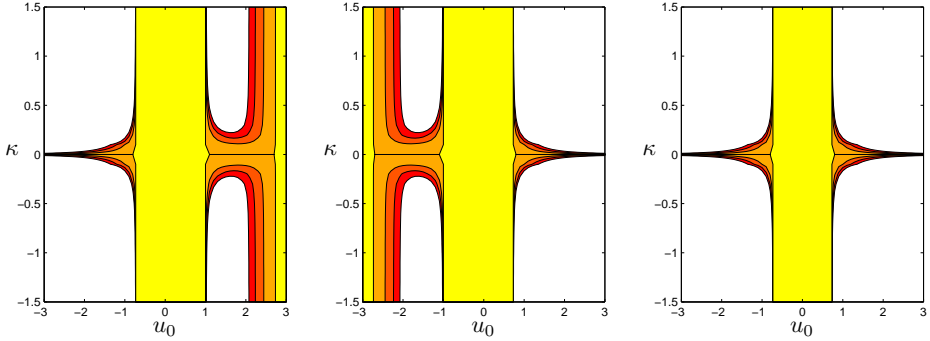


Figure 3.2: The first two figures show stability for each of the two eigenvalues in the D1Q5 system with  $\nu = 1$ , the third figure plots the minimum of the two. Contours are plotted at  $\Im(\lambda) = (-0.3, -0.2, -0.1, 0)$ , the yellow region and its boundary indicate the stable region and, the other colours, the decay from stability.

In this case we investigate the short wave asymptotics as  $|\kappa_1|, |\kappa_2| \rightarrow \infty$ . The eigenvalues of the system under such conditions are

$$\begin{aligned} \lambda_{1,2} &= \left( \frac{1}{3} - \frac{3}{2}u_{10}^2 \right) i\nu\kappa_1^2 + \left( \frac{1}{3} - \frac{3}{2}u_{20}^2 \right) i\nu\kappa_2^2 - 3i\nu u_{10} u_{20} \kappa_1 \kappa_2 \\ &\quad \pm \sqrt{- \left( \left( \frac{1}{3} - \frac{3}{2}u_{10}^2 \right) \nu\kappa_1^2 + \left( \frac{1}{3} - \frac{3}{2}u_{20}^2 \right) \nu\kappa_2^2 - 3\nu u_{10} u_{20} \kappa_1 \kappa_2 \right)}, \quad (3.89) \\ \lambda_3 &= \left( \frac{1}{3} - u_{10}^2 \right) i\nu\kappa_1^2 + \left( \frac{1}{3} - u_{20}^2 \right) i\nu\kappa_2^2 - 2i\nu u_{10} u_{20} \kappa_1 \kappa_2. \end{aligned}$$

In the 1-D examples all terms were in even powers of  $\kappa$  whereas in this case there are cross terms in the product  $\kappa_1 \kappa_2$ . Because of this it is necessary to consider the different permutations of signs for these terms. Since the condition that the third eigenvalue imposes is weaker than that of the the first two, which are equivalent, it is sufficient to find the region of stability using just one of these. Again assuming that the coefficient  $\nu$  is positive, the region is given by parameters satisfying the two conditions.

$$\begin{aligned} \left( \frac{1}{3} - \frac{3}{2}u_{10}^2 \right) + \left( \frac{1}{3} - \frac{3}{2}u_{20}^2 \right) - 3u_{10} u_{20} &\geq 0 \\ \left( \frac{1}{3} - \frac{3}{2}u_{10}^2 \right) + \left( \frac{1}{3} - \frac{3}{2}u_{20}^2 \right) + 3u_{10} u_{20} &\geq 0 \end{aligned} \quad (3.90)$$

The plot of the region generated by these inequalities is given in Figure 3.6. Similarly to the one dimensional example, in the event that  $\nu$  is negative or the constant flow speed moves outside this region, the magnitude of the Fourier perturbation will increase exponentially in time.

Again for specific parameters the stability can be calculated numerically. In the first case examine the case where  $\kappa_2, u_{20} = 0$ . Figure (3.3) shows the stability plot for the three eigenvalues and their minimum, in this case we see that while the eigenvalues are different from their counterparts in the 1-D system, the stability region is exactly the same. In Figure (3.4) we vary  $\kappa_2$  and  $u_{20}$  to see what affect

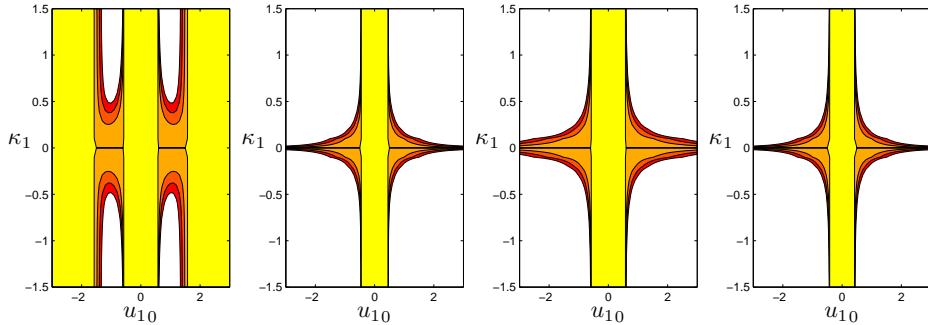


Figure 3.3: The first three figures show stability for each of the three eigenvalues in the athermal D2Q9 system with parameters  $\nu = 1, u_2 = 0, \kappa_2 = 0$ , the fourth figure plots the minimum of them. In each case the contours are plotted at  $\lambda = (-0.3, -0.2, -0.1, 0)$  therefore the yellow region and its boundary describe the stable area.

this has on the stability region. For a more complete picture we plot  $u_{10}$  against  $\kappa_2$  and again plot the stability region. In Figure (3.5) we vary  $\kappa_1$  and  $u_{20}$  across the different plots.

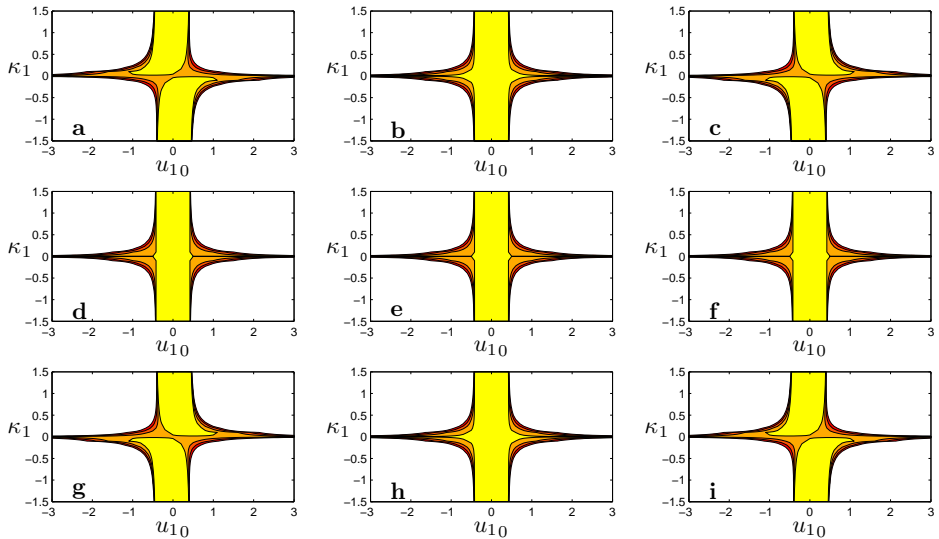


Figure 3.4: Stability regions for the athermal D2Q9 system. Contours are plotted at  $\Im(\lambda) = (-0.3, -0.2, -0.1, 0)$ , the yellow region and its boundary indicate the stable region and, the other colours, the decay from stability. The parameters are  $\nu = 1$  and additionally **a)**  $\kappa_2 = -0.1, u_{20} = -0.5$ ; **b)**  $\kappa_2 = -0.1, u_{20} = 0$ ; **c)**  $\kappa_2 = -0.1, u_{20} = 0.5$ ; **d)**  $\kappa_2 = 0, u_{20} = -0.5$ ; **e)**  $\kappa_2 = 0, u_{20} = 0$ ; **f)**  $\kappa_2 = 0, u_{20} = 0.5$ ; **g)**  $\kappa_2 = 0.1, u_{20} = -0.5$ ; **h)**  $\kappa_2 = 0.1, u_{20} = 0$ ; **i)**  $\kappa_2 = 0.1, u_{20} = 0.5$ .

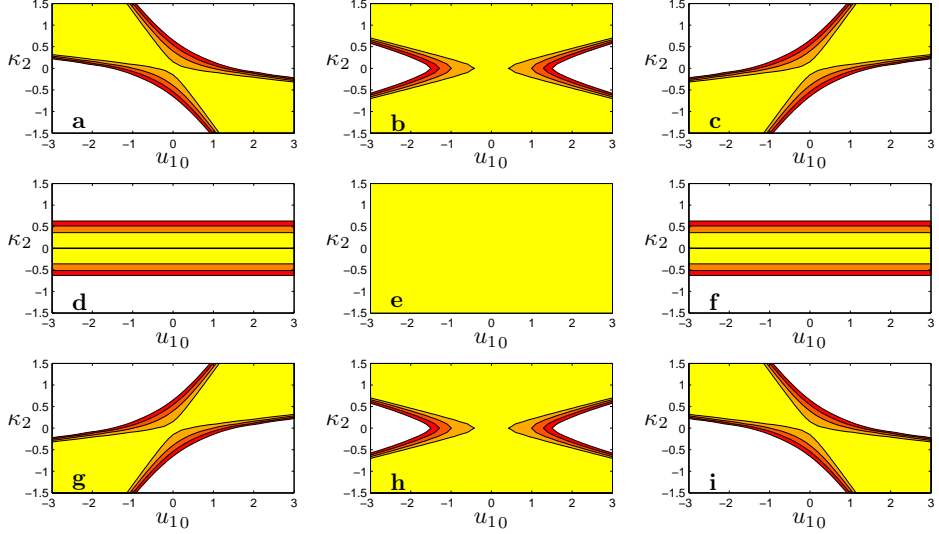


Figure 3.5: Stability regions for the athermal D2Q9 system. Contours are plotted at  $\Im(\lambda) = (-0.3, -0.2, -0.1, 0)$ , the yellow region and its boundary indicate the stable region and, the other colours, the decay from stability. The parameters are  $\nu = 1$  and additionally **a)**  $\kappa_1 = -0.1, u_{20} = -0.5$ ; **b)**  $\kappa_1 = -0.1, u_{20} = 0$ ; **c)**  $\kappa_1 = -0.1, u_{20} = 0.5$ ; **d)**  $\kappa_1 = 0, u_{20} = -0.5$ ; **e)**  $\kappa_1 = 0, u_{20} = 0$ ; **f)**  $\kappa_1 = 0, u_{20} = 0.5$ ; **g)**  $\kappa_1 = 0.1, u_{20} = -0.5$ ; **h)**  $\kappa_1 = 0.1, u_{20} = 0$ ; **i)**  $\kappa_1 = 0.1, u_{20} = 0.5$ .

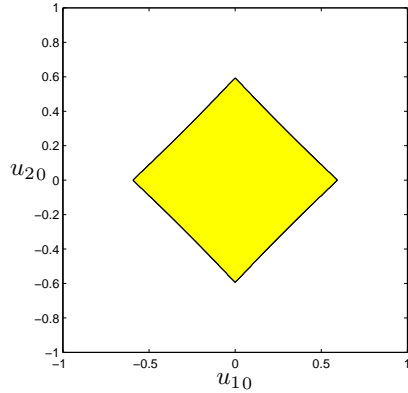


Figure 3.6: Stability regions for the athermal D2Q9 system. Contours are plotted at  $\Im(\lambda) = (-0.3, -0.2, -0.1, 0)$ , the yellow region and its boundary indicate the stable region and, the other colours, the decay from stability. The parameters are  $\nu = 1$  and  $|\kappa_1|, |\kappa_2| \rightarrow \infty$ .

## 3.4 Constructed Examples

### A constructed thermal four velocity lattice

As an example of a lattice with a thermal moment we select the velocities  $(-2, -1, 1, 2)$ .

Here our macroscopic moments will be the usual athermal moments plus an energy density moment.

$$\sum_i v_i^2 f_i^{(0)} = \rho E \quad (3.91)$$

In order to find a condition for every degree of freedom in the system we find a fourth condition by matching the fourth order moment of the continuous Maxwellian distribution. We add the condition that heat flux should be zero outside advection

$$\sum_i (v_i - u)^3 f_i^{(0)} = 0. \quad (3.92)$$

These four conditions together specify a unique quasi-equilibrium by the solution of the system

$$\begin{pmatrix} 1 & 1 & 1 & 1 \\ -2 & -1 & 1 & 2 \\ 4 & 1 & 1 & 4 \\ (-2-u)^3 & (-1-u)^3 & (1-u)^3 & (2-u)^3 \end{pmatrix} \begin{pmatrix} f_1^{(0)} \\ f_2^{(0)} \\ f_3^{(0)} \\ f_4^{(0)} \end{pmatrix} = \begin{pmatrix} \rho \\ \rho u \\ \rho E \\ 0 \end{pmatrix} \quad (3.93)$$

The resulting quasi-equilibrium is given by the population vector

$$\frac{1}{12}\rho(-2\rho + \rho + 2\rho E + 2\rho u^3 - 3\rho u E, 8\rho - 8\rho u - 2\rho E - 4\rho u^3 + 6\rho u E, 8\rho + 8\rho u - 2\rho E + 4\rho u^3 - 6\rho u E, -2\rho - \rho u + 2\rho E - 2\rho u^3 + 3\rho u E) \quad (3.94)$$

We are now interested again in the zero order terms of the moment expansion. We have for the density derivative,

$$\Psi_1^{(0)} = - \sum_i v_i \partial_x f_i^{(0)} = -\partial_x \sum_i v_i f_i^{(0)} = -\partial_x \rho u, \quad (3.95)$$

for the momentum derivative

$$\Psi_2^{(0)} = - \sum_i v_i^2 \partial_x f_i^{(0)} = -\partial_x \sum_i W_\alpha v_i^3 f_i^{(0)} = -\partial_x \rho E, \quad (3.96)$$

and this time for the energy derivative

$$\Psi_3^{(0)} = -\partial_x \sum_i v_i^3 f_i^{(0)} = -\partial_x (-2\rho u^3 + 3\rho u E) \quad (3.97)$$

We next calculate the first order terms, beginning with the density.

$$\Psi_1^{(1)} = \frac{1}{2} \sum_i v_i^2 \partial_{x^2} f_i^{(0)} - \sum_i v_i \partial_x f_i^{(1)} - \frac{1}{2} \partial_t \Psi_1^{(0)} \quad (3.98)$$

The first term is calculated directly and again the second term is the space derivative of the momentum density of the  $f_M^{(1)}$ .

$$\Psi_1^{(1)} = \frac{1}{2} \partial_{x^2} \rho E - \frac{1}{2} \partial_t \Psi_1^{(0)}. \quad (3.99)$$

The time derivative of  $\Psi^{(0)}$  can be calculated by the chain rule,

$$\begin{aligned} \partial_t \Psi_1^{(0)} &= \left( \partial_\rho \Psi_1^{(0)} \right) (\partial_t \rho) + \left( \partial_{\rho u} \Psi_1^{(0)} \right) (\partial_t \rho u) + \left( \partial_{\rho E} \Psi_1^{(0)} \right) (\partial_t \rho E) \\ &= -\partial_x \Psi_2^{(0)} = \partial_{x^2} \rho E \end{aligned} \quad (3.100)$$

Substituting this back in we have,

$$\Psi_1^{(1)} = \frac{1}{2} \partial_{x^2} \rho E - \frac{1}{2} \partial_{x^2} \rho E = 0. \quad (3.101)$$

For the momentum moment we have

$$\Psi_2^{(1)} = \frac{1}{2} \sum_i v_i^3 \partial_{x^2} f_i^{(0)} - \sum_i v_i^2 \partial_x f_i^{(1)} - \frac{1}{2} \partial_t \Psi_2^{(0)} \quad (3.102)$$

The first term can be calculated directly from the equilibrium populations, the second term is equivalent to the second order (thermal) moment used and is therefore equal to zero giving,

$$\Psi_2^{(1)} = \frac{1}{2} \partial_{x^2} (-2\rho u^3 + 3\rho u E) - \frac{1}{2} \partial_t \Psi_2^{(0)}. \quad (3.103)$$

For the time derivative of  $\Psi_2^{(0)}$  we have,

$$\begin{aligned} \partial_t \Psi_2^{(0)} &= \left( \partial_\rho \Psi_2^{(0)} \right) (\partial_t \rho) + \left( \partial_{\rho u} \Psi_2^{(0)} \right) (\partial_t \rho u) + \left( \partial_{\rho E} \Psi_2^{(0)} \right) (\partial_t \rho E) \\ &= -\partial_x \Psi_3^{(0)} = \partial_{x^2} (-2\rho u^3 + 3\rho u E). \end{aligned} \quad (3.104)$$

Substituting this in and evaluating we have then,

$$\Psi_2^{(1)} = \frac{1}{2} \partial_{x^2} (-2\rho u^3 + 3\rho u E) - \frac{1}{2} \partial_{x^2} (-2\rho u^3 + 3\rho u E) = 0. \quad (3.105)$$

For the energy moment we have,

$$\Psi_3^{(1)} = \frac{1}{2} \sum_i v_i^4 f_i^{(0)} - \sum_i \partial_x v_i^3 f_i^{(1)} - \frac{1}{2} \partial_t \Psi_3^{(0)}. \quad (3.106)$$

The first term can be calculated directly from the equilibrium populations and gives us,

$$\partial_{x^2} \sum_i v_i^4 f_i^{(0)} = \partial_{x^2} (-4\rho + 5\rho E). \quad (3.107)$$

In order to calculate the second term we need the first order populations, these are given by,

$$\begin{aligned} \frac{\omega}{1-\omega} \mathbf{f}_M^{(1)} = & \frac{1}{12} \left( -4\partial_x \rho + (-4u^3 + 3uE) \partial_x \rho u + (5 + 6u^2 - 3E) \partial_x \rho \right. \\ & + 6u\partial_x \rho u^3 - 9u\partial_x \rho u E 8\partial_x \rho + (8u^3 - 6uE) \partial_x \rho u \\ & + (-10 - 12u^2 + 6E) \partial_x \rho E - 12u\partial_x \rho u^3 + 18u\partial_x \rho u E \\ & \left. - 8\partial_x \rho + (-8u^3 + 6uE) \partial_x \rho u + (10 + 12u^2 - 6E) \partial_x \rho E \right. \\ & + 12u\partial_x \rho u^3 - 18u\partial_x \rho u E 4\partial_x \rho + (4u^3 - 3uE) \partial_x \rho u \\ & \left. + (-5 - 6u^2 + 3E) \partial_x \rho E - 6u\partial_x \rho u^3 + 9u\partial_x \rho u E \right). \end{aligned} \quad (3.108)$$

Using these populations we have,

$$\begin{aligned} \partial_x \sum_i v_i^3 f_i^{(1)} = & \partial_x \left( 4\partial_x \rho + (4u^3 - 3uE) \partial_x \rho u \right. \\ & \left. + (-5 - 6u^2 + 3E) \partial_x \rho E - 6u\partial_x \rho u^3 + 9u\partial_x \rho u E \right). \end{aligned} \quad (3.109)$$

For the time derivative of  $\Psi_3^{(0)}$  we have,

$$\begin{aligned} \partial_t \Psi_3^{(0)} &= \left( \partial_\rho \Psi_3^{(0)} \right) (\partial_t \rho) + \left( \partial_{\rho u} \Psi_3^{(0)} \right) (\partial_t \rho u) + \left( \partial_{\rho E} \Psi_3^{(0)} \right) (\partial_t \rho E) \\ &= (-4\partial_x u^3 + 3\partial_x u E) \Psi_1^{(0)} + (6\partial_x u^2 - 3\partial_x E) \Psi_2^{(0)} - 3\partial_x u \Psi_3^{(0)} \\ &= \partial_x \left( (4u^3 - 3uE) \partial_x \rho u + (-6u^2 + 3E) \partial_x \rho E - 6u\partial_x \rho u^3 + 9u\partial_x \rho u E \right). \end{aligned} \quad (3.110)$$

Combining the three terms gives us,

$$\begin{aligned}
\Psi_3^{(1)} &= \left( \frac{\omega - 1}{\omega} - \frac{1}{2} \right) \partial_x \left( 4\partial_x\rho + (4u^3 - 3uE) \partial_x\rho u \right. \\
&\quad \left. + (-5 - 6u^2 + 3E) \partial_x\rho E - 6u\partial_x\rho u^3 + 9u\partial_x\rho u E \right) \\
&= \frac{\omega - 2}{2\omega} \partial_x \left( 4\partial_x\rho + (4u^3 - 3uE) \partial_x\rho u \right. \\
&\quad \left. + (-5 - 6u^2 + 3E) \partial_x\rho E - 6u\partial_x\rho u^3 + 9u\partial_x\rho u E \right) \\
&= \frac{\omega - 2}{2\omega} \partial_x \left( (4 - 5E - 2u^4 + 3E^2) \partial_x\rho \right. \\
&\quad \left. + (-14\rho u^3 + 6\rho u E) \partial_x u + (-5\rho + 3\rho u^2 + 3\rho E) \partial_x E \right).
\end{aligned} \tag{3.111}$$

The complete moment gradients to first order are then,

$$\begin{aligned}
\partial_t\rho &= -\partial_x\rho u + o(\epsilon) \\
\partial_t\rho u &= -\partial_x\rho E + o(\epsilon) \\
\partial_t\rho E &= -\partial_x \left( -2\rho u^3 + 3\rho u E \right) \\
&\quad - \epsilon \frac{2 - \omega}{2\omega} \partial_x \left( (4 - 5E - 2u^4 + 3E^2) \partial_x\rho \right. \\
&\quad \left. + (-14\rho u^3 + 6\rho u E) \partial_x u + (-5\rho + 3\rho u^2 + 3\rho E) \partial_x E \right).
\end{aligned} \tag{3.112}$$

We see that for one dimensional system which conserves energy density then there is no viscosity.

### 3.4.1 A constructed thermal example with 8 velocities

We now construct a 2D thermal example, for the velocity set we select the 8 non-zero velocities of the D2Q9 lattice. Similarly to the 1D case we add a thermal moment for a total of 4, for four more conditions to equal the number of velocities we again

zero other high order terms. Explicitly these 5 conditions are given by

$$\begin{aligned}
\sum_i \mathbf{v}_i^2 \mathfrak{f}_i^{(0)} &= \rho E, \\
\sum_i (\mathbf{v}_i - \mathbf{u})^2 \mathfrak{f}_i^{(0)} &= 0, \\
\sum_i (v_{i,1} - u_1)(v_{i,2} - u_2) \mathfrak{f}_i^{(0)} &= 0, \\
\sum_i ((v_{i,1} - u_1)^2 - (v_{i,2} - u_2)^2) (v_{i,1} - u_1) \mathfrak{f}_i^{(0)} &= 0, \\
\sum_i ((v_{i,1} - u_1)^2 - (v_{i,2} - u_2)^2) (v_{i,2} - u_2) \mathfrak{f}_i^{(0)} &= 0.
\end{aligned} \tag{3.113}$$

For brevity the populations generated by these conditions are listed in appendix B.1, they are again used to calculate the zero order macroscopic moments

$$\begin{aligned}
\Psi_1^{(0)} &= \sum_i \left( -\mathbf{v}_i \cdot \partial_{\mathbf{x}} \mathfrak{f}_i^{(0)} \right) \\
&= -\partial_{x_1} \sum_i v_{i,1} \mathfrak{f}_i^{(0)} - \partial_{x_2} \sum_i v_{i,2} \mathfrak{f}_i^{(0)} \\
&= -\partial_{x_1} \rho u_1 - \partial_{x_2} \rho u_2
\end{aligned} \tag{3.114}$$

for the first momentum derivative

$$\begin{aligned}
\Psi_2^{(0)} &= \sum_i v_{i,1} \left( -\mathbf{v}_i \cdot \partial_{\mathbf{x}} \mathfrak{f}_i^{(0)} \right) \\
&= -\partial_{x_1} \sum_i v_{i,1}^2 \mathfrak{f}_i^{(0)} - \partial_{x_2} \sum_i v_{i,1} v_{i,2} \mathfrak{f}_i^{(0)} \\
&= -\frac{1}{2} \partial_{x_1} (\rho E + \rho u_1^2 - \rho u_2^2) - \partial_{x_2} \rho u_1 u_2
\end{aligned} \tag{3.115}$$

for the second momentum derivative

$$\begin{aligned}
\Psi_3^{(0)} &= \sum_i v_{i,2} \left( -\mathbf{v}_i \cdot \partial_{\mathbf{x}} \mathfrak{f}_i^{(0)} \right) \\
&= -\partial_{x_1} \sum_i v_{i,1} v_{i,2} \mathfrak{f}_i^{(0)} - \partial_{x_2} \sum_i v_{i,2}^2 \mathfrak{f}_i^{(0)} \\
&= -\partial_{x_1} \rho u_1 u_2 - \frac{1}{2} \partial_{x_2} (\rho E - \rho u_1^2 + \rho u_2^2)
\end{aligned} \tag{3.116}$$

and finally for the energy derivative

$$\begin{aligned}
\Psi_4^{(0)} &= \sum_i \mathbf{v}_i^2 \left( -\mathbf{v}_i \cdot \partial_{\mathbf{x}} \mathfrak{f}_i^{(0)} \right) \\
&= -\partial_{x_1} \sum_i \mathbf{v}_i^2 v_{i,1} \mathfrak{f}_i^{(0)} - \partial_{x_2} \sum_i \mathbf{v}_i^2 v_{i,2} \mathfrak{f}_i^{(0)} \\
&= -\partial_{x_1} \rho u_1 (2E - u_1^2 - u_2^2) - \partial_{x_2} \rho u_2 (2E - u_1^2 - u_2^2)
\end{aligned} \tag{3.117}$$

For the first order macroscopic moments we begin as usual with the density,

$$\Psi_1^{(1)} = \frac{1}{2} \sum_i \left( \mathbf{v}_i \cdot \partial_{\mathbf{x}} \left( \mathbf{v}_i \cdot \partial_{\mathbf{x}} \mathfrak{f}_i^{(0)} \right) \right) + \sum_i \left( -\mathbf{v}_i \cdot \partial_{\mathbf{x}} \mathfrak{f}_i^{(1)} \right) - \frac{1}{2} \partial_t \Psi_1^{(0)} \tag{3.118}$$

Again we observe that the second term is the space gradient multiplied with the momentum densities of the first order populations and hence is zero, for the first term we have

$$\begin{aligned}
\sum_i \left( \mathbf{v}_i \cdot \partial_{\mathbf{x}} \left( \mathbf{v}_i \cdot \partial_{\mathbf{x}} \mathfrak{f}_i^{(0)} \right) \right) &= \sum_i \left( \partial_{x_1^2} v_{i,1}^2 \mathfrak{f}_i^{(0)} + 2\partial_{x_1 x_2} v_{i,1} v_{i,2} \mathfrak{f}_i^{(0)} + \partial_{x_2^2} v_{i,2}^2 \mathfrak{f}_i^{(0)} \right) \\
&= \frac{1}{2} \partial_{x_1^2} (\rho E + \rho u_1^2 - \rho u_2^2) + 2\partial_{x_1 x_2} \rho u_1 u_2 + \frac{1}{2} \partial_{x_2^2} (\rho E - \rho u_1^2 + \rho u_2^2)
\end{aligned} \tag{3.119}$$

and for the third term

$$\begin{aligned}\partial_t \Psi_1^{(0)} &= \left( \partial_\rho \Psi_1^{(0)} \right) (\partial_t \rho) + \left( \partial_{\rho u_1} \Psi_1^{(0)} \right) (\partial_t \rho u_1) + \left( \partial_{\rho u_2} \Psi_1^{(0)} \right) (\partial_t \rho u_2) + \left( \partial_{\rho E} \Psi_1^{(0)} \right) (\partial_t \rho E) \\ &= -\partial_{x_1} \Psi_2^{(0)} - \partial_{x_2} \Psi_3^{(0)} = -\partial_{x_1} \left( -\frac{1}{2} \partial_{x_1} (\rho E + \rho u_1^2 - \rho u_2^2) - \partial_{x_2} \rho u_1 u_2 \right) \\ &\quad - \partial_{x_2} \left( -\partial_{x_1} \rho u_1 u_2 - \frac{1}{2} \partial_{x_2} (\rho E - \rho u_1^2 + \rho u_2^2) \right)\end{aligned}\quad (3.120)$$

hence subtracting these we have  $\Psi_1^{(1)} = 0$ . For the first second order momentum density we have

$$\Psi_2^{(1)} = \frac{1}{2} \sum_i v_{i,1} \left( \mathbf{v}_i \cdot \partial_{\mathbf{x}} \left( \mathbf{v}_i \cdot \partial_{\mathbf{x}} \mathfrak{f}_i^{(0)} \right) \right) + \sum_i v_{i,1} \left( -\mathbf{v}_i \cdot \partial_{\mathbf{x}} \mathfrak{f}_i^{(1)} \right) - \frac{1}{2} \partial_t \Psi_2^{(0)} \quad (3.121)$$

Examining each term in turn more closely we have for the first term

$$\begin{aligned}\sum_i v_{i,1} \left( \mathbf{v}_i \cdot \partial_{\mathbf{x}} \left( \mathbf{v}_i \cdot \partial_{\mathbf{x}} \mathfrak{f}_i^{(0)} \right) \right) &= \sum_i v_{i,1} \left( \partial_{x_1^2} (v_{i,1})^2 \mathfrak{f}_i^{(0)} + 2\partial_{x_1 x_2} v_{i,1} v_{i,2} \mathfrak{f}_i^{(0)} + \partial_{x_2^2} (v_{i,2})^2 \mathfrak{f}_i^{(0)} \right) \\ &= \partial_{x_1} \left( \rho \partial_{x_1} u_1 + u_1 \partial_{x_1} \rho + (-u_2 - u_1^2 - u_2^3 + 2u_2 E) \partial_{x_2} \rho \right. \\ &\quad \left. - 2\rho u_1 u_2 \partial_{x_2} u_1 + (-\rho - \rho u_1^2 - 3\rho u_2^2 + 2\rho E) \partial_{x_2} u_2 \right. \\ &\quad \left. + 2\rho u_2 \partial_{x_2} E \right) \\ &+ \partial_{x_2} \left( (-u_2 - u_1^2 u_2 - u_2^3 + 2u_2 E) \partial_{x_1} \rho - 2\rho u_1 u_2 \partial_{x_1} u_1 \right. \\ &\quad \left. + (-\rho - \rho u_1^2 - 3\rho u_2^2 + 2\rho E) \partial_{x_1} u_1 + 2\rho u_2 \partial_{x_1} E \right. \\ &\quad \left. + (-u_1 - u_1^3 - u_1 u_2^2 + 2u_1 E) \partial_{x_2} \rho \right. \\ &\quad \left. + (-\rho - 3\rho u_1^2 - \rho u_2^2 + 2\rho E) \partial_{x_2} u_1 \right. \\ &\quad \left. - 2\rho u_1 u_2 \partial_{x_2} u_2 + 2\rho u_1 \partial_{x_2} E \right)\end{aligned}\quad (3.122)$$

The first order populations for this lattice have up to 90 terms, examples of these are given in Appendix B.2, they give us for the second term

$$\begin{aligned}
\sum_i v_{i,1} \left( -\mathbf{v}_i \cdot \partial_{\mathbf{x}} \mathfrak{f}^{(1)} \right) &= - \sum_i v_{i,1} \left( \partial_{x_1} v_{i,1} \mathfrak{f}_i^{(1)} + \partial_{x_2} v_{i,2} f_M^{(1)} \right) \\
&= \frac{\omega - 1}{\omega} \left( \partial_{x_1} \left( \left( -u_1 - \frac{1}{2}u_1^3 - \frac{3}{2}u_1u_2^2 + \frac{3}{2}u_1E \right) \partial_{x_1}\rho \right. \right. \\
&\quad + \left( u_2 + \frac{3}{2}u_1^2u_2 + \frac{1}{2}u_2^3 - \frac{3}{2}u_2E \right) \partial_{x_2}\rho \\
&\quad + \left( -\rho - \rho u_1^2 - \rho u_2^2 + \rho E \right) \partial_{x_1}u_1 \\
&\quad + 3\rho u_1 u_2 \partial_{x_2}u_1 - 3\rho u_1 u_2 \partial_{x_1}u_2 \\
&\quad + \left( \rho + \rho u_1^2 + \rho u_2^2 - \rho E \right) \partial_{x_2}u_2 \\
&\quad \left. \left. + \frac{3}{2}\rho u_1 \partial_{x_1}E - \frac{3}{2}\rho u_2 \partial_{x_2}E \right) \right. \\
&\quad + \partial_{x_2} \left( \left( u_2 + \frac{3}{2}u_1^2u_2 + \frac{1}{2}u_2^3 - \frac{3}{2}u_2E \right) \partial_{x_1}\rho \right. \\
&\quad + \left( u_1 + \frac{1}{2}u_1^3 + \frac{3}{2}u_1u_2^2 - \frac{3}{2}u_1E \right) \partial_{x_2}\rho \\
&\quad + 3\rho u_1 u_2 \partial_{x_1}u_1 + \left( \rho + 2\rho u_1^2 + 2\rho u_2^2 - 2\rho E \right) \partial_{x_2}u_1 \\
&\quad + \left( \rho + 2\rho u_1^2 + 2\rho u_2^2 - 2\rho E \right) \partial_{x_1}u_2 + 3\rho u_1 u_2 \partial_{x_2}u_2 \\
&\quad \left. \left. + -\frac{3}{2}\rho u_2 \partial_{x_1}E - \frac{3}{2}\rho u_1 \partial_{x_2}E \right) \right) \right)
\end{aligned} \tag{3.123}$$

and for the third term

$$\begin{aligned}
\partial_t \Psi_2^{(0)} &= \left( \partial_\rho \Psi_2^{(0)} \right) (\partial_t \rho) + \left( \partial_{\rho u_1} \Psi_2^{(0)} \right) (\partial_t \rho u_1) + \left( \partial_{\rho u_2} \Psi_2^{(0)} \right) (\partial_t \rho u_2) + \left( \partial_{\rho E} \Psi_2^{(0)} \right) (\partial_t \rho E) \\
&= \left( \frac{\partial}{\partial x_1} (u_1^2 - u_2^2) + \partial_{x_2} u_1 u_2 \right) \Psi_1^{(0)} + (-2\partial_{x_1} u_1 - \partial_{x_2} u_2) \Psi_2^{(0)} \\
&\quad + (2\partial_{x_1} u_2 - \partial_{x_2} u_1) \Psi_3^{(0)} - \partial_{x_1} \Psi_4^{(0)} \\
&= \partial_{x_1} \left( \left( -\frac{1}{2} u_1^3 - \frac{3}{2} u_1 u_2^2 + \frac{3}{2} u_1 E \right) \partial_{x_1} \rho + \left( \frac{1}{2} u_1^2 u_2 - \frac{1}{2} u_2^3 + \frac{1}{2} u_2 E \right) \partial_{x_2} \rho \right. \\
&\quad \left. + (-\rho u_1^2 - \rho u_2^2 + \rho E) \partial_{x_1} u_1 + \rho u_1 u_2 \partial_{x_2} u_1 - 3\rho u_1 u_2 \partial_{x_1} u_2 \right. \\
&\quad \left. + (-2\rho u_2^2 + \rho E) \partial_{x_2} u_2 + \frac{3}{2} \rho u_1 \partial_{x_1} E + \frac{1}{2} \rho u_2 \partial_{x_2} E \right) \\
&\quad + \partial_{x_2} \left( \left( \frac{1}{2} u_1^2 u_2 - \frac{1}{2} u_2^3 + \frac{1}{2} u_2 E \right) \partial_{x_1} \rho + \left( -\frac{1}{2} u_1^3 + \frac{1}{2} u_1 u_2^2 + \frac{1}{2} u_1 E \right) \partial_{x_2} \rho \right. \\
&\quad \left. + \rho u_1 u_2 \partial_{x_1} u_1 + (-\rho u_1^2 + \rho u_2^2) \partial_{x_2} u_1 + (\rho u_1^2 - \rho u_2^2) \partial_{x_1} u_2 \right. \\
&\quad \left. + \rho u_1 u_2 \partial_{x_2} u_2 + \frac{1}{2} \rho u_2 \partial_{x_1} E + \frac{1}{2} \rho u_1 \partial_{x_2} E \right)
\end{aligned} \tag{3.124}$$

Combining all three terms we have

$$\begin{aligned}
\Psi_2^{(1)} = & \left( \frac{\omega - 1}{\omega} - \frac{1}{2} \right) \left( \partial_{x_1} \left( \left( -u_1 - \frac{1}{2}u_1^3 - \frac{3}{2}u_1u_2^2 + \frac{3}{2}u_1E \right) \partial_{x_1}\rho \right. \right. \\
& + \left( u_2 + \frac{3}{2}u_1^2u_2 + \frac{1}{2}u_2^3 - \frac{3}{2}u_2E \right) \partial_{x_2}\rho \\
& + (-\rho - \rho u_1^2 - \rho u_2^2 + \rho E) \partial_{x_1}u_1 + 3\rho u_1u_2\partial_{x_2}u_1 \\
& . - 3\rho u_1u_2\partial_{x_1}u_2 + (\rho + \rho u_1^2 + \rho u_2^2 - \rho E) \partial_{x_2}u_2 \\
& \left. \left. + \frac{3}{2}\rho u_1\partial_{x_1}E - \frac{3}{2}\rho u_2\partial_{x_2}E \right) \right. \\
& + \partial_{x_2} \left( \left( u_2 + \frac{3}{2}u_1^2u_2 + \frac{1}{2}u_2^3 - \frac{3}{2}u_2E \right) \partial_{x_1}\rho \right. \\
& + \left( u_1 + \frac{1}{2}u_1^3 + \frac{3}{2}u_1u_2^2 - \frac{3}{2}u_1E \right) \partial_{x_2}\rho \\
& + 3\rho u_1u_2\partial_{x_1}u_1 + (\rho + 2\rho u_1^2 + 2\rho u_2^2 - 2\rho E) \partial_{x_2}u_1 \\
& + (\rho + 2\rho u_1^2 + 2\rho u_2^2 - 2\rho E) \partial_{x_1}u_2 + 3\rho u_1u_2\partial_{x_2}u_2 \\
& \left. \left. + -\frac{3}{2}\rho u_2\partial_{x_1}E - \frac{3}{2}\rho u_1\partial_{x_2}E \right) \right)
\end{aligned} \tag{3.125}$$

Finally for the first order energy density we have

$$\Psi_4^{(1)} = \frac{1}{2} \sum_i (\mathbf{v}_i)^2 \left( \mathbf{v}_i \cdot \partial_{\mathbf{x}} \left( \mathbf{v}_i \cdot \partial_{\mathbf{x}} \mathbf{f}^{(0)} \right) \right) + \sum_i (\mathbf{v}_i)^2 \left( -\mathbf{v}_i \cdot \partial_{\mathbf{x}} \mathbf{f}^{(1)} \right) - \frac{1}{2} \partial_t \Psi_4^{(0)} \tag{3.126}$$

We have for the first term

$$\begin{aligned}
\sum_i \mathbf{v}_i^2 \left( \mathbf{v}_i \cdot \partial_{\mathbf{x}} \left( \mathbf{v}_i \cdot \partial_{\mathbf{x}} \mathbf{f}^{(0)} \right) \right) &= \sum_i \mathbf{v}_i^2 \left( \partial_{x_1^2} v_{i,1}^2 \mathbf{f}_i^{(0)} + 2\partial_{x_1 x_2} v_{i,1} v_{i,2} \mathbf{f}_i^{(0)} + \partial_{x_2^2} v_{i,2}^2 \mathbf{f}_i^{(0)} \right) \\
&= \partial_{x_1} \left( \left( -1 + \frac{1}{2} u_1^2 - \frac{1}{2} u_2^2 + \frac{3}{2} E \right) \partial_{x_1} \rho \right. \\
&\quad \left. + \rho u_1 \partial_{x_1} u_1 - \rho u_2 \partial_{x_1} u_2 + \frac{3}{2} \rho \partial_{x_1} E \right. \\
&\quad \left. + 2u_1 u_2 \partial_{x_2} \rho + 2\rho u_2 \partial_{x_2} u_1 + 2\rho u_1 \partial_{x_2} u_2 \right) \\
&\quad + \partial_{x_2} \left( 2u_1 u_2 \partial_{x_1} \rho + 2\rho u_2 \partial_{x_2} u_1 + 2\rho u_1 \partial_{x_1} u_2 \right. \\
&\quad \left. + \left( -1 - \frac{1}{2} u_1^2 + \frac{1}{2} u_2^2 + \frac{3}{2} E \right) \partial_{x_2} \rho \right. \\
&\quad \left. - \rho u_1 \partial_{x_2} u_1 + \rho u_2 \partial_{x_2} u_2 + \frac{3}{2} \rho \partial_{x_2} E \right) \\
&\tag{3.127}
\end{aligned}$$

Again using the first order populations gives us for the second term

$$\begin{aligned}
\sum_i (\mathbf{v}_i)^2 \left( -\mathbf{v}_i \cdot \partial_{\mathbf{x}} \mathbf{f}^{(1)} \right) &= - \sum_i (\mathbf{v}_i)^2 \left( \partial_{x_1} v_{i,1} \mathfrak{f}_i^{(1)} + \partial_{x_2} v_{i,2} f_M^{(1)} \right) \\
&= \frac{\omega - 1}{\omega} \left( \partial_{x_1} \left( \left( 1 - \frac{1}{2} u_1^2 + \frac{1}{2} u_2^2 - \frac{3}{2} E - \frac{3}{2} u_1^4 - u_1^2 u_2^2 \right. \right. \right. \\
&\quad \left. \left. \left. + \frac{1}{2} u_2^4 + \frac{3}{2} u_1^2 E - \frac{3}{2} u_2^2 E + E^2 \right) \partial_{x_1} \rho \right. \right. \\
&\quad \left. \left. + (-2u_1 u_2 - 2u_1^3 u_2 - 2u_1 u_2^3 + 3u_1 u_2 E) \partial_{x_2} \rho \right. \right. \\
&\quad \left. \left. + (-\rho u_1 - 7\rho u_1^3 - 3\rho u_1 u_2^2 + 4\rho u_1 E) \partial_{x_1} u_1 \right. \right. \\
&\quad \left. \left. + (-2\rho u_2 - 5\rho u_1^2 u_2 - \rho u_2^3 + 2\rho u_2 E) \partial_{x_2} u_1 \right. \right. \\
&\quad \left. \left. + (\rho u_2 - 3\rho u_1^2 u_2 + \rho u_2^3 - 2\rho u_2 E) \partial_{x_1} u_2 \right. \right. \\
&\quad \left. \left. + (-2\rho u_1 - 3\rho u_1^3 - 7\rho u_1 u_2^2 + 4\rho u_1 E) \partial_{x_2} u_2 \right. \right. \\
&\quad \left. \left. + \left( -\frac{3}{2} \rho + \frac{5}{2} \rho u_1^2 - \frac{1}{2} \rho u_2^2 + \rho E \right) \partial_{x_1} E \right. \right. \\
&\quad \left. \left. + 3\rho u_1 u_2 \partial_{x_2} E \right) \right. \\
&\quad \left. + \partial_{x_2} \left( (-2u_1 u_2 - 2u_1^3 u_2 - 2u_1 u_2^3 + 3u_1 u_2 E) \partial_{x_1} \rho \right. \right. \\
&\quad \left. \left. + \left( 1 + \frac{1}{2} u_1^2 - \frac{1}{2} u_2^2 - \frac{3}{2} E + \frac{1}{2} u_1^4 - u_1^2 u_2^2 \right. \right. \right. \\
&\quad \left. \left. \left. - \frac{3}{2} u_2^4 - \frac{3}{2} u_1^2 E + \frac{3}{2} u_2^2 E + E^2 \right) \partial_{x_2} \rho \right. \right. \\
&\quad \left. \left. + (-2\rho u_2 - 7\rho u_1^2 u_2 - 3\rho u_2^2 + 4\rho u_2 E) \partial_{x_1} u_1 \right. \right. \\
&\quad \left. \left. + (\rho u_1 + \rho u_1^3 - 3\rho u_1 u_2^2 - 2\rho u_1 E) \partial_{x_2} u_1 \right. \right. \\
&\quad \left. \left. + (-2\rho u_1 - \rho u_1^3 - 5\rho u_1 u_2^2 + 2\rho u_1 E) \partial_{x_1} u_2 \right. \right. \\
&\quad \left. \left. + (-\rho u_2 - 3\rho u_1^2 u_2 - 7\rho u_2^3 + 4\rho u_2 E) \partial_{x_2} u_2 \right. \right. \\
&\quad \left. \left. + 3\rho u_1 u_2 \partial_{x_1} E \right. \right. \\
&\quad \left. \left. + \left( -\frac{3}{2} \rho - \frac{1}{2} \rho u_1^2 + \frac{5}{2} \rho u_2^2 + \rho E \right) \partial_{x_2} E \right) \right) \right) \\
&\tag{3.128}
\end{aligned}$$

and for the third term

$$\begin{aligned}
\partial_t \Psi_4^{(0)} &= \left( \partial_\rho \Psi_4^{(0)} \right) (\partial_t \rho) + \left( \partial_{\rho u_1} \Psi_4^{(0)} \right) (\partial_t \rho u_1) + \left( \partial_{\rho u_2} \Psi_4^{(0)} \right) (\partial_t \rho u_2) + \left( \partial_{\rho E} \Psi_4^{(0)} \right) (\partial_t \rho E) \\
&= \left( \partial_{x_1} (2u_1 E - 2u_1^3 - 2u_1 u_2^2) + \partial_{x_2} (2u_2 E - 2u_1^2 u_2 - 2u_2^3) \right) \Psi_1^{(0)} \\
&\quad + \left( \partial_{x_1} (-2E + 3u_1^2 + u_2^2) + 2\partial_{x_2} u_1 u_2 \right) \Psi_2^{(0)} \\
&\quad + \left( 2\partial_{x_1} u_1 u_2 + \partial_{x_2} (-2E + u_1^2 + 3u_2^2) \right) \Psi_3^{(0)} + (-2\partial_{x_1} u_1 - 2\partial_{x_2} u_2) \Psi_4^{(0)} \\
&= \partial_{x_1} \left( \left( -\frac{3}{2}u_1^4 - u_1^2 u_2^2 + \frac{1}{2}u_2^4 + \frac{3}{2}u_1^2 E - \frac{3}{2}u_2^2 E + E^2 \right) \partial_{x_1} \rho \right. \\
&\quad \left. + (-2u_1^3 u_2 - 2u_1 u_2^3 + 3u_1 u_2 E) \partial_{x_2} \rho \right. \\
&\quad \left. + (-7\rho u_1^3 - 3\rho u_1 u_2^2 + 4\rho u_1 E) \partial_{x_1} u_1 + (-5\rho u_1^2 u_2 - \rho u_2^3 + 2\rho u_2 E) \partial_{x_2} u_1 \right. \\
&\quad \left. + (-3\rho u_1^2 u_2 + \rho u_2^3 - 2\rho u_2 E) \partial_{x_1} u_2 + (-3\rho u_1^3 - 7\rho u_1 u_2^2 + 4\rho u_1 E) \partial_{x_2} u_2 \right. \\
&\quad \left. + \left( \frac{5}{2}\rho u_1^2 - \frac{1}{2}\rho u_2^2 + \rho E \right) \partial_{x_1} E + 3\rho u_1 u_2 \partial_{x_2} E \right) \\
&\quad + \partial_{x_2} \left( \left( -2u_1^3 u_2 - 2u_1 u_2^3 + 3u_1 u_2 E \right) \partial_{x_1} \rho \right. \\
&\quad \left. + \left( \frac{1}{2}u_1^4 - u_1^2 u_2^2 - \frac{3}{2}u_2^4 - \frac{3}{2}u_1^2 E + \frac{3}{2}u_2^2 E + E^2 \right) \partial_{x_2} \rho \right. \\
&\quad \left. + (-7\rho u_1^2 u_2 - 3\rho u_2^3 + 4\rho u_2 E) \partial_{x_1} u_1 + (\rho u_1^3 - 3\rho u_1 u_2^2 - 2\rho u_1 E) \partial_{x_2} u_1 \right. \\
&\quad \left. + (-\rho u_1^3 - 5\rho u_1 u_2^2 + 2\rho u_1 E) \partial_{x_1} u_2 + (-3\rho u_1^2 u_2 - 7\rho u_2^3 + 4\rho u_2 E) \partial_{x_2} u_2 \right. \\
&\quad \left. + 3\rho u_1 u_2 \partial_{x_1} E + \left( -\frac{1}{2}\rho u_1^2 + \frac{5}{2}\rho u_2^2 + \rho E \right) \partial_{x_2} E \right) \\
&\tag{3.129}
\end{aligned}$$

Combining all three terms we have

$$\begin{aligned}
\Psi_4^{(1)} = & \left( \frac{\omega - 1}{\omega} - \frac{1}{2} \right) \left( \partial_{x_1} \left( \left( 1 - \frac{1}{2}u_1^2 + \frac{1}{2}u_2^2 - \frac{3}{2}E - \frac{3}{2}u_1^4 - u_1^2u_2^2 \right. \right. \right. \\
& \quad \left. \left. \left. + \frac{1}{2}u_2^4 + \frac{3}{2}u_1^2E - \frac{3}{2}u_2^2E + E^2 \right) \partial_{x_1}\rho \right. \\
& \quad \left. + (-2u_1u_2 - 2u_1^3u_2 - 2u_1u_2^3 + 3u_1u_2E) \partial_{x_2}\rho \right. \\
& \quad \left. + (-\rho u_1 - 7\rho u_1^3 - 3\rho u_1u_2^2 + 4\rho u_1E) \partial_{x_1}u_1 \right. \\
& \quad \left. + (-2\rho u_2 - 5\rho u_1^2u_2 - \rho u_2^3 + 2\rho u_2E) \partial_{x_2}u_1 \right. \\
& \quad \left. + (\rho u_2 - 3\rho u_1^2u_2 + \rho u_2^3 - 2\rho u_2E) \partial_{x_1}u_2 \right. \\
& \quad \left. + (-2\rho u_1 - 3\rho u_1^3 - 7\rho u_1u_2^2 + 4\rho u_1E) \partial_{x_2}u_2 \right. \\
& \quad \left. + \left( -\frac{3}{2}\rho + \frac{5}{2}\rho u_1^2 - \frac{1}{2}\rho u_2^2 + \rho E \right) \partial_{x_1}E + 3\rho u_1u_2\partial_{x_2}E \right) \\
& \quad + \partial_{x_2} \left( \left( -2u_1u_2 - 2u_1^3u_2 - 2u_1u_2^3 + 3u_1u_2E \right) \partial_{x_1}\rho \right. \\
& \quad \left. + \left( 1 + \frac{1}{2}u_1^2 - \frac{1}{2}u_2^2 - \frac{3}{2}E + \frac{1}{2}u_1^4 - u_1^2u_2^2 \right. \right. \\
& \quad \left. \left. - \frac{3}{2}u_2^4 - \frac{3}{2}u_1^2E + \frac{3}{2}u_2^2E + E^2 \right) \partial_{x_2}\rho \right. \\
& \quad \left. + (-2\rho u_2 - 7\rho u_1^2u_2 - 3\rho u_2^3 + 4\rho u_2E) \partial_{x_1}u_1 \right. \\
& \quad \left. + (\rho u_1 + \rho u_1^3 - 3\rho u_1u_2^2 - 2\rho u_1E) \partial_{x_2}u_1 \right. \\
& \quad \left. + (-2\rho u_1 - \rho u_1^3 - 5\rho u_1u_2^2 + 2\rho u_1E) \partial_{x_1}u_2 \right. \\
& \quad \left. + (-\rho u_2 - 3\rho u_1^2u_2 - 7\rho u_2^3 + 4\rho u_2E) \partial_{x_2}u_2 \right. \\
& \quad \left. + 3\rho u_1u_2\partial_{x_1}E + \left( -\frac{3}{2}\rho - \frac{1}{2}\rho u_1^2 + \frac{5}{2}\rho u_2^2 + \rho E \right) \partial_{x_2}E \right) \right) \tag{3.130}
\end{aligned}$$

The final macroscopic equations for this system up to first order are then

$$\begin{aligned}
\partial_t \rho &= -\partial_{\mathbf{x}} \rho u + o(\epsilon) \\
\partial_t \rho u_1 &= -\frac{1}{2} \partial_{x_1} (\rho E + \rho u_1^2 - \rho u_2^2) - \partial_{x_2} \rho u_1 u_2 \\
&\quad + \epsilon \frac{\omega - 2}{2\omega} \left( \partial_{x_1} \left( \left( -u_1 - \frac{1}{2} u_1^3 - \frac{3}{2} u_1 u_2^2 + \frac{3}{2} u_1 E \right) \partial_{x_1} \rho \right. \right. \\
&\quad \left. \left. + \left( u_2 + \frac{3}{2} u_1^2 u_2 + \frac{1}{2} u_2^3 - \frac{3}{2} u_2 E \right) \partial_{x_2} \rho \right. \right. \\
&\quad \left. \left. + (-\rho - \rho u_1^2 - \rho u_2^2 + \rho E) \partial_{x_1} u_1 + 3\rho u_1 u_2 \partial_{x_2} u_1 \right. \right. \\
&\quad \left. \left. - 3\rho u_1 u_2 \partial_{x_1} u_2 + (\rho + \rho u_1^2 + \rho u_2^2 - \rho E) \partial_{x_2} u_2 \right. \right. \\
&\quad \left. \left. + \frac{3}{2} \rho u_1 \partial_{x_1} E - \frac{3}{2} \rho u_2 \partial_{x_2} E \right) \right. \\
&\quad \left. + \partial_{x_2} \left( \left( u_2 + \frac{3}{2} u_1^2 u_2 + \frac{1}{2} u_2^3 - \frac{3}{2} u_2 E \right) \partial_{x_1} \rho \right. \right. \\
&\quad \left. \left. + \left( u_1 + \frac{1}{2} u_1^3 + \frac{3}{2} u_1 u_2^2 - \frac{3}{2} u_1 E \right) \partial_{x_2} \rho \right. \right. \\
&\quad \left. \left. + 3\rho u_1 u_2 \partial_{x_1} u_1 + (\rho + 2\rho u_1^2 + 2\rho u_2^2 - 2\rho E) \partial_{x_2} u_1 \right. \right. \\
&\quad \left. \left. + (\rho + 2\rho u_1^2 + 2\rho u_2^2 - 2\rho E) \partial_{x_1} u_2 + 3\rho u_1 u_2 \partial_{x_2} u_2 \right. \right. \\
&\quad \left. \left. + -\frac{3}{2} \rho u_2 \partial_{x_1} E - \frac{3}{2} \rho u_1 \partial_{x_2} E \right) \right)
\end{aligned} \tag{3.131}$$

$$\begin{aligned}
\partial_t \rho E &= -\partial_{x_1} \rho u_1 (2E - u_1^2 - u_2^2) - \partial_{x_2} \rho u_2 (2E - u_1^2 - u_2^2) \\
&\quad + \epsilon \frac{\omega - 2}{2\omega} \left( \partial_{x_1} \left( \left( 1 - \frac{1}{2}u_1^2 + \frac{1}{2}u_2^2 - \frac{3}{2}E - \frac{3}{2}u_1^4 - u_1^2 u_2^2 \right. \right. \right. \\
&\quad \left. \left. \left. + \frac{1}{2}u_2^4 + \frac{3}{2}u_1^2 E - \frac{3}{2}u_2^2 E + E^2 \right) \partial_{x_1} \rho \right. \\
&\quad + (-2u_1 u_2 - 2u_1^3 u_2 - 2u_1 u_2^3 + 3u_1 u_2 E) \partial_{x_2} \rho \\
&\quad + (-\rho u_1 - 7\rho u_1^3 - 3\rho u_1 u_2^2 + 4\rho u_1 E) \partial_{x_1} u_1 \\
&\quad + (-2\rho u_2 - 5\rho u_1^2 u_2 - \rho u_2^3 + 2\rho u_2 E) \partial_{x_2} u_1 \\
&\quad + (\rho u_2 - 3\rho u_1^2 u_2 + \rho u_2^3 - 2\rho u_2 E) \partial_{x_1} u_2 \\
&\quad + (-2\rho u_1 - 3\rho u_1^3 - 7\rho u_1 u_2^2 + 4\rho u_1 E) \partial_{x_2} u_2 \\
&\quad + \left( -\frac{3}{2}\rho + \frac{5}{2}\rho u_1^2 - \frac{1}{2}\rho u_2^2 + \rho E \right) \partial_{x_1} E + 3\rho u_1 u_2 \partial_{x_2} E \Big) \\
&\quad + \partial_{x_2} \left( (-2u_1 u_2 - 2u_1^3 u_2 - 2u_1 u_2^3 + 3u_1 u_2 E) \partial_{x_1} \rho \right. \\
&\quad \left. + \left( 1 + \frac{1}{2}u_1^2 - \frac{1}{2}u_2^2 - \frac{3}{2}E + \frac{1}{2}u_1^4 - u_1^2 u_2^2 \right. \right. \\
&\quad \left. \left. - \frac{3}{2}u_2^4 - \frac{3}{2}u_1^2 E + \frac{3}{2}u_2^2 E + E^2 \right) \partial_{x_2} \rho \right. \\
&\quad + (-2\rho u_2 - 7\rho u_1^2 u_2 - 3\rho u_2^3 + 4\rho u_2 E) \partial_{x_1} u_1 \\
&\quad + (\rho u_1 + \rho u_1^3 - 3\rho u_1 u_2^2 - 2\rho u_1 E) \partial_{x_2} u_1 \\
&\quad + (-2\rho u_1 - \rho u_1^3 - 5\rho u_1 u_2^2 + 2\rho u_1 E) \partial_{x_1} u_2 \\
&\quad + (-\rho u_2 - 3\rho u_1^2 u_2 - 7\rho u_2^3 + 4\rho u_2 E) \partial_{x_2} u_2 \\
&\quad \left. + 3\rho u_1 u_2 \partial_{x_1} E + \left( -\frac{3}{2}\rho - \frac{1}{2}\rho u_1^2 + \frac{5}{2}\rho u_2^2 + \rho E \right) \partial_{x_2} E \right) \Big)
\end{aligned}$$

Again the second momentum density derivative is just the reflection of the first.

## 3.5 Macroscopic Stability of Constructed Examples

We are now concerned with the stability of the discrete dynamics of the constructed examples under a short wave perturbation. Again we are concerned with the stability of the linear part of the dynamics only. Also we again reinforce that this linear macroscopic stability is not equivalent to stability of the complete microscopic dynamics.

### 3.5.1 The Thermal 1D System

Again we perform a stability analysis using the same perturbation for the energy,

$$\begin{aligned}\rho &= \rho_0 + Ae^{i(\lambda t + \kappa x)} \\ u &= u_0 + Be^{i(\lambda t + \kappa x)} \\ E &= E_0 + Ce^{i(\lambda t + \kappa x)}\end{aligned}\tag{3.132}$$

Substituting these perturbations into the macroscopic system we find an order 3 matrix analogously to the two moment case. The characteristic polynomial of the system in  $\lambda$  is

$$\begin{aligned}\lambda^3 + &\left(3u_0\kappa - 5i\nu\kappa^2 + 3i\nu u_0^2\kappa^2 + 3i\nu\kappa^2 E_0\right)\lambda^2 \\ &+ \left(6u_0^2\kappa^2 - 3E_0\kappa^2 + 14i\nu u_0^3\kappa^3 - 6i\nu u_0 E_0\kappa^3\right)\lambda \\ &+ 4u_0^3\kappa^3 + 4i\nu\kappa^4 + 12i\nu u_0^4\kappa^4 - 9i\nu u_0^2 E_0\kappa^4 - 3u_0 E_0\kappa^3\end{aligned}\tag{3.133}$$

In this case the stability region for the limit of large  $\kappa$  is simply calculated numerically. The graph of this stability region is given in Figure 3.9. For some other parameter values we can also plot the stability numerically, these are given in Fig-

ures 3.7,3.8. We can speculate a little on the causes of the shape shown in Figure

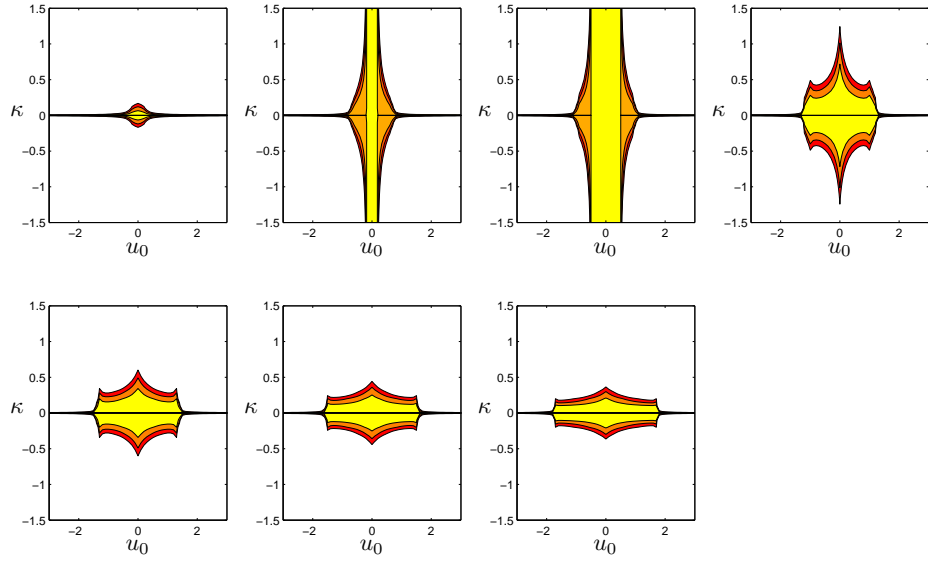


Figure 3.7: Regions of stability for the thermal 1D system. Contours are plotted at  $\Im(\lambda) = (-0.3, -0.2, -0.1, 0)$ , therefore the yellow region and its boundary indicate the stable region and, the other colours, the decay from stability. The parameters for the plots are  $\nu = 1$  and additionally **a)**  $E_0 = 0$ ; **b)**  $E_0 = 0.5$ ; **c)**  $E_0 = 1$ ; **d)**  $E_0 = 1.5$ ; **e)**  $E_0 = 2$ ; **f)**  $E_0 = 2.5$ ; **g)**  $E_0 = 3$ .

3.9. The two main sources of instability are possibly down to negative diffusivity for larger mach numbers on the  $u_0$  axis versus sound speeds which the discrete velocity system cannot support on the  $E_0$  axis.

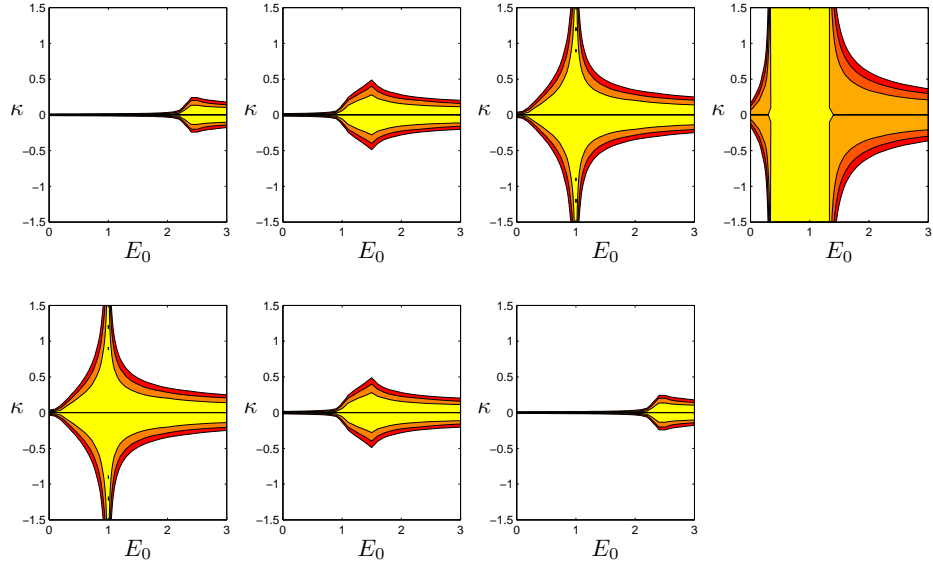


Figure 3.8: Regions of stability for the thermal 1D system. Contours are plotted at  $\Im(\lambda) = (-0.3, -0.2, -0.1, 0)$ , therefore the yellow region and its boundary indicate the stable region and, the other colours, the decay from stability. The parameters for the plots are  $\nu = 1$  and additionally **a)**  $u_0 = -1.5$ ; **b)**  $u_0 = -1$ ; **c)**  $u_0 = -0.5$ ; **d)**  $u_0 = 0$ ; **e)**  $u_0 = 0.5$ ; **f)**  $u_0 = 1$ ; **g)**  $u_0 = 1.5$ .

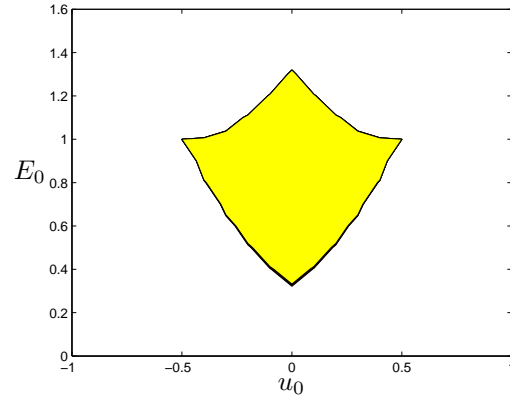


Figure 3.9: Regions of stability for the thermal 1D system. Contours are plotted at  $\Im(\lambda) = (-0.3, -0.2, -0.1, 0)$ , therefore the yellow region and its boundary indicate the stable region and, the other colours, the decay from stability. The parameters are  $\nu = 1$  and  $\kappa \rightarrow \infty$ .

### 3.6 The Thermal 2D system

We again extend the stability analysis with the addition of a perturbation from constant energy.

$$\begin{aligned} \rho &= \rho_0 + A e^{i(\lambda t + \kappa_1 x_1 + \kappa_2 x_2)} \\ u_1 &= u_{10} + B_1 e^{i(\lambda t + \kappa_1 x_1 + \kappa_2 x_2)} \\ u_2 &= u_{20} + B_2 e^{i(\lambda t + \kappa_1 x_1 + \kappa_2 x_2)} \\ E &= E_0 + C e^{i(\lambda t + \kappa_1 x_1 + \kappa_2 x_2)} \end{aligned} \quad (3.134)$$

In Figure (3.10) we vary  $\kappa_2$  and  $u_{20}$  with a fixed energy level to see what affect this has on the stability region. For this example we find that an energy level of 0.75 is in the centre of the most stable region. In Figure (3.11) we vary  $\kappa_1$  and  $u_{20}$  across the

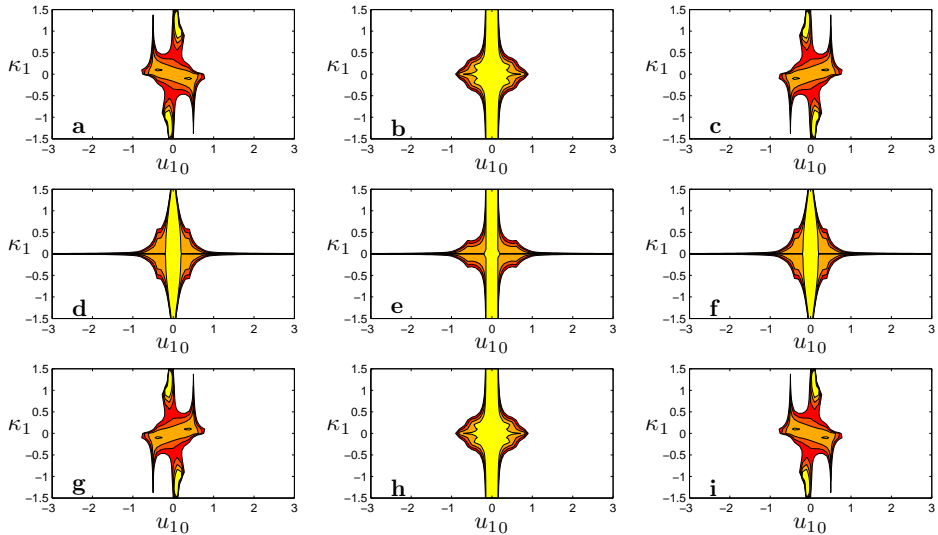


Figure 3.10: Stability regions for the thermal 8 velocity 2D system. Contours are plotted at  $\Im(\lambda) = (-0.3, -0.2, -0.1, 0)$ , the yellow region and its boundary indicate the stable region and, the other colours, the decay from stability. The parameters are  $E_0 = 0.75$ ,  $\nu = 1$  and additionally **a)**  $\kappa_2 = -0.1, u_{20} = -0.5$ ; **b)**  $\kappa_2 = -0.1, u_{20} = 0$ ; **c)**  $\kappa_2 = -0.1, u_{20} = 0.5$ ; **d)**  $\kappa_2 = 0, u_{20} = -0.5$ ; **e)**  $\kappa_2 = 0, u_{20} = 0$ ; **f)**  $\kappa_2 = 0, u_{20} = 0.5$ ; **g)**  $\kappa_2 = 0.1, u_{20} = -0.5$ ; **h)**  $\kappa_2 = 0.1, u_{20} = 0$ ; **i)**  $\kappa_2 = 0.1, u_{20} = 0.5$ .

different plots. We also plot the effects of varying the energy constant  $E_0$ . Finally

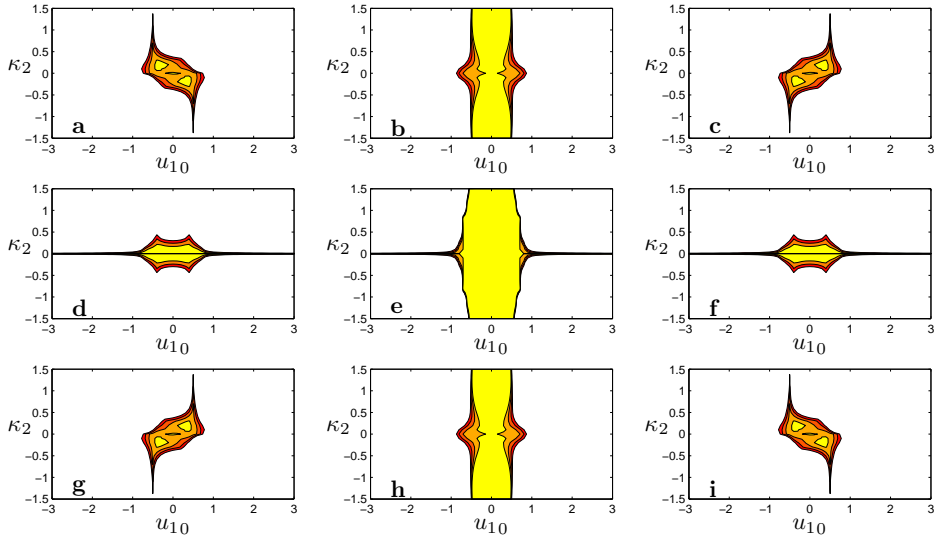


Figure 3.11: Stability regions for the thermal 8 velocity 2D system. Contours are plotted at  $\Im(\lambda) = (-0.3, -0.2, -0.1, 0)$ , the yellow region and its boundary indicate the stable region and, the other colours, the decay from stability. The parameters are  $E_0 = 0.75, \nu = 1$  and additionally **a)**  $\kappa_1 = -0.1, u_{20} = -0.5$ ; **b)**  $\kappa_1 = -0.1, u_{20} = 0$ ; **c)**  $\kappa_1 = -0.1, u_{20} = 0.5$ ; **d)**  $\kappa_1 = 0, u_{20} = -0.5$ ; **e)**  $\kappa_1 = 0, u_{20} = 0$ ; **f)**  $\kappa_1 = 0, u_{20} = 0.5$ ; **g)**  $\kappa_1 = 0.1, u_{20} = -0.5$ ; **h)**  $\kappa_1 = 0.1, u_{20} = 0$ ; **i)**  $\kappa_1 = 0.1, u_{20} = 0.5$ .

we again plot the short wave asymptotics of the system with varying energy levels.

Figure 3.13 along with Figure 3.12 indicates that there is an energy interval where the first order manifold is stable at zero velocity. Below  $E_0 = 0.5$  there exists no stable region in the limit of  $|\kappa_1|, |\kappa_2|$  being large, above  $E_0 = 1$  such regions exist but they do not include the zero velocity region of parameter space.

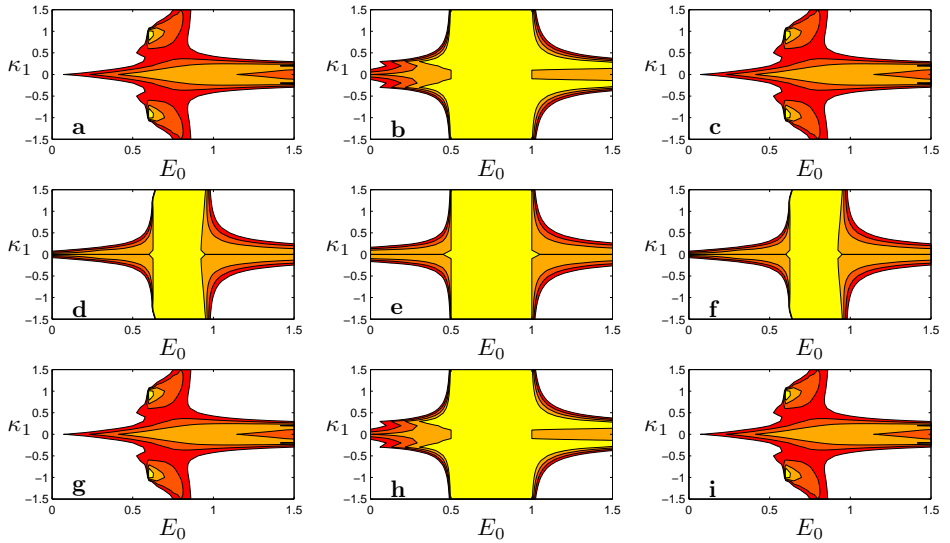


Figure 3.12: Stability regions for the thermal 8 velocity 2D system. Contours are plotted at  $\Im(\lambda) = (-0.3, -0.2, -0.1, 0)$ , the yellow region and its boundary indicate the stable region and, the other colours, the decay from stability. The parameters are  $u_{10} = 0, \nu = 1$  and additionally **a**)  $\kappa_2 = -0.1, u_{20} = -0.5$ ; **b**)  $\kappa_2 = -0.1, u_{20} = 0$ ; **c**)  $\kappa_2 = -0.1, u_{20} = 0.5$ ; **d**)  $\kappa_2 = 0, u_{20} = -0.5$ ; **e**)  $\kappa_2 = 0, u_{20} = 0$ ; **f**)  $\kappa_2 = 0, u_{20} = 0.5$ ; **g**)  $\kappa_2 = 0.1, u_{20} = -0.5$ ; **h**)  $\kappa_2 = 0.1, u_{20} = 0$ ; **i**)  $\kappa_2 = 0.1, u_{20} = 0.5$ .

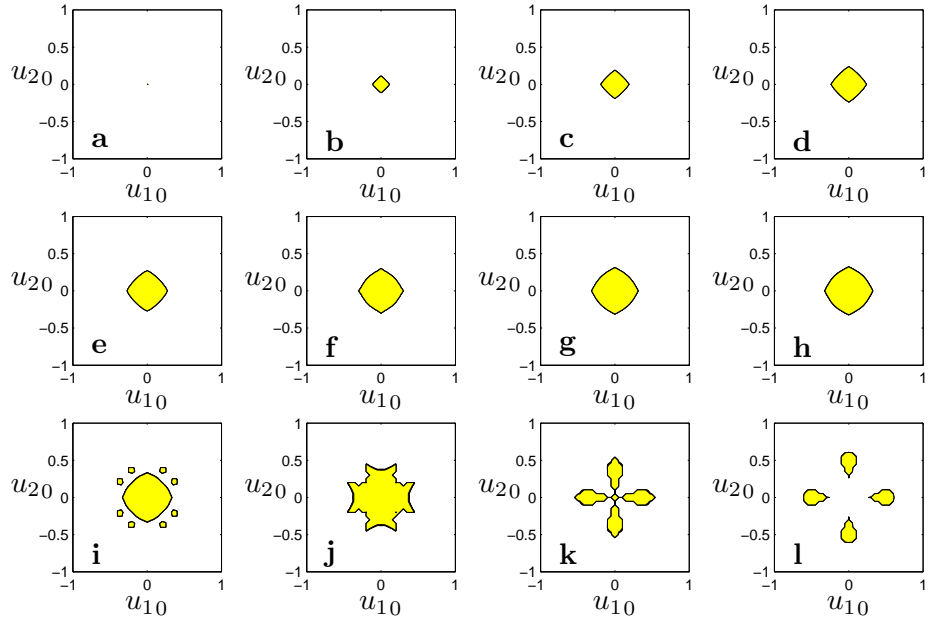


Figure 3.13: Stability regions for the thermal 8 velocity 2D system. Contours are plotted at  $\Im(\lambda) = (-0.3, -0.2, -0.1, 0)$ , the yellow region and its boundary indicate the stable region and, the other colours, the decay from stability. The parameters are large  $\kappa_1, \kappa_2$  and additionally **a)**  $E_0 = 0.5$ ; **b)**  $E_0 = 0.55$ ; **c)**  $E_0 = 0.6$ ; **d)**  $E_0 = 0.65$ ; **e)**  $E_0 = 0.7$ ; **f)**  $E_0 = 0.75$ ; **g)**  $E_0 = 0.8$ ; **h)**  $E_0 = 0.85$ ; **i)**  $E_0 = 0.9$ ; **j)**  $E_0 = 0.95$ ; **k)**  $E_0 = 1$ ; **l)**  $E_0 = 1.05$ .

# Chapter 4

## Generalizations of BGK

In order to improve the stability of lattice Boltzmann methods, some generalizations of the BGK collision operation have been proposed. In this section a brief description of these enhancements is made.

### 4.1 ELBM

In the continuous case the Maxwellian distribution maximizes entropy, as measured by the Boltzmann  $H$  function. In the context of lattice Boltzmann methods a discrete form of the  $H$ -theorem has been suggested as a way to introduce thermodynamic control to the system [7, 41, 42].

From this perspective the goal is to find an equilibrium state equivalent to the Maxwellian in the continuum which will similarly maximize entropy. Before the equilibrium can be found an appropriate  $H$  function must be known for a given lattice. These functions have been constructed in a lattice dependent fashion in [38], and  $H = -S$  with  $S$  from (4.2) is an example of a  $H$  function constructed in this way.

One way to implement an ELBM is as a variation on the LBGK, known as

the ELBGK [2]. The BGK operation 2.9 has its single coefficient  $\omega$  replaced by a composite coefficient  $\alpha\beta$ ,

$$f_i \mapsto f_i + \alpha\beta(f_i^{\text{eq}} - f_i). \quad (4.1)$$

In this case  $\beta$  is used to manipulate the viscosity and  $\alpha$  is varied to ensure a constant entropy condition according to the discrete  $H$ -theorem. In general the entropy function is based upon the lattice and cannot always be found explicitly. However for some examples such as the simple one dimensional lattice with velocities  $\mathbf{v} = (-c, 0, c)$  and corresponding populations  $\mathbf{f} = (f_-, f_0, f_+)$  an explicit Boltzmann style entropy function is known [38]:

$$S(\mathbf{f}) = -f_- \log(f_-) - f_0 \log(f_0/4) - f_+ \log(f_+). \quad (4.2)$$

With knowledge of such a function  $\alpha$  is found as the non-trivial root of the entropic involution equation,

$$S(\mathbf{f}) = S(\mathbf{f} + \alpha(\mathbf{f}^{\text{eq}} - \mathbf{f})), \quad (4.3)$$

finding this root may be called ‘performing the involution’. The trivial root  $\alpha = 0$  returns the entropy value of the original populations. ELBGK then finds the non-trivial  $\alpha$  such that (4.3) holds. This version of the BGK collision one calls entropic BGK (or EBGK) collision. A solution of (4.3) must be found at every time step and lattice site. Entropic equilibria (also derived from the  $H$ -theorem) are always used for ELBGK.

The definition of ELBM for a given entropy equation (4.3) is incomplete. First of all, it is possible that the non-trivial solution does not exist. Moreover, for most of the known entropies (like the perfect entropy [38]) there always exist such  $\mathbf{f}$  that the equation (4.3) for the ELBM collision has no non-trivial solutions. These  $\mathbf{f}$  should

be sufficiently far from equilibrium. For completeness, every user of ELBM should define collisions when the non-trivial root of (4.3) does not exist. We know two rules for this situation:

1. The most radical approach gives the Ehrenfest rule [8, 22, 29, 27]: "if the solution does not exist then go to equilibrium", i.e. if the solution does not exists then take  $\alpha = 1$ .
2. The most gentle solution gives the "positivity rule" [10, 50, 64, 59]: to take the maximal value of  $\alpha$  that guarantees  $f_i + \alpha(f_i^{\text{eq}} - f_i) \geq 0$  for all  $i$ .

In general, the Ehrenfest rule prescribes to send the most non-equilibrium sites to equilibrium and the positivity rule is applied for any LBM as a recommendation to substitute the non-positive vectors  $\mathbf{f}$  by the closest non-negative on the interval of the straight line  $[\mathbf{f}, \mathbf{f}^{\text{eq}}]$  that connects  $\mathbf{f}$  to equilibrium. These rules give the examples of the pointwise LBM limiter and we discuss them separately.

It is possible demonstrate the population function values where the involution cannot be performed for some simple examples. We study the entropic involution in the distribution simplex  $\Sigma$  given by  $\sum f_i = \text{const} > 0$ ,  $f_i \geq 0$ . We demonstrate for some simple examples that the simplex of distributions can be split into two subsets  $A$  and  $B$ : in the set  $A$  the entropic involution exists, and for distributions from the set  $B$  equation (4.3) has no non-trivial solutions.

These examples uses the standard 1-D lattice with the discrete entropy function given in Eq 4.2. The first example is an LBM with only one conserved moment in collision, namely density. The equilibrium is  $f_-^{\text{eq}} = \frac{\rho}{6}$ ,  $f_0^{\text{eq}} = \frac{2\rho}{3}$ ,  $f_+^{\text{eq}} = \frac{\rho}{6}$ .

In Fig. 4.1, the simplex  $\Sigma$  of positive populations with a fixed density  $\rho = 1$  is the triangle given by the intersection of three half-planes,  $f^+ > 0$ ,  $f^- > 0$ , and  $1 - f^+ - f^- > 0$ . Within that region we plot several entropy level contours  $S(\mathbf{f}) = c$  and the unique equilibrium point. The region is divided into the parts where the

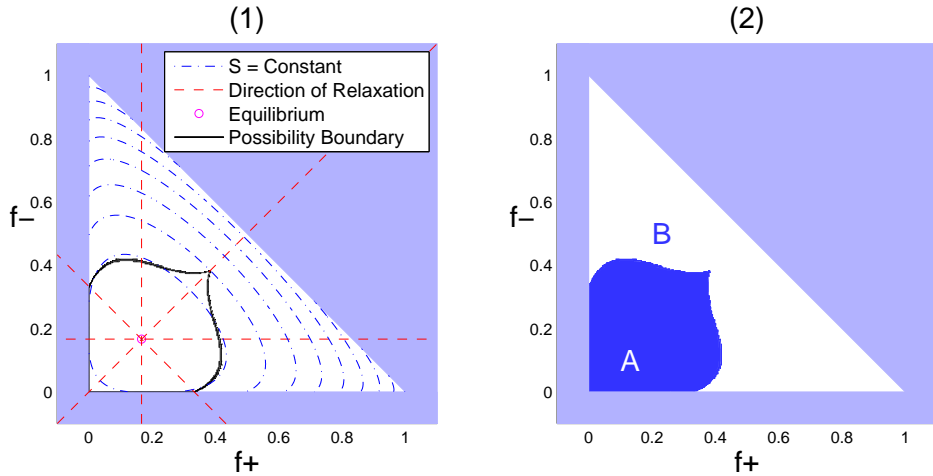


Figure 4.1: The simplex  $\Sigma$  is given by the white background. (1) Populations relax through the equilibrium given by the single point to an equal entropy point, if possible. The boundary of this possibility is given. (2) The regions  $A$  (the entropic involution is possible) and  $B$  (the involution is impossible) as subsets of the simplex divided by this boundary are presented.

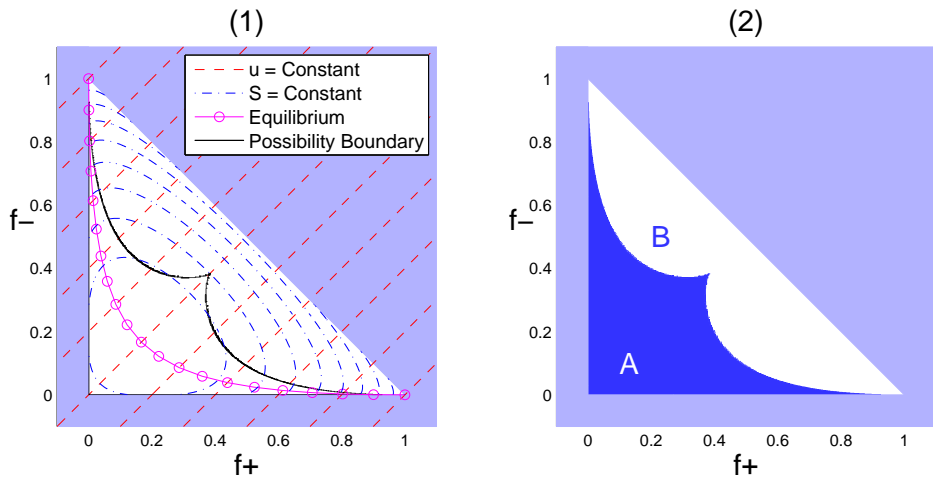


Figure 4.2: The simplex  $\Sigma$  is given by the white background. (1) Populations relax through their corresponding equilibrium point along the line given by constant  $u$  to an equal entropy point, if possible. The boundary of this possibility is given. (2) The regions  $A$  and  $B$  separated by this boundary are presented.

entropic involution is possible (around the equilibrium) and where it is impossible.

A more common use of lattice Boltzmann involves a second fixed moment, momentum. The entropic equilibria used by the ELBGK are available explicitly as the maximum of the entropy function (4.2),

$$f_{\mp}^{\text{eq}} = \frac{\rho}{6}(\mp 3u - 1 + 2\sqrt{1+3u^2}), \quad f_0^{\text{e}} = \frac{2\rho}{3}(2 - \sqrt{1+3u^2}). \quad (4.4)$$

In this case the dimension of the equilibrium is one greater. In Fig. 4.2 all relaxation occurs parallel to the lines of constant  $u$ . The region where entropic involution is possible is again given.

In each experiment the region is discretized into many individual points. For each point a value for  $\alpha$  is attempted to be found. The method used is simply to begin with a guess of  $\alpha = 1$  and then add increments of  $10^{-3}$  until a solution of Eq. 4.3 occurs, or the edge of the positivity domain is reached. This method would be inappropriate to use in a usual ELBM, due to the very large computational cost, but it is very robust and hence useful for this experiment with many highly non-equilibrium distributions. Another approach (with the same result) implies calculation of the entropic involution for all the boundary points where it exists. In this method we draw a straight line  $l$  through a boundary point  $\mathbf{f}$  and the equilibrium and find the intersection  $l \cap \Sigma$  which consists of all points on  $l$  with non-negative coordinates. One end of this interval is  $\mathbf{f}$ , another end is also a boundary point,  $\mathbf{f}'$ . The entropic involution for  $\mathbf{f}$  exists if and only if  $S(\mathbf{f}') \leq S(\mathbf{f})$ . After we check this inequality, we can solve Eq. (4.3). The images of these involutions form the border that separates sets  $A$  and  $B$  (see Figs).

Another source for additional dissipation in the ELBM may be the numerical method used for the solution of (4.3). For the full description of ELBM we have to select a numerical method for this equation. This method has to have an uniform

accuracy in the wide range of parameters, for all possible deviation from equilibrium (distribution of these deviations has “heavy tails” [10]).

In order to investigate the stabilization properties of ELBGK it is therefore necessary to craft a numerical method capable of finding the non-trivial root in (4.3). In this section we fix the population vectors  $\mathbf{f}$  and  $\mathbf{f}^{\text{eq}}$ , and are concerned only with this root finding algorithm. We recast (4.3) as a function of  $\alpha$  only:

$$S_f(\alpha) = S(\mathbf{f} + \alpha(\mathbf{f}^{\text{eq}} - \mathbf{f})) - S(\mathbf{f}). \quad (4.5)$$

In this setting we attempt to find the non-trivial root  $r$  of (4.5) such that  $S_f(r) = 0$ . It should be noted that as we search for  $r$  numerically we should always take care that the approximation we use is less than  $r$  itself. An upper approximation could result in negative entropy production. A simple algorithm for finding the roots of a concave function, based on local quadratic approximations to the target function, has cubic convergence order. Assume that we are operating in a neighbourhood  $r \in N$ , in which  $S'_f$  is negative (as well of course  $S''_f$  is negative). At each iteration the new estimate for  $r$  is the greater root of the parabola  $P$ , the second order Taylor polynomial at the current estimate. Analogously to the case for Newton iteration, the constant in the estimate is the ratio of third and first derivatives in the interval of iteration:

$$\begin{aligned} |(r - \alpha_{n+1})| &\leq C|\alpha_n - r|^3, \\ \text{where } C &= \tfrac{1}{6} \sup_{a \in N} |S'''_f(a)| / \inf_{b \in N} |S'_f(b)|, \end{aligned}$$

where  $\alpha_n$  is the evaluation of  $r$  on the  $n$ th iteration.

We use a Newton step to estimate the accuracy of the method at each iteration:

because of the concavity of  $S$

$$|\alpha_n - r| \lesssim |S_f(\alpha_n)/S'_f(\alpha_n)|. \quad (4.6)$$

In fact we use a convergence criteria based not solely on  $\alpha$  but on  $\alpha||\mathbf{f}^{\text{eq}} - \mathbf{f}||$ , this has the intuitive appeal that in the case where the populations are close to the local equilibrium, then non equilibrium entropy,

$$\Delta S = S(\mathbf{f}^{\text{eq}}) - S(\mathbf{f}), \quad (4.7)$$

will be small and a very precise estimate of  $\alpha$  is unnecessary. We have some freedom in the choice of the norm used and we select between the standard  $L_1$  norm and the entropic norm. The entropic norm is defined as

$$||\mathbf{f}^{\text{eq}} - \mathbf{f}||_{\mathbf{f}^{\text{eq}}} = -((\mathbf{f}^{\text{eq}} - \mathbf{f}), D^2 S|_{\mathbf{f}^{\text{eq}}} (\mathbf{f}^{\text{eq}} - \mathbf{f})),$$

where  $D^2 S|_{\mathbf{f}^{\text{eq}}}$  is the second differential of entropy at point  $\mathbf{f}^{\text{eq}}$ , and  $(x, y)$  is the standard scalar product.

The final root finding algorithm then is beginning with the LBGK estimate  $x_0 = 2$  to iterate using the roots of successive parabolas. We stop the method at the point,

$$|\alpha_n - r| \cdot ||\mathbf{f}^{\text{eq}} - \mathbf{f}|| < \epsilon. \quad (4.8)$$

To ensure that we use an estimate that is less than the root, at the point where the method has converged we check the sign of  $S_f(\alpha_n)$ . If  $S_f(\alpha_n) > 0$  then we have achieved a lower estimate, if  $S_f(\alpha_n) < 0$  we correct the estimate to the other side of

the root with a double length Newton step,

$$\alpha_n = \alpha_n - 2 \frac{S_f(\alpha_n)}{S'_f(\alpha_n)}. \quad (4.9)$$

At each time step before we begin root finding we eliminate all sites with  $\Delta S < 10^{-15}$ . For these sites we make a simple LBGK step. At such sites we find that round off error in the calculation of  $S_f$  by solution of equation (4.3) can result in the root of the parabola becoming imaginary. In such cases a mirror image given by LBGK is effectively indistinct from the exact ELBGK collision. Using this criteria, in the numerical examples given in this work the case where the non-trivial root of the entropy parabola does not exist was not encountered.

## 4.2 Entropic Limiting

The single relaxation time limiters reviewed in this section [10] vary the size but not shape of the non-equilibrium dynamics on a pointwise basis. They may be implemented as a post process to the collision operation as an additional contraction towards equilibrium,

$$\mathbf{f} \mapsto \mathbf{f}^{\text{eq}} + \lambda(\mathbf{f} - \mathbf{f}^{\text{eq}}), \quad 0 \leq \lambda < 1. \quad (4.10)$$

Just as the BGK collision cannot alter the macroscopic moments (as  $m(\mathbf{f}) = m(\mathbf{f}^{\text{eq}})$ ) so neither can a limiter of this form.

An easily understandable introduction to this concept is the idea of a positivity filter[9, 50, 59, 64]. If we understand the population function to physically represent the density of particles moving with a certain velocity then we should expect that these densities should be non-negative. If a collision operation produces a negative value of a population function then the distribution should return in the direction

of the equilibrium until all population values become non-negative. In the context of Eq 4.10 this entails finding the greatest value of  $\lambda$  such that the map produces non-negative populations.

Another logic for the use of a filter of this type is not to manage the signs of the populations but simply their distance from equilibrium. Obviously there are a number of reasonable choices for a metric to use for this distance. In this work the one used is the non-equilibrium entropy (Eq. 4.7). Where the non-equilibrium entropy is large, above a certain threshold, then an entropic limiter can be applied. One option is to equilibrate the populations using an Ehrenfest's Step[22, 29, 8]. In the setting of Eq 4.10 this corresponds to setting  $\lambda = 0$ . We can also choose  $\lambda$  dynamically.

The prescription for ‘Median Filtering’ is given in [10]. First for a given site  $\mathbf{x}$  we calculate the value of  $\Delta S(x)$ , and call this value  $\Delta S_x$ . If the value of  $\Delta S_x$  is above the thresholds, we find the median value of  $\Delta S$  in some local neighbourhood surrounding  $\mathbf{x}$  including itself, calling this value  $\Delta S_{med}$ . Now the post process Eq. 4.7 is applied with  $\lambda$  selected by  $\sqrt{\Delta S_{med}/\Delta S_x}$ . A standard choice of the local neighbourhood are the sites linked directly with the site to be filtered by a discrete velocity.

Most lattice Boltzmann models, which we consider to be defined by the choice of velocity set and local equilibrium, are not entropic and hence do not have an entropy function [67, 68]. In such a situation the Kullback relative entropy function [43],

$$S_K(\mathbf{f}) = \sum_i f_i \ln \left( \frac{f_i}{f_i^{\text{eq}}} \right), \quad (4.11)$$

may be used to complete the definition of  $\Delta S$ .

## 4.3 MRT

Multiple Relaxation Times (MRT) has been proposed as a generalization from the BGK collision operation[18, 16, 19, 20, 21, 46, 47], where the additional degrees of freedom arising from a symmetric velocity set are exploited to introduce varying levels of dissipation on different modes of the system. This class of techniques can include methods which do not self identify as MRT but exhibit the same idea of exploiting extra degrees of freedom in the system [17, 25, 36, 40, 45, 54, 55]. Usually this involves a change of basis for the collision operation, the change of basis matrix can be denoted  $M$ . In this new basis a diagonal relaxation matrix  $\Omega$  can be used to relax the different modes independently before the change of basis is reverted, we define the composite matrix  $A = M^{-1}\Omega M$  and the MRT collision operation,

$$\mathbf{f} \mapsto \mathbf{f} + A(\mathbf{f}^{\text{eq}} - \mathbf{f}). \quad (4.12)$$

The choice of which basis  $M$  is ‘best’ is not obvious. Several components of the basis are necessary, in particular the macroscopic moments should form a part of the basis. The next components of the basis should be chosen to implement the viscous stress in the Navier Stokes equations. The most interesting selection is the completion of the basis following this, corresponding to the post Navier-Stokes quantities.

To consider a choice of basis it is instructive to imagine the collision operation as a reduction in the non-equilibrium volume of a system. If for example we have a 9 velocity system with 3 conserved macroscopic moments then this non-equilibrium volume is 6-dimensional. For the single relaxation time BGK operation this volume shrinks uniformly along any axis passing through the equilibrium. MRT allows us the possibility to shrink this volume independently along different axes, the choice of the MRT basis is equivalent to the choice of these axes. If the higher order modes

are equilibrated at every time step then that component of the volume is removed entirely during any collision. When we are concerned with dynamically shrinking this volume however the choice of basis becomes especially important. We would like to choose a basis which will target the non-physical oscillations in the system.

One way to make use of the extra degrees of freedom is to take a different approach from Eq 4.12. Rather than using a different collision operator, a different equilibrium can be built [36, 40, 45, 54, 55]. The new equilibrium contains extra terms which in the macroscopic equations give rise to the Navier-Stokes viscous stress terms. With the use of such an equilibrium the collision operation can chosen to simply go to equilibrium each time step. Although the literature around these methods does not describe it as such, using an LBM of this type corresponds to deleting the component of the post Navier-Stokes dynamics which is spanned by the velocity set.

Our computational examples will be calculated on the D2Q9 lattice, usually with the standard polynomial equilibrium, the dynamics of which were explored earlier in Section 3.1.3,

$$f_i^{\text{eq}} = w_i \rho \left( 1 + 3\mathbf{v}_i \cdot \mathbf{u} + \frac{9}{2}(\mathbf{v}_i \cdot \mathbf{u})^2 - \frac{3}{2}\mathbf{u}^2 \right), \quad (4.13)$$

$$w_i = \left\{ \frac{4}{9}, \frac{1}{9}, \frac{1}{9}, \frac{1}{9}, \frac{1}{9}, \frac{1}{36}, \frac{1}{36}, \frac{1}{36}, \frac{1}{36} \right\}. \quad (4.14)$$

In one later test we use ELBM, in that case we use an entropic equilibrium which is simply the product of two 1D entropic equilibria (Eq 4.4). For convenience we repeat the horizontal and vertical components of the velocity set here,

$$\begin{aligned} v_{x_1} &= (0, 1, 0, -1, 0, 1, -1, -1, 1) \\ v_{x_2} &= (0, 0, 1, 0, -1, 1, 1, -1, -1). \end{aligned} \quad (4.15)$$

### 4.3.1 Lallemand and Luo's MRT

One choice of basis which has been suggested is an  $\ell_2$  orthogonal extension of the macroscopic moments made by cross powers of the velocity set [20, 21, 46, 47].

This basis is chosen to represent specific macroscopic quantities and in our velocity system is as follows,

$$M_1 = \begin{pmatrix} 1 & 1 & 1 & 1 & 1 & 1 & 1 & 1 & 1 \\ -4 & -1 & -1 & -1 & -1 & 2 & 2 & 2 & 2 \\ 4 & -2 & -2 & -2 & -2 & 1 & 1 & 1 & 1 \\ 0 & 1 & 0 & -1 & 0 & 1 & -1 & -1 & 1 \\ 0 & -2 & 0 & 2 & 0 & 1 & -1 & -1 & 1 \\ 0 & 0 & 1 & 0 & -1 & 1 & 1 & -1 & -1 \\ 0 & 0 & -2 & 0 & 2 & 1 & 1 & -1 & 1 \\ 0 & 1 & -1 & 1 & -1 & 0 & 0 & 0 & 0 \\ 0 & 0 & 0 & 0 & 0 & 1 & -1 & 1 & -1 \end{pmatrix} \quad (4.16)$$

As an alternative we could complete the basis simply using higher powers of the velocity vectors, the basis would be  $1, v_x, v_y, v_x^2 + v_y^2, v_x^2 - v_y^2, v_x v_y, v_x^2 v_y, v_x v_y^2, v_x^2 v_y^2$ , in

our velocity system then this change of basis matrix is as follows,

$$M_2 = \begin{pmatrix} 1 & 1 & 1 & 1 & 1 & 1 & 1 & 1 & 1 \\ 0 & 1 & 0 & -1 & 0 & 1 & -1 & -1 & 1 \\ 0 & 0 & 1 & 0 & -1 & 1 & 1 & -1 & -1 \\ 0 & 1 & 1 & 1 & 1 & 2 & 2 & 2 & 2 \\ 0 & 1 & -1 & 1 & -1 & 0 & 0 & 0 & 0 \\ 0 & 0 & 0 & 0 & 0 & 1 & -1 & 1 & -1 \\ 0 & 0 & 0 & 0 & 0 & 1 & -1 & -1 & 1 \\ 0 & 0 & 0 & 0 & 0 & 1 & 1 & -1 & -1 \\ 0 & 0 & 0 & 0 & 0 & 1 & 1 & 1 & 1 \end{pmatrix} \quad (4.17)$$

Once in moment space we can apply a diagonal relaxation matrix  $\Omega_1$  to the populations and then the inverse moment transformation matrix  $M_1^{-1}$  to switch back into population space, altogether  $A_1 = M_1^{-1}\Omega_1 M_1$ . If we use the standard athermal polynomial equilibria then three entries on the diagonal of  $\Omega_1$  are actually not important as the macroscopic moments will be automatically conserved since  $m(\mathbf{f}) = m(\mathbf{f}^{\text{eq}})$ , for simplicity we set them equal to 0 or 1 to reduce the complexity of the terms in the collision matrix. There are 6 more parameters on the diagonal matrix  $\Omega$  which we can set. Three of these correspond to second order moments, one each is required for shear and bulk viscosity which are called  $s_e$  and  $s_\nu$  respectively and one for isotropy. Two correspond to third order moments, one gives a relaxation rate  $s_q$  and again one is needed for isotropy. Finally one is used to give a relaxation rate  $s_\epsilon$  for the single fourth order moment. We have then in total four relaxation

parameters which appear on the diagonal matrix in the following form:

$$\Omega_1 = \begin{pmatrix} 1 & 0 & 0 & 0 & 0 & 0 & 0 & 0 & 0 \\ 0 & s_e & 0 & 0 & 0 & 0 & 0 & 0 & 0 \\ 0 & 0 & s_\epsilon & 0 & 0 & 0 & 0 & 0 & 0 \\ 0 & 0 & 0 & 1 & 0 & 0 & 0 & 0 & 0 \\ 0 & 0 & 0 & 0 & s_q & 0 & 0 & 0 & 0 \\ 0 & 0 & 0 & 0 & 0 & 1 & 0 & 0 & 0 \\ 0 & 0 & 0 & 0 & 0 & 0 & s_q & 0 & 0 \\ 0 & 0 & 0 & 0 & 0 & 0 & 0 & s_\nu & 0 \\ 0 & 0 & 0 & 0 & 0 & 0 & 0 & 0 & s_\nu \end{pmatrix}. \quad (4.18)$$

Apart from the parameter  $s_\nu$  which is used to control shear viscosity, in an incompressible system the other properties can be varied to improve accuracy and stability. In particular, there exists a variant of MRT known as TRT (two relaxation time) [25] where the relaxation rates  $s_e, s_\epsilon$  are made equal to  $s_\nu$ . In a system with boundaries the final rate is calculated  $s_q = 8(2 - s_\nu)/(8 - s_\nu)$ , this is done, in particular, to regulate numerical slip on the boundaries of the system so that it no longer depends upon the relaxation time  $s_\nu$ .

We should say that in some of the literature regarding MRT the equilibrium is actually built in moment space, that is the collision operation would be written,

$$F(\mathbf{f}) = \mathbf{f} + M_1^{-1}\Omega_1(\mathbf{m}^{\text{eq}} - M_1\mathbf{f}). \quad (4.19)$$

This could be done to increase efficiency, depending on the implementation, however each moment equilibrium  $\mathbf{m}^{\text{eq}}$  has an equivalent population space equilibrium  $\mathbf{f}^{\text{eq}} = M_1^{-1}\mathbf{m}^{\text{eq}}$ , so the results of implementing either system should be the same up to rounding error.

We can also conceive of using an MRT type collision as a limiter, that is to apply it only on a small number of points on the lattice where non equilibrium entropy passes a certain threshold. This answers a criticism of the single relaxation time limiters that they fail to preserve dissipation on physical modes. As well as using the standard MRT form given above we can build an MRT limiter using the alternative change of basis matrix  $M_2$ .

The limiter in this case is based on the idea of sending every mode except shear viscosity directly to equilibrium again the complete relaxation matrix is given by  $A_2 = M_2^{-1}\Omega_2 M_2$  where,

$$\Omega_2 = \begin{pmatrix} 1 & 0 & 0 & 0 & 0 & 0 & 0 & 0 & 0 \\ 0 & 1 & 0 & 0 & 0 & 0 & 0 & 0 & 0 \\ 0 & 0 & 1 & 0 & 0 & 0 & 0 & 0 & 0 \\ 0 & 0 & 0 & 1 & 0 & 0 & 0 & 0 & 0 \\ 0 & 0 & 0 & 0 & s_\nu & 0 & 0 & 0 & 0 \\ 0 & 0 & 0 & 0 & 0 & s_\nu & 0 & 0 & 0 \\ 0 & 0 & 0 & 0 & 0 & 0 & 1 & 0 & 0 \\ 0 & 0 & 0 & 0 & 0 & 0 & 0 & 1 & 0 \\ 0 & 0 & 0 & 0 & 0 & 0 & 0 & 0 & 1 \end{pmatrix}. \quad (4.20)$$

This could be considered a very *aggressive* form of the MRT which maximizes regularization on every mode except shear viscosity and may not be appropriate for general use in a system, especially as the assumption of almost incompressibility is sometimes not adhered to and hence bulk viscosity is not small. Nevertheless it has been applied as a system-wide collision operation [45], in such a context it has also been called ‘regularised collisions’[48]. The advantage of using the different change of basis matrix is that the complete collision matrix  $A_2$  is relatively sparse with just twenty-four off diagonal elements and hence is easy to implement and not

too expensive to compute with. We call this limiter the Aggressive MRT or AMRT limiter.

### 4.3.2 Dellar's MRT

Another choice is to use the basis used by Dellar[16] which has the alternative property of being orthogonal in the weighted inner product given by the quadrature weights. To define the basis completely a supplementary vector is used,

$$g = (1, -2, -2, -2, -2, 4, 4, 4, 4), \quad (4.21)$$

this may be expressed in terms of the velocity set,

$$g_i = 1 - \frac{15}{2}|\mathbf{v}_i|^2 + \frac{9}{2}|\mathbf{v}_i|^4. \quad (4.22)$$

Altogether then the change of basis matrix can be given by a matrix consisting of the 9 following rows, where just in this instance  $I$  represents a row of ones, all vector multiplications are implied elementwise,

$$M = [I; v_{x_1}; v_{x_2}; v_{x_1}^2 - I/3; v_{x_2}^2 - I/3; v_{x_1}v_{x_2}; gv_{x_1}; gv_{x_2}; g]. \quad (4.23)$$

The first three modes in this basis correspond to the conserved macroscopic moments and no relaxation is performed on these modes. In principle the other modes can be modified separately. In practice we use the same relaxation coefficient for the next three modes which together control bulk and shear viscosity. The next two modes are denoted  $\mathbf{J}$  and could be modified to improve stability or give isotropy at the third order, in fact for these modes we just follow Dellar and use the same rate as the hydrodynamic modes. Our use of MRT then is limited to varying the relaxation rate of the final mode consisting of even order components, this mode is denoted  $N$ .

In fact for a numerical implementation it is not necessary to explicitly form the complete change of basis operation. Again following Dellar, as the macroscopic moments are calculated we also calculate the non-hydrodynamic mode we are interested in modifying,

$$N = \sum_{i=1}^n g_i f_i. \quad (4.24)$$

After that the MRT lattice Boltzmann can be implemented,

$$f_i(\mathbf{x} + \epsilon \mathbf{v}_i, t + \epsilon) = f_i(\mathbf{x}, t) + \omega(f_i^{\text{eq}}(\mathbf{x}, t) - f_i(\mathbf{x}, t)) - (\omega_N - \omega)w_i g_i N(\mathbf{x}, t)/4. \quad (4.25)$$

Altogether then, in this version of the MRT we have just two relaxation rate parameters, the standard rate  $\omega$  used to control viscosity and a further parameter separately controlling the relaxation of the ghost mode  $\omega_N$ . Evidently in the case  $\omega = \omega_N$  this system reduces to the standard BGK collision operation.

A popular choice of rate for the ghost mode is to equilibrate it by setting  $\omega_N = 1$  and for the rest of this work doing so will be referred to as the ‘standard’ or ‘usual’ DMRT (Dellar MRT) operation. Since the equilibrium of this mode is zero this corresponds to deleting this component of the dynamics. This could be the most effective choice of parameter in terms of stability, however it may not be without penalty. Despite being orthogonal in the collision this mode is coupled to the hydrodynamics by means of the advection operation. In terms of the macroscopic dynamics this rate affects dissipation at a post Navier-Stokes level.

We are interested in implementing a median filter for the separate modes of the MRT collision operation. In an MRT setting our post-processing operation is given by,

$$f_i \mapsto f_i^{\text{eq}} + \delta(f_i - f_i^{\text{eq}}) + (\delta_N - \delta)w_i g_i N/4. \quad (4.26)$$

Evidently in the case  $\delta = \delta_N$  this reduces to the single relaxation time limiter.

In this setting we have two parameters we may wish to manipulate,  $\delta$  and  $\delta_N$ , and there are a few ideas we can present as to how to utilize them;

1. We can use the standard BGK collision across the system, set  $\delta = 1$  and dynamically choose  $\delta_N$ . This corresponds to not filtering the Navier-Stokes level modes at all, we attempt to locally trim out the oscillations in the ghost mode  $N$ . This is a weaker operation than using a full MRT (which would be equivalent to setting  $\delta_N = 0$  everywhere) but we hope it will be nearly as effective while adding less dissipation.
2. We can use the full MRT collision everywhere and dynamically choose  $\delta$ . This corresponds to equilibrating the ghost mode  $N$  and trimming out oscillations in the other dynamics. This is a stronger operation than the usual MRT and might be appropriate for use at Reynolds numbers where the standard MRT fails to stabilize the system. It also adds dissipation on the hydrodynamic and  $\mathbf{J}$  moments.
3. We can use the BGK collision everywhere and dynamically and separately choose both  $\delta$  and  $\delta_N$ . The rationale for doing so is that we filter all the modes as in the single relaxation time setting, but due to the extra freedom in parameters we can treat separate modes independently. Therefore if oscillations appearing in different modes can be targetted for deletion separately, without adding undue dissipation on all modes.

As  $\delta_N$  controls the dissipation on a single mode it is relatively straightforward to create a strategy to select a value for it. We simply take the ratio of absolute value of the mode to the median absolute value of its neighbours,  $\delta_N = |N|/|N|_{med}$  where  $|N|_{med}$  is the median of the absolute values of  $N$  locally. It is also simple to select which sites to apply the filter at, we simply take the sites where  $|N|$  is above a certain threshold.

Selecting a relaxation for the combined remaining nodes is not so obvious as again there are a number of reasonable choices. We use the quadratic approximation to the non-equilibrium entropy of the populations with the contribution due to  $N$  moment stripped out, we can define an auxiliary set of populations,

$$f_i^* = f_i - w_i g_i N/4. \quad (4.27)$$

Then the non-equilibrium entropy of this component of the dynamics is

$$\Delta S^* = - \sum_i (f_i^* - f_i^{\text{eq}})^2 / f_i^{\text{eq}}. \quad (4.28)$$

So the coefficient  $\delta$  may be calculated as  $\delta = \sqrt{\Delta S_{\text{med}}^*/\Delta S^*}$  where again  $\Delta S_{\text{med}}^*$  is the median value of  $\Delta S^*$  locally.

Due to the differing methods for calculating the post processing coefficients  $\delta$  and  $\delta_N$ , as well as the relative size of the modes, it is not appropriate to use the same threshold for selecting filtering sites. A separate threshold should be chosen for each, which selects a small proportion of the sites for filtering.

# Chapter 5

## Numerical Experiments

In this chapter details of some numerical experiments are given where the effectiveness of the generalizations of LBM in improving stability are tested.

### 5.1 1D Shock Tube

A standard experiment for the testing of LBMs is the one-dimensional shock tube problem. The lattice velocities used are  $\mathbf{v} = (-1, 0, 1)$ , so that space shifts of the velocities give lattice sites separated by the unit distance. 800 lattice sites are used and are initialized with the density distribution

$$\rho(x) = \begin{cases} 1, & 1 \leq x \leq 400, \\ 0.5, & 401 \leq x \leq 800. \end{cases}$$

Initially all velocities are set to zero. We compare the ELBGK equipped with the parabola based root finding algorithm using the entropic norm with the standard LBGK method using both standard polynomial and entropic equilibria. The poly-

nomial equilibria are given in [62, 5]:

$$f_-^{\text{eq}} = \frac{\rho}{6} (1 - 3u + 3u^2), \quad f_0^{\text{eq}} = \frac{2\rho}{3} \left(1 - \frac{3u^2}{2}\right), \\ f_+^{\text{eq}} = \frac{\rho}{6} (1 + 3u + 3u^2).$$

The entropic equilibria also used by the ELBGK are available explicitly as the maximum of the entropy function (4.2),

$$f_-^{\text{eq}} = \frac{\rho}{6} (-3u - 1 + 2\sqrt{1+3u^2}), \quad f_0^{\text{eq}} = \frac{2\rho}{3} (2 - \sqrt{1+3u^2}), \\ f_+^{\text{eq}} = \frac{\rho}{6} (3u - 1 + 2\sqrt{1+3u^2}).$$

Now following the prescription fromm Sec. 4.1 the governing equations for the simulation are

$$f_-(x, t+1) = f_-(x+1, t) + \alpha\beta(f_-^{\text{eq}}(x+1, t) - f_-(x+1, t)), \\ f_0(x, t+1) = f_0(x, t) + \alpha\beta(f_0^{\text{eq}}(x, t) - f_0(x, t)), \\ f_+(x, t+1) = f_+(x-1, t) + \alpha\beta(f_+^{\text{eq}}(x-1, t) - f_+(x-1, t)).$$

From this experiment we observe no benefit in terms of regularization in using the ELBGK rather than the standard LBGK method (Fig. 5.1). In both the medium and low viscosity regimes ELBGK does not supress the spurious oscillations found in the standard LBGK method. The observation is in full agreement with the Tadmor and Zhong [63] experiments for schemes with precise entropy balance.

We also consider regularizing the LBGK method using median filtering at a single point. We follow the prescription detailed in Section 4.2. First, at each time step, we locate the single lattice site  $x$  with the maximum value of  $\Delta S$ . That single site is post processed using the median filter. For this experiment the discrete equilibrium used is the entropic one, hence the standard entropy function is used

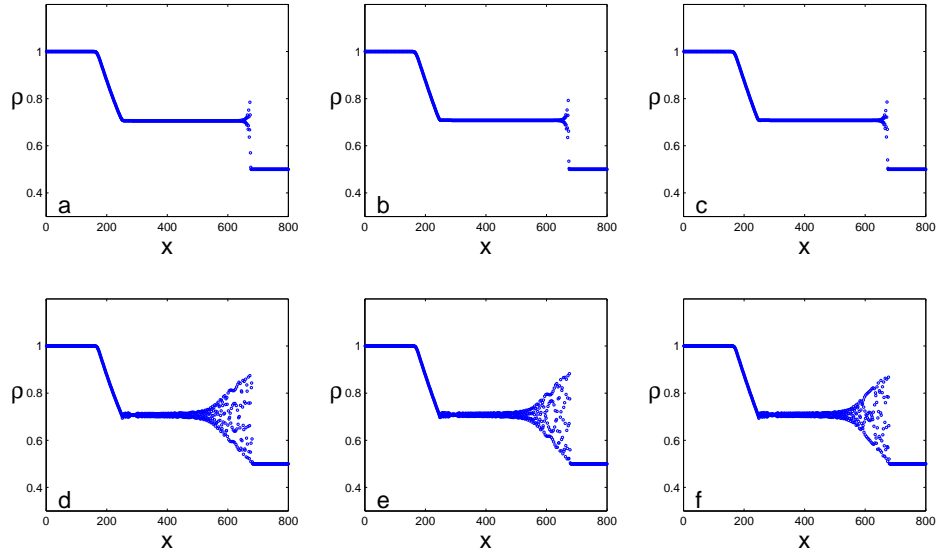


Figure 5.1: Density profile of the simulation of the shock tube problem following 400 time steps using (a) LBGK with polynomial equilibria [ $\nu = (1/3) \cdot 10^{-1}$ ]; (b) LBGK with entropic equilibria [ $\nu = (1/3) \cdot 10^{-1}$ ]; (c) ELBGK [ $\nu = (1/3) \cdot 10^{-1}$ ]; (d) LBGK with polynomial equilibria [ $\nu = 10^{-9}$ ]; (e) LBGK with entropic equilibria [ $\nu = 10^{-9}$ ]; (f) ELBGK [ $\nu = 10^{-9}$ ].

and the Kullback relative entropy function is not needed.

We observe that filtering a single point at each time step still results in a significant amount of regularization (Fig. 5.2).

We also examine in each case the lattice site where the filtering is applied. The zero position is defined as the rightmost lattice site with  $\Delta S > 0$  at each time step and the position of the filtering is measured relative to this site. The occurrences at each relative position are then summed over the experiment. We can see (Fig. 5.3) that the majority of filtering takes place on the shock. However, in the low viscosity case, we observe that at a small number of time steps the filtered site moves significantly ‘behind’ the shockwave.

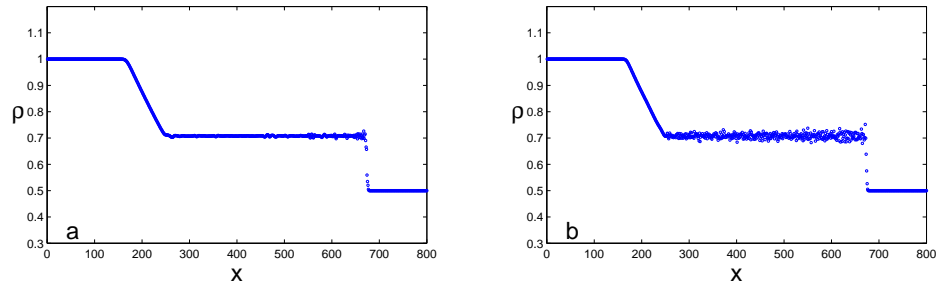


Figure 5.2: Density profile of the simulation of the shock tube problem following 400 time steps using (a) LBGK with entropic equilibria and one point median filtering [ $\nu = (1/3) \cdot 10^{-1}$ ]; (b) LBGK with entropic equilibria and one point median filtering [ $\nu = 10^{-9}$ ].

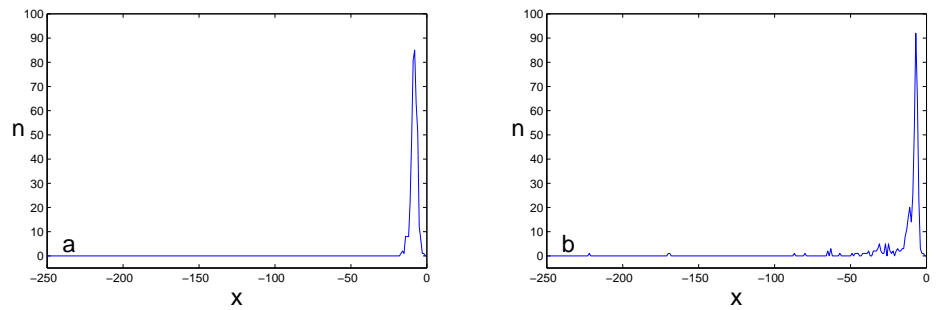


Figure 5.3: Distribution of median filtering sites relative to the position of the shock following 400 time steps using (a) LBGK with entropic equilibria and one point median filtering [ $\nu = (1/3) \cdot 10^{-1}$ ]; (b) LBGK with entropic equilibria and one point median filtering [ $\nu = 10^{-9}$ ].

## 5.2 2D Lid Driven Cavity

Our next 2D example is the benchmark 2D lid driven cavity. This benchmark has already been used for the study lattice Boltzmann methods[1, 37], including in particular for the comparison of collision operations[52]. In this case this is a square system of side length 129. Bounce back boundary conditions are used and the top boundary imposes a constant velocity of  $u_{\text{wall}} = 0.1$ . For a variety of Reynolds numbers we run experiments for up to 10000000 time steps and check which methods have remained stable up until that time step.

The bounce-back boundary conditions for a moving top wall may be implemented by [52],

$$f_i = f_j - 2w_i \rho \frac{v_{i,1} u_{\text{wall}}}{c_s^2}, \quad i = \{4, 7, 8\}, j = \{2, 5, 6\} \quad (5.1)$$

The methods which we test are the standard BGK system, the BGK system equipped with Ehrenfest steps, the BGK system equipped with the MRT limiter, the TRT system, a Lallemand and Luo (L&L) MRT system with the TRT relaxation rate for the third order moment and the other rates  $s_e = 1.64$ ,  $s_\epsilon = 1.54$  and finally an MRT system which we call L&L MRT1 with the rates  $s_q = 1.9s_e = 1.64$ ,  $s_\epsilon = 1.54$  [46]. In each case of the system equipped with limiters the maximum number of sites where the limiter is used is 9.

All methods are equipped with the standard 2nd order compressible quasi-equilibrium, which is available as the product of the 1D equilibria (Eq 5.1).

Additionally we measure Enstrophy  $\mathcal{E}$  in each system over time. Enstrophy is calculated as the sum of vorticity squared across the system, normalized by the number of lattice sites. The vorticity and the stream function are both calculated with second order central differences in lattice units. This statistic is useful as vorticity is theoretically only dissipated due to shear viscosity, at the same time in the lid driven system vorticity is produced by the moving boundary. For these

systems  $\mathcal{E}$  becomes constant as the vorticity field becomes steady. The value of this constant indicates where the *balance* between dissipation and production of vorticity is found. The lower the final value of  $\mathcal{E}$  the more dissipation produced in the system.

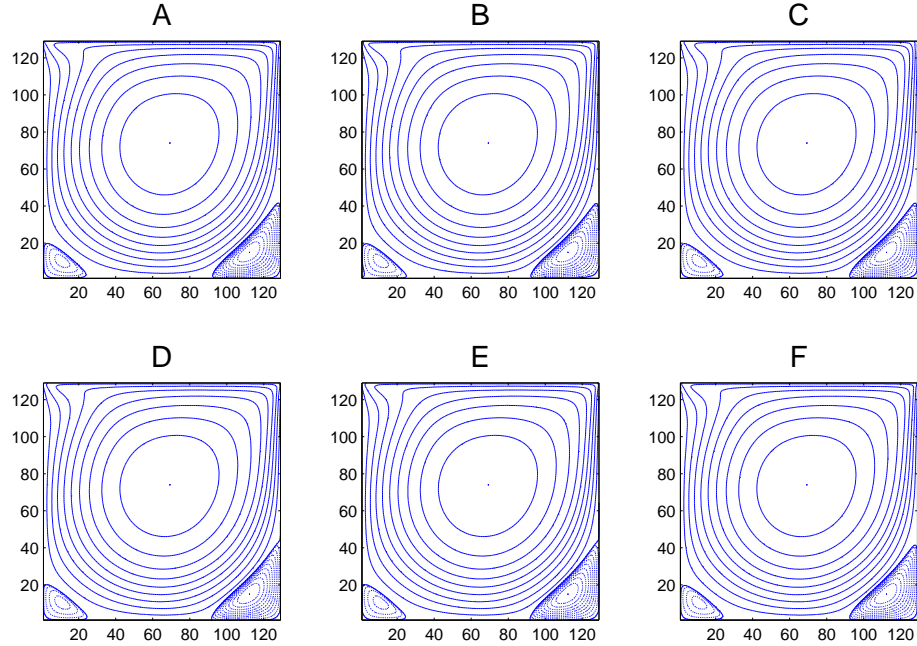


Figure 5.4: Contour plots of stream functions of A: BGK, B: BGK + Ehrenfest Steps, C: BGK + MRT Limiter, D: TRT, E: L&L MRT, F: L&L MRT1 following 10000000 time steps at Re1000 (negative regions in dashed lines).

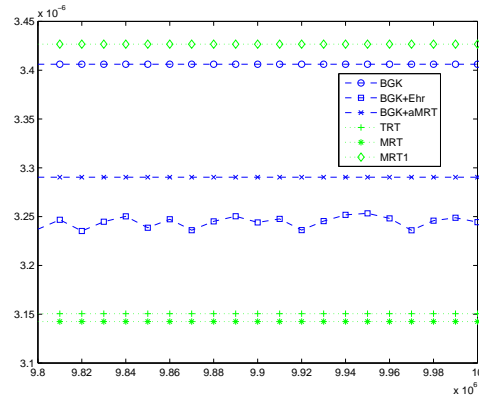


Figure 5.5: Enstrophy in the Re1000 systems during the final  $2 \cdot 10^5$  time steps

All of these systems are stable for Re1000, the contour plots of the final state

are given in Figure 5.4 and there appears only small differences. We calculate the average enstrophy in each system and plot it as a function of time in Figure 5.5. We can see that in the different systems that enstrophy and hence dissipation varies. Compared with the BGK system all the other systems except L&L MRT1 exhibit a lower level of enstrophy indicating a higher rate of dissipation. For L&L MRT1 the fixed relaxation rate of the third order mode is actually less dissipative than the BGK relaxation rate for this Reynolds number, hence the increased enstrophy. An artifact of using the pointwise filtering techniques is that they introduce small scale local oscillations in the modes that they regularize, therefore the system seems not to be asymptotically stable. This might be remedied by increasing the threshold of  $\Delta S$  below which no regularization is performed. Nevertheless in these experiments after sufficient time the enstrophy values remain within a small enough boundary for the results to be useful.

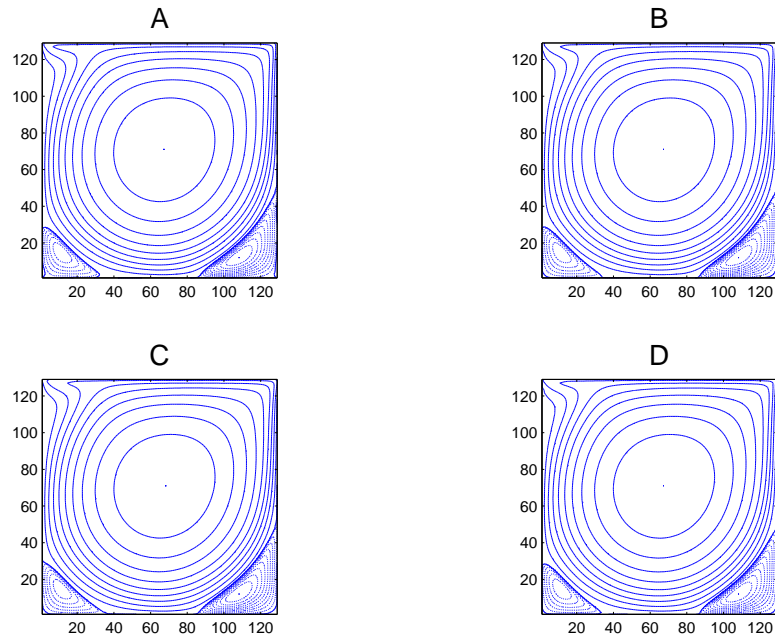


Figure 5.6: Contour plots of stream functions of A: BGK + Ehrenfest Steps, B: BGK + AMRT Limiter, C: TRT, D: L&L MRT1, following 10000000 time steps at Re2500 (negative regions in dashed lines).

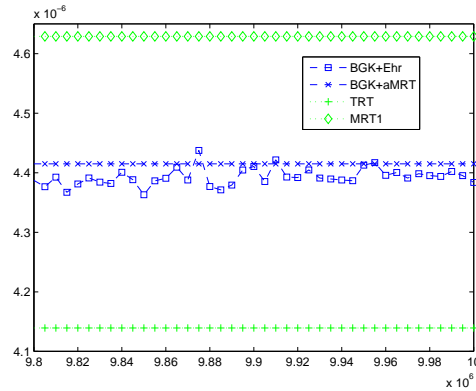


Figure 5.7: Enstrophy in the Re2500 systems during the final  $2 \cdot 10^5$  time steps

The next Reynolds number we choose is Re2500. Only 4 of the original 6 systems complete the full number of time steps for this Reynolds number, the contour plots of the final stream functions are given in Figure 5.6. Of the systems which did not complete the simulation it should be said that the L&L MRT system survived a few 10s of thousands of time steps while the BGK system diverged almost immediately, indicating that it does provide stability benefits which are not apparent at the coarse granularity of Reynolds numbers used in this study. O

Again we check the enstrophy of the systems and give the results for the final timesteps in Figure 5.7. Due to the failure of the BGK system to complete this simulation there is no "standard" result to compare the improved methods with. The surviving methods maintain their relative positions with respect to enstrophy production.

For the theoretical Reynolds number of 5000 only two systems remain, their streamfunction plots are given in Figure 5.8. At this Reynolds number the upper left vortex has appeared in the Ehrenfest limited simulation, however a new discrepancy has arisen. The lower right corner exhibits a very low level of streaming.

In Figure 5.9 the enstrophy during the final parts of the simulation is given. We note that for the first time the L&L MRT1 system produces less enstrophy (is more dissipative) than the BGK system with Ehrenfest limiter.

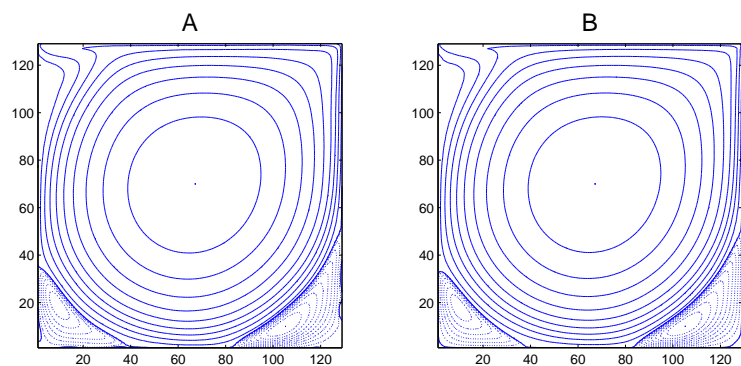


Figure 5.8: Contour plots of stream functions of A: BGK + Ehrenfest Steps, B: L&L MRT1, following 10000000 time steps at Re2500 (negative regions in dashed lines).

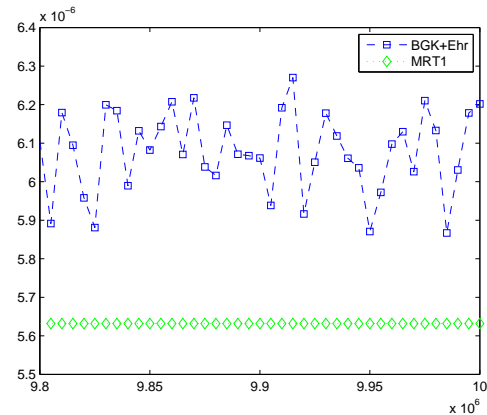


Figure 5.9: Enstrophy in the Re5000 systems during the final  $2 \cdot 10^5$  time steps

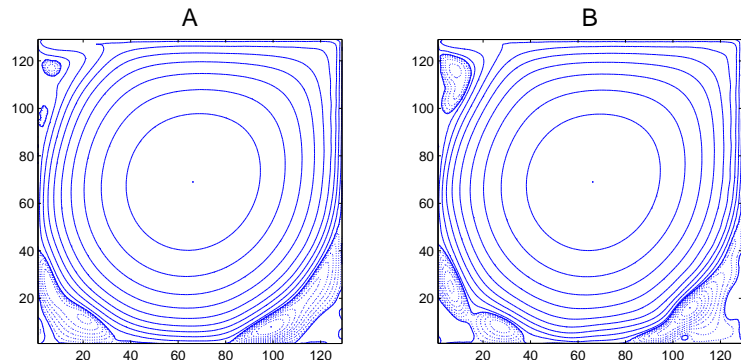


Figure 5.10: Contour plots of stream functions of A: Re7500 and B: Re10000 BGK + Ehrenfest systems, following 10000000 time steps at Re5000 (negative regions in dashed lines).

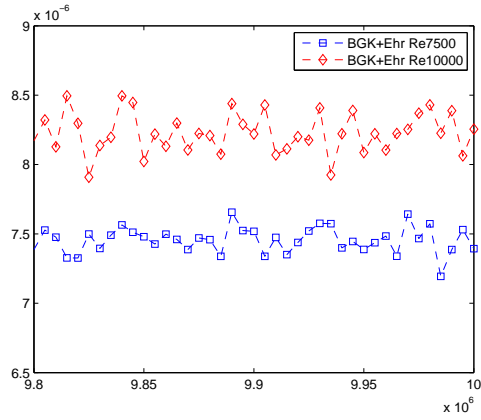


Figure 5.11: Enstrophy in the Re7500 and Re10000 BGK + Ehrenfest systems during the final  $2 \cdot 10^5$  time steps

For the final two Reynolds numbers we use, 7500 and 10000, only the BGK system with the Ehrenfest limiter completes the simulation. The corresponding streamfunction plots are given in Figure 5.10 and they exhibit multiple vortices in the corners of the domain.

The enstrophy plots are given in Figure 5.11, as the theoretical Reynolds number increases so does the level of enstrophy.

### 5.2.1 First Hopf Bifurcation

As we have seen the moving lid boundary condition drives the formation of vortices, which for low Reynolds numbers form a steady state and, for high Reynolds numbers, periodic or chaotic results. This transition begins with a Hopf bifurcation where the steady state evolves into a periodic flow, and localizing this bifurcation will be our goal in this section. This offers an alternative method of measuring dissipation in the system, the more artificial dissipation is produced, the higher the Reynolds number at which the bifurcation is observed.

In this study we use diffusive boundary conditions [3, 12]. The essence of the condition is that populations reaching a boundary are reflected, proportional to

equilibrium, such that mass-balance (in the bulk) and detail-balance are achieved. The boundary condition coincides with ‘bounce-back’ in each corner of the cavity.

To illustrate, immediately following the advection of populations consider the situation of a wall, aligned with the lattice, moving with tangential velocity  $u_{\text{wall}}$  and with inward normal in the down direction. The implementation of the diffusive Maxwell boundary condition at a boundary site  $\mathbf{x}$  on this wall consists of the update

$$f_i = \gamma f_i^{\text{eq}}(u_{\text{wall}}), \quad i = 4, 7, 8, \quad (5.2)$$

with

$$\gamma = \frac{f_2 + f_5 x + f_6}{f_4^{\text{eq}}(u_{\text{wall}}) + f_7^{\text{eq}}(u_{\text{wall}}) + f_8^{\text{eq}}(u_{\text{wall}})}. \quad (5.3)$$

The reason for the selection of this boundary condition vs the standard ‘bounce-back’ condition, is that this choice results in reduced noise in the populations functions and therefore the macroscopic moments. When using the bounce-back boundary conditions this noise makes the transition from a steady to a periodic flow difficult to detect.

A survey of available literature reveals that the precise value of  $\text{Re}$  at which the first Hopf bifurcation occurs is somewhat contentious, with most current studies (all of which are for incompressible flow) ranging from around  $\text{Re} = 7400\text{--}8500$  [11, 53, 56]. Here, we do not intend to give a precise value, rather we will be content to approximately localise the first bifurcation and by doing so measure the relative amount of dissipation produced by different systems.

To localise the first bifurcation we take the following algorithmic approach. The initial uniform fluid density profile is  $\rho = 1.0$  and the velocity of the lid is  $u_{\text{wall}} = 1/10$  (in lattice units). We use 101 interior lattice points in each direction for the domain. We then record the velocity data at a single control point with coordinates  $(6, 18)$  (relative to the upper left corner) and run the simulation for  $5000L/u_0$  time steps.

We denote the final 0.1% of the time series given by this signal by  $\mathbf{u}_{\text{sig}}$ .

For this test we switch from using the L&L MRT to the DMRT. The relaxation parameters chosen for the L&L MRT are predicated on the use of bounce-back boundary conditions, which are not appropriate for use in this test. Since the varying boundary conditions also affect the stability of the systems, even for the standard BGK collision operation, the stability results from the previous section are not directly comparable with the results in this section. To be specific the use of these diffusive boundary conditions usually increases stability.

In this problem the standard BGK system becomes unsteady before the first bifurcation occurs, at approximately Re2500. For our next benchmark test we examine the bifurcation in the standard DMRT system.

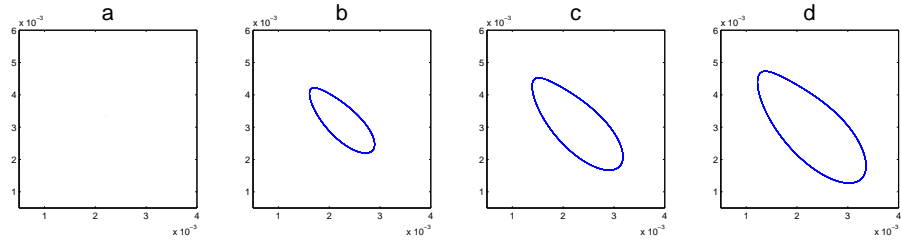


Figure 5.12: Mean filtered  $\mathbf{u}_{\text{sig}}$  for the DMRT at a) Re7400, b) Re7600, c) Re7800, d) Re8000

In Figure 5.12 the emergence of a periodic state in the standard DMRT system is observed. Again we do not precisely locate the bifurcation, only noting that it appears to emerge between a steady state solution at Re7400 and a periodic solution at Re7600. We should note that any additional dissipation produced by this operation has an extremely limited effect as the first bifurcation is detected in the expected region.

The next benchmark is the BGK system with the single relaxation time Median Filter. In Figure 5.13 we see that this system similarly seems to pick a bifurcation between Re7400 and Re7600, although the form of that bifurcation is somewhat

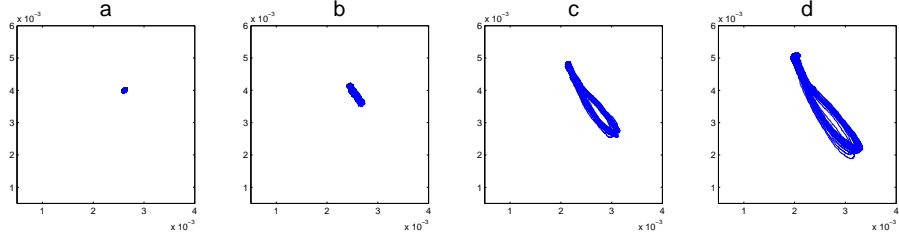


Figure 5.13: Mean filtered  $\mathbf{u}_{\text{sig}}$  for the BGK system equipped with the single relaxation time median filter at a) Re7400, b) Re7600, c) Re7800, d) Re8000

different and the system is subject to some noise due to the non-constant application of the limiter.

The final benchmark is the test of the ELBM system. In this experiment the system becomes unsteady before the first bifurcation at approximately Re6700.

The next test involves filtering only the  $N$  moment as discussed previously. In this case we set a threshold of  $10^{-2}$  for sites where the filter is applied. In particular we make two tests where we observe the following:

- In a test where the relaxation rate  $\delta_N$  is selected dynamically the system becomes unsteady before the first bifurcation at approximately Re3800. In this instance approximately 23 lattice sites per time step are selected for filtering.
- In a test where the relaxation rate  $\delta_N$  is always chosen as zero the system becomes unsteady before the first bifurcation at approximately Re4700. In this instance approximately 20 lattice sites per time step are selected for filtering.

Altogether we observe that applying an MRT operation in this manner is considerably less effective at stabilizing the system than the standard method of applying it uniformly everywhere in the system.

Although ELBM and these MRT-filtered systems become unsteady before the first bifurcation the systems do complete the requested number of time steps (they do not ‘blow up’) but in fact complete the simulation up to higher values of Reynolds

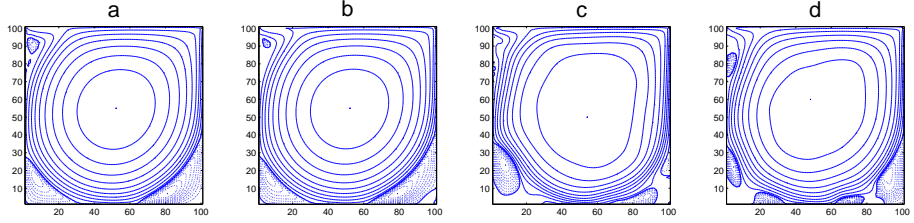


Figure 5.14: Steam function of a) Full MRT, b) BGK equipped with the single relaxation time median filter c) BGK with MRT Limiter with  $\delta_N$  dynamically chosen, d) ELBM at the final time step of the Re7000 simulations (negative regions in dashed lines)

numbers . Nevertheless the results of these simulations are not useful as can be seen in Figure 5.14. The form of the stream function varies significantly from the standard DMRT and median filtered BGK systems which reproduce the proper form of the stream function.

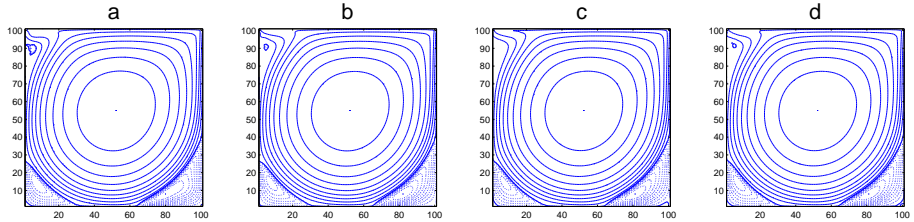


Figure 5.15: Steam function of a)BGK, b) Full DMRT, c) BGK equipped with the single relaxation time median filter, d) ELBM at the final time step of the Re5000 simulations (negative regions in dashed lines)

The other side of the coin is that although simulations may not be completely steady before the bifurcation, the results may be quite good. In Figure 5.15 the stream functions are given for all the benchmark tests at Re5000. For this Reynolds number BGK is unsteady (having non-zero disturbance energy), nevertheless the stream function is rather close to the steady solutions given by the three primary

stabilizing techniques. We presume that in this case the disturbances in the pure BGK systems consist of minor fluctuations which average out in time. This explains the good results for vortex centres for BGK at this Reynolds number and grid resolution given elsewhere[10].

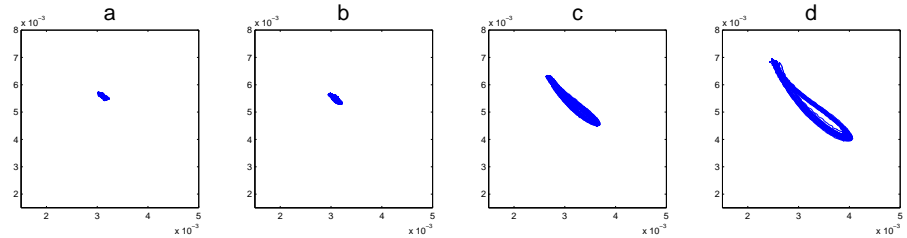


Figure 5.16: Mean filtered  $\mathbf{u}_{\text{sig}}$  for the full MRT system equipped with the median filter as a post-processor at a) Re7400, b) Re7600, c) Re7800, d) Re8000

The next test represents using the full MRT everywhere and applying the Median Filter as a post-processor. We can see from Figure 5.16 that although this system also picks out the first bifurcation, it does so at a larger Reynolds.

The final techniques to test are the combinations of filtering both parameters  $\delta$  and  $\delta_N$ . We try two options, in both for the Navier-Stokes part we use the Median Filtering where  $\Delta S^*$  is above the threshold. For the  $N$  component in the first option we dynamically choose  $\delta_N$ , in the second option we just set  $\delta_N = 0$ , where the magnitude of  $N$  exceeds the threshold.

In Figures 5.17, 5.18 we see the systems with the median-filter Navier Stokes dynamics as well as the median filtered/ selectively equilibrated ghost mode respectively. In these systems we see the bifurcation develop into a very noisy phase before seeming to return to a more structured dynamic.

To further examine the relative positions of the bifurcations in the systems we measure the mean squared deviation of  $\mathbf{u}_{\text{sig}}$  from its own average in that time, this

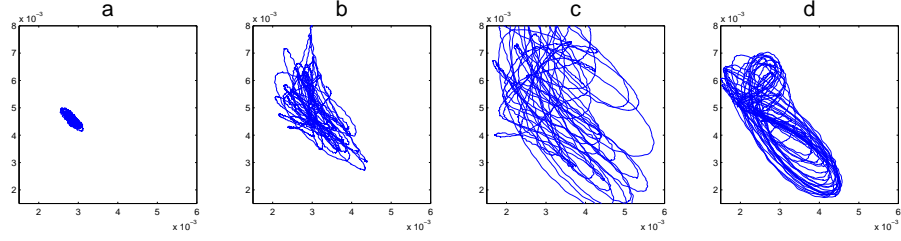


Figure 5.17: Mean filtered  $\mathbf{u}_{\text{sig}}$  for the BGK system with the Navier-Stokes modes and ghost mode median filters as a post-processor at a) Re7400, b) Re7600, c) Re7800, d) Re8000

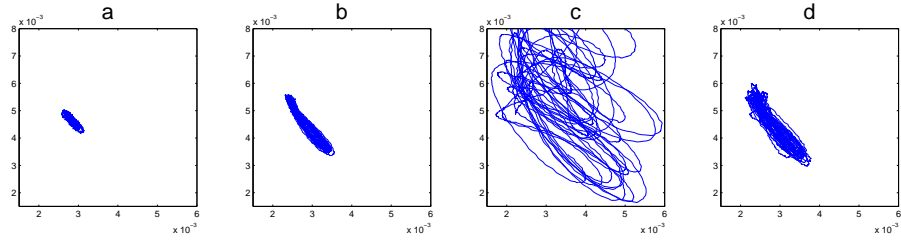


Figure 5.18: Mean filtered  $\mathbf{u}_{\text{sig}}$  for the BGK system with the Navier-Stokes modes and ghost mode selectively equilibrated as a post-processor at a) Re7400, b) Re7600, c) Re7800, d) Re8000

gives the ‘disturbance energy’ of the signal,

$$E = \|(u_{\text{sig}} - \overline{u_{\text{sig}}})\|_2^2. \quad (5.4)$$

Since the transition between steady and periodic flow in the lid-driven cavity is known to belong to the class of standard Hopf bifurcations we are assured that  $E \propto \text{Re}$  [24].

In Figure 5.19 we plot  $E$  as a function of Reynolds number, including the results of the benchmark tests. The emergence of the first bifurcation in the systems shown in Figures 5.12, 5.13, 5.16, 5.17, 5.18 can also be observed here. From this figure we can see that the standard MRT as well as the two limiters which filter the modes

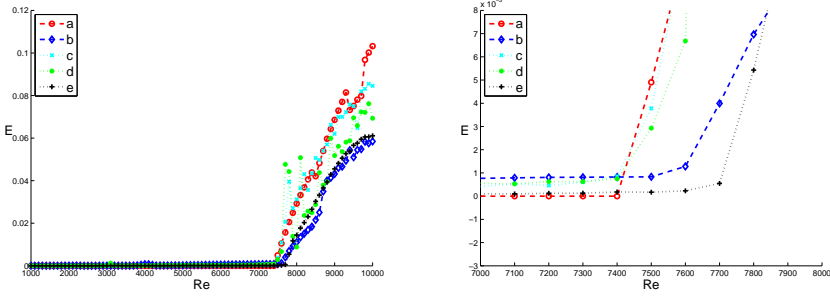


Figure 5.19: Disturbance energy (Eq. 5.4) in the systems with collision operations  
**a)**Full DMRT **b)**BGK with single relaxation time Median Filtering **c)**BGK with Median Filtering the Navier-Stokes and ghost modes independently **d)** BGK with Median Filtering the Navier-Stokes modes and selectively equilibrating the ghost mode **e)** Full DMRT with Median Filtering the Navier-Stokes modes; at Re10000 to Re100000 ; at Re1000 to Re10000

independently produce marginally less dissipation.

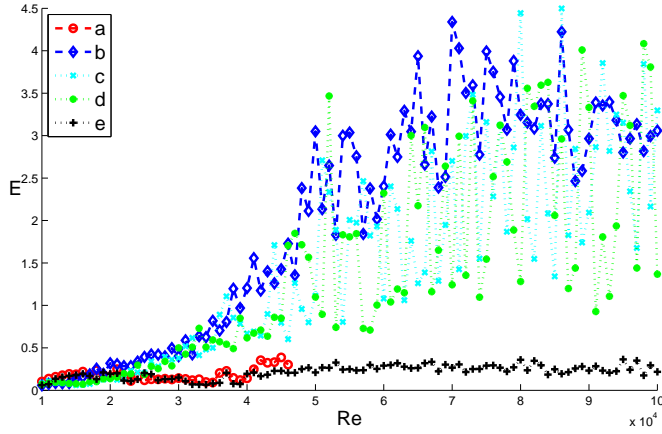


Figure 5.20: Disturbance energy (Eq. 5.4) in the systems with collision operations  
**a)**Full DMRT **b)**BGK with single relaxation time Median Filtering **c)**BGK with Median Filtering the Navier-Stokes and ghost modes independently **d)** BGK with Median Filtering the Navier-Stokes modes and selectively equilibrating the ghost mode **e)** Full DMRT with Median Filtering the Navier-Stokes modes; at Re10000 to Re100000 ; at Re1000 to Re10000

In Figure 5.20 we extend the range of Reynolds numbers up to 100000. The scope of energy exhibited by the systems diverges apart perhaps from the full DMRT and the full DMRT with Median Filter which stay relatively close together until the full DMRT becomes unstable at approximately Re44000.

# Chapter 6

## Conclusions

In the analysis of the continuous Boltzmann equation, the Chapman-Enskog procedure is known to reproduce the Navier-Stokes equations[33, 39, 62] at the first order. This is achieved by a perturbation by a small parameter, the Knudsen number. At higher orders which were not discussed here the Burnett equations arise.

The discrete Boltzmann schemes studied here are defined by the requirement that the Euler equations are recovered at the zero order. In common with the continuous scheme, dissipative terms arise at the first order, however in the discrete case there appear additional viscous terms. In parallel with Goodman and Lax[26] we view the additional dissipative part of the fluid as a direct consequence of the discrete scheme used. In this work we have used the idea of invariant manifolds[30] to calculate the macroscopic dynamics arising from discrete time Boltzmann schemes. This technique is based on an expansion in a different small parameter, the time step  $\epsilon$ . Dynamics at the zero and first orders again correspond to the conservative and dissipative parts of a fluid respectively. Although in this work we calculate these dynamics up to the first order only, the methodology can be extended to calculate higher orders. Under some hypotheses about the smoothness of the distribution function we prove conditional stability of these expansions up to some finite order.

To compute a solution to the Boltzmann system it is also necessary to discretize velocity space. We have calculated the exact macroscopic dynamics up to first order of common discrete velocity schemes, and their continuous counterparts. Although the dynamics of these two schemes match at the zero order, in the discrete velocity case additional erroneous terms arise at the first order. Such errors might be expected due to the way the quasi-equilibria in the discrete case are defined. If we view the discrete velocity summation as a quadrature approximation to the continuous velocity integral, then we should expect an error of integration. At the zero order we find no such error. This is due to an equilibrium being constructed specifically that the zero order moments are calculated exactly. This equilibrium consists of merely the second order Taylor expansion of the continuous equilibrium about the zero momentum position. It should, perhaps then, be no surprise that the dissipative dynamics in the discrete system approach those of the continuous system only in the limit of momentum going to zero, and that the error terms are third order.

We perform a stability analysis of the linear part of the macroscopic dynamics of the discrete velocity schemes under a short wave perturbation. In common with other authors using similar Fourier techniques [59, 61], and with our own earlier assumptions, we find that two lattice parameters are critical for stability. These are the time step  $\epsilon$  which must be positive, and the relaxation parameter  $\omega$ , which must be chosen for non-zero flow speed in the interval  $(-1, 1)$ . We also analytically and graphically give the permissible range of macroscopic quantities for stability. For the athermal systems study the density  $\rho$  can be any value, whereas the momentum  $u$  should be within an area centered around the zero point. The exact shape of this region is determined by the choice of velocity discretization.

Some enhancements of the standard single relaxation time BGK collision operation have been presented. Particular implementations of these have been tested to find their comparative benefits.

Our first numerical test involves implementing ELBM and the median filter and testing them on the standard 1D shock tube benchmark. We present three main conclusions from this study. Firstly we do not find any evidence that maintaining the proper balance of entropy regularizes spurious oscillations the Lattice Boltzmann method. For ELBGK we confirm the conclusions of Lax [26] and Levermore with Liu [49] that *dispersive oscillations* are unavoidable in numerical simulation of shocks.

Secondly, in order to clean up the parasitic dispersive oscillations in the Lattice Boltzmann method it is effective to filter the entropy in some way, so as to reduce the extremely-localised incidents of high non-equilibrium entropy; see [10], other (nonlocal) algorithms of filtering were proposed recently [57].

Finally for the 1D shock tube, one only needs to filter the entropy at one point per time step (usually very local to the shock), even at very low viscosity, in order to effectively eliminate the post-shock oscillation. The entropy filtering for non-entropic equilibria is possible [10] with use of the Kullback–Leibler distance from current distribution to equilibrium (the relative entropy).

In the 2D lid driven cavity test we observe that implementing TRT[25] or the L&L MRT[46] with certain relaxation rates can improve stability. The increase in stability from using TRT can be attributed to the correction of the numerical slip on the boundary, as well as modifying dissipation. What is the best set of parameters to choose for MRT is not a closed question. The parameters used in this work are those originally proposed by Lallemand and Luo [46]. Certain choices of relaxation parameters may improve stability while qualitatively changing the flow, so parameter choices should be justified theoretically, or alternatively the results of simulations should be somehow validated. Nevertheless the parameters used in this work exhibit an improvement in stability over the standard BGK system.

Modifying the relaxation rates of the different modes changes the production of dissipation of different components at different orders of the dynamics. The higher

order dynamics of lattice Boltzmann methods include higher order space derivatives of the distribution functions. MRT could exhibit the very nice property that where these derivatives are near to zero that MRT has little effect, while where these derivatives are large (near shocks and oscillations) that additional dissipation could be added, regularizing the system.

Using entropic limiters explicitly adds dissipation locally[10]. The Ehrenfest steps succeed to stabilize the system at Reynolds numbers where other tested methods fail, at the cost of the smoothness of the flow. We also implemented an entropic limiter using MRT technology called AMRT, which maximises dissipation on all non-shear modes. This also succeeded in stabilizing the system to a degree, however the amount of dissipation added is less than an Ehrenfest step and hence it is less effective. The particular advantage of a limiter of this type over the Ehrenfest step is that it can preserve the correct production of dissipation on physical modes across the system. Other MRT type limiters can easily be invented by simply varying the relaxation parameters.

As previously mentioned there have been more filtering operations proposed[57]. These have a similar idea of local (but not pointwise) filtering of lattice Boltzmann simulations. A greater variety of variables to filter have been examined, for example the macroscopic fields can be filtered rather than the mesoscopic population functions.

We can use the Enstrophy statistic to measure effective dissipation in the system. The results from the lid-driven cavity experiment indicate that increased total dissipation does not necessarily increase stability. The increase in dissipation needs to be targeted onto specific parts of the domain or specific modes of the dynamics to be effective

If we use some non-standard boundary conditions we can measure dissipation in a slightly different way, by the location of the first Hopf Bifurcation. The first

observation is that in both the DMRT and Median Filtered simulations the first bifurcation is detected in the expected range. We should not say that the bifurcation appears at the proper value, as we do not have a precise expectation of what it should be. Rather we can just say that both techniques add a minor and comparable amount of dissipation into the system, while improving the stability relative to the BGK system.

The other primary technique outlined in this work, ELBGK, stabilized the system up to a higher Reynolds number than the basic LBGK system, however not enough to reach the first bifurcation. On the basis of this test this technique cannot be recommended as a stabilizer for lattice Boltzmann systems as it not only performs worse, but is significantly more computationally expensive than an application of MRT or Median Filtering, due to the requirement to solve Eq 4.5 at every lattice site and time step.

The experiments which only filtered the ghost mode  $N$  were also not stable up to the first bifurcation. While it may be interesting that such minor modifications to the BGK system (altering only the post Navier-Stokes dynamics at a small number of sites) provides a stability increase by Re1000-2000, on the basis of this test this limiter cannot be recommended very strongly. The reasons being that the standard DMRT is considerably more effective, exhibits a reasonable value for the first bifurcation (and hence adds little dissipative error) and doesn't bear the computational overhead of applying a post-processing operation in addition to evaluating the field  $N$  at each time step.

The combination of the full DMRT and the Median Filter as a post process introduces an additional quantity of dissipation which delays the onset of the first bifurcation, as might be expected as the combination of two smoothing techniques.

The systems we tested which attempted to filter the modes independently also stabilize the system, picking a reasonable value of the Reynolds number for the first

bifurcation but with some additional noise in the dynamics.

According to Figure 5.19 the systems which pick the bifurcation at the lowest value of  $Re$  are the Full DMRT system and the two systems which filter the modes independently. All the results will be affected by the particular choice of the thresholds used to select the sites where filtering is applied. Fewer applications of any filter would be expected to move the bifurcation to a lower Reynolds number. No investigation was made in this work into varying these thresholds, they were simply chosen via some initial tests as values which selected a very small proportion of lattice sites.

We also observe that in the realm of higher Reynolds numbers (Figure 5.20) that the energy of the systems at the monitoring point diverges. Another method of validation should be used at these lower viscosities to realize which technique is most accurate in this regime.

Altogether we have observed that two existing techniques for stabilizing lattice Boltzmann methods by generalizing the BGK collision operation succeed in picking the first Hopf Bifurcation at a reasonable value of the Reynolds number. Of course these two operations can be combined to produce even more artificial dissipation and hence move the bifurcation to a greater value of the Reynolds number. This is obviously undesirable but such a procedure may be useful at very low viscosities to produce a stable system. ELBGK performs more poorly, providing less stability benefits while being more computationally expensive. The newly created limiters, which filter the modes independently, also pick a reasonable of the Reynolds number for the first bifurcation. A fuller investigation into the effects of altering the threshold parameters needs to be made to see if this performance can be further improved. The fact that the ‘parent’ methods of these limiters, namely MRT and Median Filtering, perform so well, indicates that any performance gains from using a limiter of this type will be fairly marginal.

Finally we should note that the stability of lattice Boltzmann systems depends on more than one parameter. In all these numerical tests the Reynolds number was modified by altering the rate of production of shear viscosity. In particular, for the lid driven cavity the Reynolds number could be varied by altering the lid speed, which was fixed at 0.1 in all of these simulations. Since the different modes of the dynamics include varying powers of velocity, this would affect the stability of the system in a different manner to simply changing the shear viscosity coefficient. In such systems the relative improvements offered by these methods over the BGK system could be different.

## Appendix A

# First order populations for the D2Q9 lattice with standard polynomial quasi-equilibria

$$\begin{aligned}
\frac{\omega}{1-\omega} f^{1\dots 3,(1)} = & \frac{4}{9} \left( -u_1 \partial_{x_1} \rho - u_2 \partial_{x_2} \rho + \left( 1 + \frac{3}{2} u^2 \right) \partial_{x_1} \rho u_1 \right. \\
& + \left( 1 + \frac{3}{2} u^2 \right) \partial_{x_2} \rho u_2 - 3u_1 \partial_{x_1} \rho u_1^2 - 3u_2 \partial_{x_2} \rho u_2^2 \\
& \left. - 3u_1 \partial_{x_2} \rho u_1 u_2 - 3u_2 \partial_{x_1} \rho u_1 u_2 \right), \\
& \frac{1}{9} \left( 2u_1 \partial_{x_1} \rho - u_2 \partial_{x_2} \rho + \left( -2 - 3u_1^2 + \frac{3}{2} u_2^2 \right) \partial_{x_1} \rho u_1 \right. \\
& + \left( 1 - 3u_1^2 + \frac{3}{2} u_2^2 \right) \partial_{x_2} \rho u_2 + 6u_1 \partial_{x_1} \rho u_1^2 + \frac{3}{2} \partial_{x_1} \rho u_2^2 \quad (\text{A.1}) \\
& \left. - 3u_2 \partial_{x_2} \rho u_2^2 - 3u_2 \partial_{x_1} \rho u_1 u_2 + (3 + 6u_1) \partial_{x_2} \rho u_1 u_2 \right), \\
& \frac{1}{9} \left( -u_1 \partial_{x_1} \rho + 2u_2 \partial_{x_2} \rho + \left( 1 + \frac{3}{2} u_1^2 - 3u_2^2 \right) \partial_{x_1} \rho u_1 \right. \\
& + \left( -2 + \frac{3}{2} u_1^2 - 3u_2^2 \right) \partial_{x_2} \rho u_2 + 6u_2 \partial_{x_2} \rho u_2^2 + \frac{3}{2} \partial_{x_2} \rho u_1^2 \\
& \left. - 3u_1 \partial_{x_1} \rho u_1^2 - 3u_1 \partial_{x_2} \rho u_1 u_2 + (3 + 6u_2) \partial_{x_1} \rho u_1 u_2 \right).
\end{aligned}$$

$$\begin{aligned}
\frac{\omega}{1-\omega} f^{4 \dots 7,(1)} = & \frac{1}{9} \left( 2u_1 \partial_{x_1} \rho - u_2 \partial_{x_2} \rho + \left( -2 - 3u_1^2 + \frac{3}{2}u_2^2 \right) \partial_{x_1} \rho u_1 \right. \\
& + \left( 1 - 3u_1^2 + \frac{3}{2}u_2^2 \right) \partial_{x_2} \rho u_2 + 6u_1 \partial_{x_1} \rho u_1^2 - \frac{3}{2} \partial_{x_1} \rho u_2^2 \\
& \left. - 3u_2 \partial_{x_2} \rho u_2^2 - 3u_2 \partial_{x_1} \rho u_1 u_2 + (-3 + 6u_1) \partial_{x_2} \rho u_1 u_2 \right), \\
& \frac{1}{9} \left( -u_1 \partial_{x_1} \rho + 2u_2 \partial_{x_2} \rho + \left( 1 + \frac{3}{2}u_1^2 - 3u_2^2 \right) \partial_{x_1} \rho u_1 \right. \\
& + \left( -2 + \frac{3}{2}u_1^2 - 3u_2^2 \right) \partial_{x_2} \rho u_2 + 6u_2 \partial_{x_2} \rho u_2^2 - \frac{3}{2} \partial_{x_2} \rho u_1^2 \\
& \left. - 3u_1 \partial_{x_1} \rho u_1^2 - 3u_1 \partial_{x_2} \rho u_1 u_2 + (-3 + 6u_2) \frac{\partial}{\partial x_1} \rho u_1 u_2 \right) \\
& \frac{1}{36} (2u_1 \partial_{x_1} \rho + 2u_2 \partial_{x_2} \rho + 3u_1 \partial_{x_2} \rho + 3u_2 \partial_{x_1} \rho \\
& + (-2 - 3u_1^2 - 9u_1 u_2 - 3u_2^2) \partial_{x_1} \rho u_1 \\
& + (-2 - 3u_1^2 - 9u_1 u_2 - 3u_2^2) \partial_{x_2} \rho u_2 \\
& - 3\partial_{x_1} \rho u_2 - 3\partial_{x_2} \rho u_1 - 3\partial_{x_1} \rho u_2^2 - 3\partial_{x_2} \rho u_1^2 \tag{A.2} \\
& + (6u_1 + 9u_2) \partial_{x_1} \rho u_1^2 + (9u_1 + 6u_2) \partial_{x_2} \rho u_2^2 \\
& + (-6 + 9u_1 + 6u_2) \partial_{x_1} \rho u_1 u_2 \\
& + (-6 + 9u_1 + 6u_2) \partial_{x_2} \rho u_1 u_2), \\
& \frac{1}{36} (2u_1 \partial_{x_1} \rho + 2u_2 \partial_{x_2} \rho - 3u_1 \partial_{x_2} \rho - 3u_2 \partial_{x_1} \rho \\
& + (-2 - 3u_1^2 + 9u_1 u_2 - 3u_2^2) \partial_{x_1} \rho u_1 \\
& + (-2 - 3u_1^2 + 9u_1 u_2 - 3u_2^2) \partial_{x_2} \rho u_2 \\
& + 3\partial_{x_1} \rho u_2 + 3\partial_{x_2} \rho u_1 + 3\partial_{x_1} \rho u_2^2 - 3\partial_{x_2} \rho u_1^2 \\
& + (6u_1 - 9u_2) \partial_{x_1} \rho u_1^2 + (-9u_1 + 6u_2) \partial_{x_2} \rho u_2^2 \\
& + (-6 - 9u_1 + 6u_2) \partial_{x_1} \rho u_1 u_2 \\
& + (6 - 9u_1 + 6u_2) \partial_{x_2} \rho u_1 u_2),
\end{aligned}$$

$$\begin{aligned}
\frac{\omega}{1-\omega} f^{8\dots 9,(1)} = & \frac{1}{36} (2u_1 \partial_{x_1} \rho + 2u_2 \partial_{x_2} \rho + 3u_1 \partial_{x_2} \rho + 3u_2 \partial_{x_1} \rho \\
& + (-2 - 3u_1^2 - 9u_1 u_2 - 3u_2^2) \partial_{x_1} \rho u_1 \\
& + (-2 - 3u_1^2 - 9u_1 u_2 - 3u_2^2) \partial_{x_2} \rho u_2 \\
& - 3\partial_{x_1} \rho u_2 - 3\partial_{x_2} \rho u_1 + 3\partial_{x_1} \rho u_2^2 + 3\partial_{x_2} \rho u_1^2 \\
& + (6u_1 + 9u_2) \partial_{x_1} \rho u_1^2 + (9u_1 + 6u_2) \partial_{x_2} \rho u_2^2 \\
& + (6 + 9u_1 + 6u_2) \partial_{x_1} \rho u_1 u_2 \\
& + (6 + 9u_1 + 6u_2) \partial_{x_2} \rho u_1 u_2), \\
& \frac{1}{36} (2u_1 \partial_{x_1} \rho + 2u_2 \partial_{x_2} \rho - 3u_1 \partial_{x_2} \rho - 3u_2 \partial_{x_1} \rho \\
& + (-2 - 3u_1^2 + 9u_1 u_2 - 3u_2^2) \partial_{x_1} \rho u_1 \\
& + (-2 - 3u_1^2 + 9u_1 u_2 - 3u_2^2) \partial_{x_2} \rho u_2 \\
& + 3\partial_{x_1} \rho u_2 + 3\partial_{x_2} \rho u_1 - 3\partial_{x_1} \rho u_2^2 + 3\partial_{x_2} \rho u_1^2 \\
& + (6u_1 - 9u_2) \partial_{x_1} \rho u_1^2 + (-9u_1 + 6u_2) \partial_{x_2} \rho u_2^2 \\
& + (6 - 9u_1 + 6u_2) \partial_{x_1} \rho u_1 u_2 \\
& + (-6 - 9u_1 + 6u_2) \partial_{x_2} \rho u_1 u_2)
\end{aligned} \tag{A.3}$$

## Appendix B

# Populations for the constructed 2D thermal example

### B.1 Zero order populations for the 8 velocity lattice with a thermal moment

$$\begin{aligned}
f^{1\dots 8,(0)} = & \frac{1}{4}\rho(2 + 4u_1 + u_1^2 - u_2^2 - E + 2u_1^3 + 2u_1u_2^2 - 4u_1E), \\
& \frac{1}{4}\rho(2 + 4u_2 - u_1^2 + u_2^2 - E + 2u_1^2u_2 + 2u_2^3 - 4u_2E), \\
& \frac{1}{4}\rho(2 - 4u_1 + u_1^2 - u_2^2 - E - 2u_1^3 - 2u_1u_2^2 + 4u_1E), \\
& \frac{1}{4}\rho(2 - 4u_2 - u_1^2 + u_2^2 - E - 2u_1^2u_2 - 2u_2^3 + 4u_2E), \\
& \frac{1}{4}\rho(-1 - u_1 - u_2 + u_1u_2 + E - u_1^3 - u_1^2u_2 - u_1u_2^2 - u_2^3 + 2u_1E + 2u_2E), \\
& \frac{1}{4}\rho(-1 + u_1 - u_2 - u_1u_2 + E + u_1^3 - u_1^2u_2 + u_1u_2^2 - u_2^3 - 2u_1E + 2u_2E), \\
& \frac{1}{4}\rho(-1 + u_1 + u_2 + u_1u_2 + E + u_1^3 + u_1^2u_2 + u_1u_2^2 + u_2^3 - 2u_1E - 2u_2E), \\
& \frac{1}{4}\rho(-1 - u_1 + u_2 - u_1u_2 + E - u_1^3 + u_1^2u_2 - u_1u_2^2 + u_2^3 + 2u_1E - 2u_2E)
\end{aligned} \tag{B.1}$$

## B.2 Example first order populations for the 8 velocity lattice with a thermal moment

$$\begin{aligned}
\frac{\omega}{1-\omega} f^{1,(1)} = & \frac{1}{4} (-2 - 2u_1 - u_2^2 + u_1^2 + 3E - 3u_1u_2^2 - u_1^3 + 3u_1E - u_2^4 + 2u_1^2u_2^2 \\
& + 3u_1^4 - 3u_1^2E + 3u_2^2E - 2E^2) \partial_{x_1}\rho \\
& + \frac{1}{4} (2u_2 + 4u_1u_2 + 3u_1^2u_2 + u_2^3 - 3u_2E + 4u_1^3u_2 + 4u_1u_2^3 - 6u_1u_2E) \partial_{x_2}\rho \\
& + \frac{1}{4}\rho (-2 + 2u_1 - 2u_1^2 - 2u_2^2 + 2E - 8u_1E + 14u_1^3 + 6u_1u_2^2) \partial_{x_1}u_1 \\
& + \frac{1}{4}\rho (4u_2 + 6u_1u_2 + 10u_1^2u_2 + u_2^3 - 4u_2E) \partial_{x_2}u_1 \\
& + \frac{1}{4}\rho (-2u_2 - 6u_1u_2 + 6u_1^2u_2 - 2u_2^3 + 4u_2E) \partial_{x_1}u_2 \\
& + \frac{1}{4}\rho (2 + 4u_1 + 2u_1^2 + 2u_2^2 - 2E + 6u_1^3 + 14u_1u_2^2 - 8u_1E) \partial_{x_2}u_2 \\
& + \frac{1}{4}\rho (3 + 3u_1 - 5u_1^2 + u_2^2 - 2E) \partial_{x_1}E + \frac{1}{4}\rho (-3u_2 - 6u_1u_2) \partial_{x_2}E
\end{aligned} \tag{B.2}$$

$$\begin{aligned}
\frac{\omega}{1-\omega} f^{5,(1)} = & \frac{1}{4} (2 + 2u_2 - u_1^2 - 4u_1u_2 + u_2^2 - 3E + 3u_2u_1^2 + u_2^3 - 3u_2E - 3u_1^4 - 4u_1^3u_2 \\
& - 2u_1^2u_2 - 4u_1u_2^3 + u_2^4 + 3u_1^2E + 6u_1u_2E - 3u_2^2E + 2E^2) \partial_{x_1}\rho \\
& + \frac{1}{4} (2 + 2u_1 + u_1^2 - 4u_1u_2 - u_2^2 - 3E + u_1^3 + 3u_1u_2^2 - 3u_1E + u_1^4 - 4u_1^3u_2 \\
& - 2u_1^2u_2^2 - 4u_1u_2^3 - 3u_2^4 - 3u_1^2E + 6u_1u_2E + 3u_2^2E + 2E^2) \partial_{x_2}\rho \\
& + \frac{1}{4}\rho (-2\rho u_1 - 4\rho u_2 - 14\rho u_1^3 - 14\rho u_1^2u_2 - 6\rho u_1u_2^2 - 6\rho u_2^3 \\
& + 8\rho u_1E + 8\rho u_2E) \partial_{x_1}u_1 \\
& + \frac{1}{4}\rho (2\rho + 2\rho u_1 - 4\rho u_2 + 4\rho u_1^2 - 4\rho E + 4\rho u_2^2 + 2\rho u_1^3 \\
& - 10\rho u_1^2u_2 - 6\rho u_1u_2^2 - 2\rho u_2^3 - 4\rho u_1E + 4\rho u_2E) \partial_{x_2}u_1 \\
& + \frac{1}{4}\rho (2\rho - 4\rho u_1 + 2\rho u_2 + 4\rho u_1^2 + 4\rho u_2^2 - 4\rho E - 2\rho u_1^3 \\
& - 6\rho u_1^2u_2 - 10\rho u_1u_2^2 + 2\rho u_2^3 + 4\rho u_1E - 4\rho u_2E) \partial_{x_1}u_2 \\
& + \frac{1}{4}\rho (-4\rho u_1 - 2\rho u_2 - 6\rho u_1^3 - 6\rho u_1^2u_2 - 14\rho u_1u_2^2 - 14\rho u_2^3 \\
& + 8\rho u_1E + 8\rho u_2E) \partial_{x_2}u_2 \\
& + \frac{1}{4}\rho (-3\rho - 3\rho u_2 + 5\rho u_1^2 + 6\rho u_1u_2 - \rho u_2^2 + 2\rho E) \partial_{x_1}E \\
& + \frac{1}{4}\rho (-3\rho - 3\rho u_1 - \rho u_1^2 + 6\rho u_1u_2 + 5\rho u_2^2 + 2\rho E) \partial_{x_2}E
\end{aligned}$$

(B.3)

# Bibliography

- [1] S. Ansumali, S. S. Chikatamarla, C. E. Frouzakis, I. V. Karlin, and I. G. Kevrekidis. *Model Reduction and Coarse-Graining Approaches for Multiscale Phenomena*, chapter Lattice Boltzmann Method and Kinetic Theory. 2006.
- [2] Santosh Ansumali and Iliya V. Karlin. Stabilization of the lattice Boltzmann method by the H theorem: A numerical test. *Phys. Rev. E*, 62:7999–8003, Dec 2000.
- [3] Santosh Ansumali and Iliya V. Karlin. Kinetic boundary conditions in the lattice Boltzmann method. *Phys. Rev. E*, 66:026311, Aug 2002.
- [4] G.K. Batchelor. *An introduction to fluid dynamics*. Cambridge mathematical library. Cambridge University Press, 2000.
- [5] R. Benzi, S. Succi, and M. Vergassola. The lattice boltzmann equation: theory and applications. *Physics Reports*, 222(3):145 – 197, 1992.
- [6] P. L. Bhatnagar, E. P. Gross, and M. Krook. A model for collision processes in gases. i. small amplitude processes in charged and neutral one-component systems. *Phys. Rev.*, 94:511–525, May 1954.
- [7] B. M. Boghosian, P. J. Love, and J. Yepez. Entropic lattice boltzmann model for burgers’s equation. *Philosophical Transactions of the Royal Society of London*.

*Series A: Mathematical, Physical and Engineering Sciences*, 362(1821):1691–1701, 2004.

- [8] R. A. Brownlee, A. N. Gorban, and J. Levesley. Stabilization of the lattice boltzmann method using the ehrenfests' coarse-graining idea. *Phys. Rev. E*, 74:037703, Sep 2006.
- [9] R. A. Brownlee, A. N. Gorban, and J. Levesley. Stability and stabilization of the lattice boltzmann method. *Phys. Rev. E*, 75:036711, Mar 2007.
- [10] R.A. Brownlee, A.N. Gorban, and J. Levesley. Nonequilibrium entropy limiters in lattice boltzmann methods. *Physica A: Statistical Mechanics and its Applications*, 387(2-3):385 – 406, 2008.
- [11] Charles-Henri Bruneau and Mazen Saad. The 2d lid-driven cavity problem revisited. *Computers & Fluids*, 35(3):326 – 348, 2006.
- [12] Cercignani C. *Theory and application of the Boltzmann equation*. Scottish Academic Press, 1975.
- [13] S. Chapman and T. G. Cowling. *The Mathematical Theory of Non-uniform Gases*. January 1991.
- [14] Hudong Chen, Shiyi Chen, and William H. Matthaeus. Recovery of the navier-stokes equations using a lattice-gas boltzmann method. *Phys. Rev. A*, 45:R5339–R5342, Apr 1992.
- [15] S Chen and GD Doolen. Lattice Boltzmann method for fluid flows. *Annual Review of Fluid Dynamics*, 30:329–364, 1998.
- [16] P. J. Dellar. Incompressible limits of lattice boltzmann equations using multiple relaxation times. *J. Comput. Phys.*, 190:351–370, 2003.

- [17] Paul J. Dellar. Bulk and shear viscosities in lattice boltzmann equations. *Phys. Rev. E*, 64:031203, Aug 2001.
- [18] P.J. Dellar. Non-hydrodynamic modes and a priori construction of shallow water lattice Boltzmann equations. *Phys. Rev. E*, 65:036309 (12 pages), 2002.
- [19] P.J. Dellar. Non-hydrodynamic modes and general equations of state in lattice boltzmann equations. *Physica A: Statistical Mechanics and its Applications*, 362(1):132 – 138, 2006.
- [20] D. d'Humieres. Rarefied gas dynamics: Theory and simulations. 159:450–458, 1992.
- [21] D. d'Humieres, I. Ginzburg, M. Krafczyk, P. Lallemand, and L. S. Luo. Multiple-relaxation-time lattice boltzmann models in three dimensions. *Philosophical Transactions of the Royal Society of London. Series A: Mathematical, Physical and Engineering Sciences*, 360(1792):437–451, 2002.
- [22] P. Ehrenfest and T. Ehrenfest. *The conceptual foundations of the statistical approach in mechanics*.
- [23] U. Frisch, B. Hasslacher, and Y. Pomeau. Lattice-gas automata for the navier-stokes equation. *Phys. Rev. Lett.*, 56:1505–1508, Apr 1986.
- [24] N. K. Ghaddar, K. Z. Korczak, B. B. Mikic, and A. T. Patera. Numerical investigation of incompressible flow in grooved channels. I - Stability and self-sustained oscillations. *Journal of Fluid Mechanics*, 163:99–127, February 1986.
- [25] Irina Ginzburg. Generic boundary conditions for lattice boltzmann models and their application to advection and anisotropic dispersion equations. *Advances in Water Resources*, 28(11):1196 – 1216, 2005.

- [26] Jonathan Goodman and Peter D. Lax. On dispersive difference schemes. i. *Communications on Pure and Applied Mathematics*, 41(5):591–613, 1988.
- [27] A. N. Gorban. *Model Reduction and Coarse-Graining Approaches for Multiscale Phenomena*, chapter Basic Types of Coarse-Graining, page 117. 2006.
- [28] Alexander N. Gorban, Iliya V. Karlin, Patrick Ilg, and Hans Christian Correactions and enhancements of quasi-equilibrium states. *Journal of Non-Newtonian Fluid Mechanics*, 96(1-2):203 – 219, 2001.
- [29] Alexander N. Gorban, Iliya V. Karlin, Hans Christian Öttinger, and Larisa L. Tatarinova. Ehrenfest’s argument extended to a formalism of nonequilibrium thermodynamics. *Phys. Rev. E*, 63:066124, May 2001.
- [30] A.N. Gorban. *Invariant Manifolds for Physical and Chemical Kinetics*. Springer, 2005.
- [31] H. Grad. Note on n-dimensional hermite polynomials. *Comm. Pure. Appl. Math*, 2:325–330, 1949.
- [32] SK Gudunov. A difference scheme for numerical solution of discontinuous solution of hydrodynamic equations. *Math Sbornik*, pages 271–306, 1959.
- [33] Xiaoyi He and Li-Shi Luo. Lattice boltzmann model for the incompressible navier-stokes equation. *Journal of Statistical Physics*, 88:927–944, 1997. 10.1023/B:JOSS.0000015179.12689.e4.
- [34] Xiaoyi He and Li-Shi Luo. Theory of the lattice boltzmann method: From the boltzmann equation to the lattice boltzmann equation. *Phys. Rev. E*, 56:6811–6817, Dec 1997.
- [35] F. J. Higuera, S. Succi, and R. Benzi. Lattice gas dynamics with enhanced collisions. *EPL (Europhysics Letters)*, 9(4):345, 1989.

- [36] F.L. Hinton, M.N. Rosenbluth, S.K. Wong, Y.R. Lin-Liu, and R.L. Miller. Modified lattice Boltzmann method for compressible fluid simulations. *Phys. Rev. E*, 63:061212, 2001.
- [37] Shuling Hou, Qisu Zou, Shiyi Chen, Gary Doolen, and Allen C. Cogley. Simulation of cavity flow by the lattice boltzmann method. *J. Comput. Phys.*, 118:329–347, May 1995.
- [38] I. V. Karlin, A. Ferrante, and H. C. Öttinger. Perfect entropy functions of the lattice boltzmann method. *Europhys. Lett.*, 47(2):182–188, 1999.
- [39] C. E. Frouzakus I. V. Karlin, S. Ansumali and S. S. Chikatamarla. Elements of the lattice boltzmann method i: Linear advection equation. *Communications in Computational Physics*, 1:1–45, 2006.
- [40] Takaji Inamuro. A lattice kinetic scheme for incompressible viscous flows with heat transfer. *Phil. Trans. Roy. Soc. London. Series A*, 360:477–484, 2002.
- [41] Iliya V. Karlin, Alexander N. Gorban, S. Succi, and V. Boffi. Maximum entropy principle for lattice kinetic equations. *Phys. Rev. Lett.*, 81:6–9, Jul 1998.
- [42] Iliya V. Karlin, Larisa L. Tatarinova, Alexander N. Gorban, and Hans Christian Öttinger. Irreversibility in the short memory approximation. *Physica A: Statistical Mechanics and its Applications*, 327(3-4):399–424, September 2003.
- [43] S. Kullback. *Information theory and statistics*. Wiley, 1959.
- [44] D. Kuzmin, R. Lohner, and S. Turek. *Flux Corrected Transport*. Springer, 2005.
- [45] Anthony J. C. Ladd. Numerical simulations of particulate suspensions via a discretized boltzmann equation. part 1. theoretical foundation. *Journal of Fluid Mechanics*, pages 285–309, 1994.

- [46] Pierre Lallemand and Li-Shi Luo. Theory of the lattice boltzmann method: Dispersion, dissipation, isotropy, galilean invariance, and stability. *Phys. Rev. E*, 61:6546–6562, Jun 2000.
- [47] Pierre Lallemand and Li-Shi Luo. Theory of the lattice boltzmann method: Acoustic and thermal properties in two and three dimensions. *Phys. Rev. E*, 68:036706, Sep 2003.
- [48] J. Latt and B. Chopard. Lattice boltzmann method with regularized pre-collision distribution functions. *Math. Comput. Sim.*, 72:165–168, 2006.
- [49] C.David Levermore and Jian-Guo Liu. Large oscillations arising in a dispersive numerical scheme. *Physica D: Nonlinear Phenomena*, 99(2-3):191 – 216, 1996.
- [50] Y. Li, R. Shock, R. Zhang, and H. Chen. Numerical study of flow past an impulsively started cylinder by the lattice-Boltzmann method. *Journal of Fluid Mechanics*, 519:273–300, November 2004.
- [51] Li-Shi Luo. *Lattice-Gas and lattice Boltzmann equations for two dimensional hydrodynamics*. PhD thesis, Georgia Institute of Technology, 1993.
- [52] Li-Shi Luo, Wei Liao, Xingwang Chen, Yan Peng, and Wei Zhang. Numerics of the lattice boltzmann method: Effects of collision models on the lattice boltzmann simulations. *Phys. Rev. E*, 83:056710, May 2011.
- [53] T. W. Pan and R. Glowinski. A projection/wave-like equation method for the numerical simulation of incompressible viscous fluid flow modeled by the navier–stokes equations. *Comp. Fluid Dyn. J.*, 9:28–42, 2000.
- [54] Y. Peng, C. Shu, Y. T. Chew, and T. Inamuro. Lattice kinetic scheme for the incompressible viscous thermal flows on arbitrary meshes. *Phys. Rev. E*, 69:016703–, 2004.

- [55] Y. Peng, C. Shu, Y. T. Chew, and H. W. Zheng. New lattice kinetic schemes for incompressible viscous flows. *Int. J. Mod. Phys. C*, 15:1197–1213, 2004.
- [56] Yih-Ferng Peng, Yuo-Hsien Shiau, and Robert R. Hwang. Transition in a 2-d lid-driven cavity flow. *Computers & Fluids*, 32(3):337 – 352, 2003.
- [57] Denis Ricot, Simon Mari, Pierre Sagaut, and Christophe Bailly. Lattice boltzmann method with selective viscosity filter. *Journal of Computational Physics*, 228(12):4478 – 4490, 2009.
- [58] CJ Roy. Grid convergence error analysis for mixed-order numerical schemes. *AIAA Journal*, 41:595–604, 2003.
- [59] Borja Servan-Camas and Frank T. C. Tsai. Non-negativity and stability analyses of lattice boltzmann method for advection-diffusion equation. *J. Comput. Phys.*, 228:236–256, January 2009.
- [60] Xiaowen Shan and Xiaoyi He. Discretization of the velocity space in the solution of the boltzmann equation. *Phys. Rev. Lett.*, 80:65–68, Jan 1998.
- [61] J. D. Sterling and S. Chen. Stability analysis of lattice boltzmann methods. 1996.
- [62] S. Succi. *The lattice Boltzmann equation for fluid dynamics and beyond*. Numerical mathematics and scientific computation. Clarendon Press, 2001.
- [63] E. Tadmor and W. Zhong. Entropy stable approximations of navier-stokes equations with no artificial numerical viscosity. *Journal of Hyperbolic Differential Equations*, 3:529–559, 2006.
- [64] F. Tosi, S. Ubertini, S. Succi, H. Chen, and I.V. Karlin. Numerical stability of entropic versus positivity-enforcing lattice boltzmann schemes. *Mathematics*

*and Computers in Simulation*, 72(2-6):227 – 231, 2006. Discrete Simulation of Fluid Dynamics in Complex Systems.

- [65] J.R. Weimar and J.P. Boon. Nonlinear reactions advected by a flow. *Physica A*, 224:207–215, 1996.
- [66] J. M. Yeomans. Mesoscale simulations: Lattice Boltzmann and particle algorithms. *Physica A Statistical Mechanics and its Applications*, 369:159–184, September 2006.
- [67] Wen-An Yong and Li-Shi Luo. Nonexistence of  $H$  theorems for the athermal lattice boltzmann models with polynomial equilibria. *Phys. Rev. E*, 67:051105, May 2003.
- [68] Wen-an Yong and Li-Shi Luo. Nonexistence of H theorem for some lattice boltzmann models. *Journal of Statistical Physics*, 121:91–103, 2005. 10.1007/s10955-005-5958-9.